Yücel Karabiyik

Quantitative Doppler analysis using color flow imaging and adaptive signal processing

Thesis for the degree of Philosophiae Doctor

Trondheim, June 2017

Norwegian University of Science and Technology
Faculty of Medicine
Department of Circulation and Medical Imaging

NTNU
Innovation and Creativity

Kvantitative Doppler-målinger fra farge-Doppler ved bruk av adaptiv signalprosessering

Medisinsk ultralyd er et viktig verktøy i obstetrikk for å vurdere mors helse og fosterets utvikling gjennom svangerskapet. Doppler-ultralyd brukes for å estimere blodstrømshastigheter og i svangerskap kan Dopplermålinger fra blant annet navlesnoren avsløre risikosvangerskap. Ultralydskannere er relativt billige og svangerskapsultralyd er et vanlig tilbud til gravide i industrialiserte land, mens det i utviklingsland er mangel på både ultralydskannere og kvalifiserte operatører.

Målet gjennom doktorgradsarbeidet har vært å utvikle Doppler-metoder som kan effektivisere arbeidsflyt og gi kvantitative Dopplermålinger automatisk, spesielt for uerfarne operatører. Metodene skal være implementerbare også på billige, uvanserte skannere som ofte er aktuelle for utviklingsland. Farge-Doppler brukes i dag som en kvalitativ metode som visualiserer blodstrøm. I dette arbeidet har de kvantitative mulighetene til farge-Doppler blitt undersøkt, spesielt med tanke på nøyaktighet og bilderate. Når flere avbildningssekvenser brukes samtidig (duplex/triplex mode), synker bilderaten drastisk, noe som kan motvirkes ved å avbilde et mindre område og bruke mindre data til hastighetsestimering. For å unngå triplex-sekvenser, ble det dermed først undersøkt om adaptiv spektralestimering kunne brukes til å estimere middelhastigheten til blodstrømmen slik som i farge-Doppler. Det ble vist at dette kunne gjøres selv uten å måtte filtrere bort vevssignalet først, noe som ga mer nøyaktige hastighetsestimat for de lavere blodstrømshastighetene som ellers ville blitt ødelagt av vevsfilteret ved bruk av farge-Doppler.

For å effektivisere arbeidsflyt og unngå duplex/triplex-sekvenser, er det deretter utviklet en metode som gir hastighetsspekter fra alle punkt i farge-Dopplerbildet ved hjelp av adaptiv spektralestimering og romlig midling. I tillegg ble det utviklet en metode for å estimere envelopen til hastighetsspektrene for å lettere finne maksimumshastigheter og relevante Dopplerindekser.

Den siste metoden som er presentert i dette doktorgradsarbeidet prøver å minimere spredning i hastighetsspekteret for å unngå overestimering av maksimumshastigheter. Metoden gir hastighetsspekter av høy kvalitet basert på få datapunkt som er forenelig med farge-Doppler. En ultralydskanner med en kombinasjon av metodene som er presentert i denne avhandlingen, vil oppnå en forbedret farge-Doppler-metode med mulighet for kvantitative blodstrømsmålinger. Metoden vil være enkel å ta i bruk og kan redusere variasjoner i målinger og mellom operatører.

Yücel Karabiyik
Institutt for Sirkulasjon og Bildediagnostikk, NTNU
Hovedveileder: Lasse Løvstakken
Biveiledere: Hans Torp, Ingvild Kinn Ekroll, Sturla H. Eik-Nes
Finansieringskilde: Umoja Project

Ovennevnte avhandling er funnet verdig til forsvares offentlig for graden Philosophiae Doctor (PhD) i medisinsk teknologi. Disputas finner sted i Auditoriet, MTA i Medisinsk teknisk forskningssenter, tirsdag 29. august 2017 kl. 12:15.

Abstract

Medical ultrasound is an essential tool used routinely in obstetrics for assessing fetal and maternal health. In particular, Doppler ultrasound and estimation of relevant Doppler indices are crucial for identifying high risk pregnancies. Technological advancements have made ultrasound systems relatively cheap and available for the general population in developed countries. Due to economic hardship in developing countries, however, both ultrasound scanners equipped with Doppler capabilities and qualified personnel in the field of obstetrics are lacking.

The work presented here is aimed at providing Doppler methods that can facilitate efficient work flow and automated quantitative analysis, in particular for the inexperienced user, and that can be implemented on low/mid-end ultrasound scanners. Specifically, the quantitative abilities of color flow imaging (CFI) were investigated, where the accuracy of blood velocity estimation and trade-off towards frame rate was investigated. The time-sharing approach in duplex and triplex imaging modes, where acquisition of data for each mode is interleaved, limits the amount of available data for blood velocity quantification. This decreases the frame rate, robustness of the velocity estimates and the region where the velocities are estimated. A method that employs adaptive spectral estimation methods was proposed for mean velocity estimation in CFI without prior clutter filtering. It was shown that the method could decrease the bias of the estimates in the transition region of the clutter filters where low blood velocity estimates are corrupted.

In order to avoid switching between the scanning modes during examination, and to provide quantitative analysis of the blood flow anywhere on the color flow image, a method was proposed where the velocity spectra are estimated using adaptive spectral estimators by utilizing 2-D spatial averaging. In addition, a spectral envelope estimation method was developed to estimate the maximum velocities and provide Doppler index estimation. The methods were evaluated with string phantom experiments and *in vivo* acquisitions; it was shown that robust estimates could be achieved with limited number of available samples as in conventional CFI (8-16).

Finally, a method to decrease spectral broadening in quantitative analysis was proposed to alleviate overestimation of maximum velocities. The method requires fewer samples than previous methods to achieve high spectral resolution and can potentially be used with conventionally acquired CFI data. A system that combines all the proposed methods can provide improved mean velocity estimates and more easy-to-use analysis with a potential to decrease intra/inter-observer variability.

Preface

This thesis is submitted in partial fulfilment of the requirements for the degree of *Philosophiae Doctor* (Ph.D.) at the Faculty of Medicine of the Norwegian University of Science and Technology (NTNU). The research was funded by the UMOJA project which is a joint effort between three main partners: The National Center for Fetal Medicine (NCFM) at St. Olavs Hospital and NTNU, the Department of Circulation and Medical Imaging (ISB) at NTNU, and GE Vingmed Ultrasound AS., and was carried out at ISB. The main supervisor has been Professor Lasse Løvstakken from ISB and co-supervisors have been Professor Hans Torp and Dr. Ingvild Kinn Ekroll from ISB, and Professor Sturla H. Eik-Nes from the Department of Laboratory Medicine, Children's and Women's Health, NTNU.

Acknowledgements

My journey at ISB started with my master's studies in 2011. I have met many people along the way who made my journey worth it and influenced my work. First of all, I would like to express my gratitude and appreciation to my main supervisor Lasse for his continuous support since the beginning of this journey. His great guidance, motivation, profound knowledge and ideas helped me throughout my research and writing of this thesis. I would also like to thank my co-supervisors: Ingvild, for being invaluable help at every stage of my work, for motivating me and always being available for discussions, and Hans, for his important suggestions and feedback and for always welcoming me with a smile when I entered his office and taking his time for discussions.

I would also like to express my sincere gratitude to my co-supervisor Sturla and Eva for their invaluable support on the clinical aspects of the project. A special thanks goes to Jørgen for the fruitful discussions and his help with the research scanner. I would like to thank Alfonso for his great help with all kinds of phantoms and scanners and for creating practical solutions to my lab problems. I would also like to thank all the co-authors for great cooperation.

I would like to thank Solveig and Morten for being the *unofficial organizing committee* and organizing all the fun social events. I would like to thank Stefano for his "cake support" which gave Fridays another meaning, Sebastien for being the entertaining party guy, Sigurd for being a fun and supportive office mate and all the colleagues in the ultrasound family at ISB for the great work environment.

I would like to thank my friends back home who motivated and supported me through difficult times and friends here who supported me and gave a second home to me in Norway; *tusen hjertelig takk!* Finally, I would like to thank my family for their love and support throughout my life.

Table of Contents

Abbreviations xii

1 Introduction **1**
1.1 The UMOJA Project 2
1.2 Aims of study 3
1.3 Previous work 4
1.4 Thesis outline 5
1.5 Summary of Contributions 6
1.5.1 Improving estimation of mean velocities for CFI in time-shared systems 6
1.5.2 A method to estimate maximum velocities for quantitative Doppler analysis 7
1.5.3 Extending the use of CFI to quantitative Doppler analysis . . . 8
1.5.4 Decreasing OW length and spectral broadening 8
1.6 Discussion 9
1.7 Concluding remarks and future work 14
1.8 Publication list 15
References 17

2 Background **23**
2.1 Medical ultrasound imaging 23
2.2 Data acquisition 24
2.2.1 Line-by-line acquisition 24
2.2.2 Parallel beamforming 24
2.3 Color flow imaging 26
2.3.1 The autocorrelation estimator 26
2.4 Spectral Doppler 27
2.4.1 Power spectral Capon 31
2.4.2 The APES power spectral estimator 32
2.4.3 Blood iterative adaptive approach 33
2.5 Clutter filtering 34
2.5.1 Infinite impulse response filters 34
2.5.2 Finite impulse response filters 34
2.5.3 Polynomial regression filters 35

2.5.4 Adaptive clutter filtering . . . 35
2.6 Diagnostic value of CFI and PW-Doppler . . . 35
References . . . 38

3 Adaptive Spectral Estimation Methods in Color Flow Imaging 45
3.1 Introduction . . . 45
3.2 Methods . . . 47
3.2.1 PSD Estimators . . . 47
3.2.2 Mean Velocity Estimators . . . 50
3.2.3 Clutter Filtering . . . 52
3.2.4 Signal Model and Simulation Setup . . . 53
3.2.5 Data Acquisition and Processing . . . 53
3.3 Results . . . 55
3.3.1 Simulations . . . 55
3.3.2 In-vivo . . . 61
3.3.3 Flow phantom . . . 64
3.4 Discussion . . . 65
3.5 Conclusions . . . 70
References . . . 71

4 Adaptive Spectral Envelope Estimation for Doppler Ultrasound 75
4.1 Introduction . . . 75
4.2 Algorithm Description . . . 78
4.2.1 Maximum Velocity Point Detection . . . 78
4.2.2 Maximum Velocity Envelope Estimation . . . 81
4.2.3 Algorithm for Pulsatility Index Estimation . . . 82
4.3 Evaluation Methods . . . 83
4.3.1 Signal Model for Simulations . . . 83
4.3.2 Data Acquisition and Processing . . . 85
4.4 Results . . . 87
4.4.1 Comparison with Existing Methods . . . 87
4.4.2 Testing for Robustness to Varying SNR . . . 89
4.4.3 Varying Doppler angle and peak velocity . . . 92
4.4.4 Estimation of Clinical Indices based on Spectral Envelope . . . 93
4.5 Discussion . . . 95
4.5.1 Method Establishment . . . 95
4.5.2 Reliability of Maximum Velocity Estimation . . . 96
4.5.3 Robustness to SNR . . . 98
4.5.4 Blood flow measurements based on envelope . . . 98
4.6 Conclusion . . . 99
References . . . 99

5 Quantitative Doppler Analysis using Conventional Color Flow Imaging Acquisitions **105**
5.1 Introduction . . . 105
5.2 Methods . . . 107
5.2.1 PSD Estimators . . . 107
5.2.2 Maximum Velocity Envelope Estimation . . . 108
5.2.3 Data Acquisition and Processing . . . 110
5.3 Results . . . 112
5.3.1 String phantom results . . . 113
5.3.2 In vivo results . . . 115
5.4 Discussion . . . 119
5.5 Conclusions . . . 121
5.6 Acknowledgements . . . 121
References . . . 121

6 Data Adaptive 2-D Tracking Doppler **131**
6.1 Introduction . . . 131
6.2 Methods . . . 132
6.3 Experiments . . . 133
6.4 Results . . . 135
6.5 Discussion . . . 137
6.6 Conclusion . . . 138
References . . . 139

Abbreviations

A-mode	Amplitude mode
APES	Amplitude and phase estimation
AR	Autoregressive
ARMA	Autoregressive moving average
BAPES	Amplitude and phase estimation
BIAA	Blood iterative adaptive approach
B-mode	Brightness mode
BPSC	Blood power spectral Capon
BSLIM	Blood sparse learning via iterative minimization
CCA	Common carotid artery
CFI	Color flow imaging
DFT	Digital Fourier transform
DOA	Direction of arrival
EDV	End diastolic velocity
FFT	Fast Fourier transform
FIR	Finite impulse response
$F_{\#}$	F-number
FOV	Field of view
Fps	Frames per second
GM	Geometric method
IAA	Iterative adaptive approach
IIR	Infinite impulse response
IPS	Integrated power spectrum
IUGR	Intra uterine growth restriction
MA	Moving average
MGM	Modified geometric method
MLA	Multi line acquisition
MUSIC	Multiple signal classification
MV	Minimum variance

OW	Observation window
PI	Pulsatility index
PRF	Pulse repetition frequency
PRT	Pulse repetition time
PSD	Power spectral density
PSV	Peak systolic velocity
PW-Doppler	Pulsed wave Doppler
RI	Resistivity index
ROI	Region of interest
SNR	Signal-to-noise ratio
SNSI	Signal noise slope intersection
TAV	Time averaged velocity
T_t	Transit time
UNFPA	United Nations Population Fund

Chapter 1

Introduction

The introduction of medical ultrasound has changed the way diagnoses are made in various fields in medicine. Today it is an essential tool used routinely in specialities like cardiology, obstetrics and emergency medicine. The technology has gone through a great evolution following advancements in hardware design and signal processing techniques. The developments in sonar (sound navigation and ranging) and radar (radio detection and ranging) led to the idea of using ultrasound on the human body for treatment and diagnostic purposes [1]. The pulse-echo technique employed in radar was later applied using ultrasound waves to examine the human body. In radar, pulsed electromagnetic waves are transmitted through a transmitter and the reflected waves from an object picked up by the receiver are used for estimation of the object's location and speed. A basic application of this technique in medical ultrasound is the A-mode (amplitude mode) display where the amplitude of the scattered wave is displayed versus depth. It was used on the human body in the late 1940s and early 1950s [2–5]. This paved the way to the generation of B-mode (brightness mode) ultrasound images where the pulses are transmitted in different directions to cover a 2-D region and the amplitude of each reflected wave is represented by the brightness of a dot in the image for visualization of anatomical structures [6, 7].

As for the investigation of the moving targets in the human body, I. Edler and C.H. Hertz, in Sweden in 1953, probed the human heart motions using a flaw detector which was based on the pulse-echo technique [8, 9]. Shigeo Satomura, published his method for inspection of cardiac functions by utilizing the Doppler effect; his device was the first Doppler ultrasound device used for medical diagnostics [10, 11]. The first ultrasound application in the field of obstetrics and gynaecology was published by Ian Donald, John McVicar and Tom Brown in 1958; they investigated abdominal masses and published the first ultrasound images of the fetus [12]. The first ultrasonic Doppler application in this field was the detection of the fetal heart movement published in 1964 [13].

Improvements in the electronics resulted in the development of real-time ultrasound scanners and diagnostic use of ultrasound became widespread. In the 1980s, color flow imaging (CFI) was introduced where the mean blood velocities estimated in a 2-D region were mapped to colors and overlaid on B-mode images [14, 15]. The method known as the autocorrelation method is used for estimation of mean blood velocities in most commercial ultrasound imaging systems [16]. In CFI, several pulses are transmitted in one direction with a fixed time interval called the pulse repetition

time (PRT), and the number of pulses transmitted in each direction is usually referred to as the *ensemble length* or *packet size* and will be used interchangeably in this work. The packet size is usually kept low (8-16 samples) in order to cover a large spatial region at reasonable imaging frame rates. This trade-off sets a limit to the achievable color flow image quality in terms of robustness and estimated velocity span; the estimates within the packet have high variance and the low number of samples makes clutter filtering challenging. The echoes from the stationary or near stationary tissue can be 20-80 dB stronger than the signal from blood and must be attenuated before velocity estimation. Filters used for attenuation have a certain transition band between the stop band and pass band region. It is desired to keep the transition region narrow and have sufficient stop band attenuation in order to remove the clutter completely while estimating the blood velocity without bias. However, generating such a filter is not straight forward, resulting in an attenuation of the low blood velocities in the transition band.

Since the introduction of CFI, many data acquisition and processing techniques have been proposed to estimate the mean blood velocities [17–24]. Combination of broad beams and parallel beamforming can be used to cover larger areas for each transmit event than is possible with focused, line-by-line imaging. When used for color flow imaging, these methods can increase the frame rates and the packet size substantially. Methods such as ultrafast Doppler imaging that employs broad transmit waves allow for estimation of the whole spectrum of blood flow velocities anywhere in the image [17]. Conventionally, spectral estimation is done by transmitting additional narrow bandwidth pulses with low PRT, and the velocity spectrum is provided at one sample volume location. This mode is referred to as pulsed wave Doppler (PW-Doppler), and is the main modality used for quantification of blood velocities in the clinic. The advantages of parallel beamforming come with the cost of decreased contrast and lateral resolution as well as increased data processing and acquisition workload. Therefore, high quality real time ultrafast imaging applications are realized on high-end and costly ultrasound scanners for the time being [25].

1.1 The UMOJA Project

Reducing maternal and child deaths is a global priority. The levels of maternal and perinatal mortality are beyond acceptable, around 303 000 women [26] die and 2.6 million babies are stillborn [27] every year. Most of these deaths could be prevented, as the health-care solutions to prevent or manage complications are well known. Women living in rural areas are the least likely to receive the health care needed which causes a higher maternal mortality rate. Most of all maternal and perinatal deaths occur in developing countries [28].

Today, Doppler measurements are an integrated part of most ultrasound scanning systems. Diagnostic ultrasound is the primarily used imaging method in pregnancy and easily accessed by the general population in developed countries. However, in rural and remote areas of developing countries diagnostic imaging is often insufficient or completely lacking [29]. Moreover, the challenging financial situation

causes investment in cheap, low quality equipment that does not include the Doppler technology, which is, considered as advanced ultrasonography implemented on sophisticated equipment [30]. Doppler technology, however, is essential for the determination of high-risk pregnancies [31] such as hypertension in pregnancy, which is one of the major factors responsible for maternal death [32].

In addition to lack of diagnostic imaging, the shortage of qualified health professionals is a major factor regarding the high levels of maternal and child deaths in low-income countries. The State of the Worlds Midwifery 2014 report of the United Nations Population Fund (UNFPA) states that there is a need to train and deploy more midwives, particularly in remote and rural areas of developing countries [28].

The work described in this thesis is a part of the UMOJA project which aims to develop a low-cost and portable ultrasound imaging system that is easy to use for the inexperienced user, and specifically designed for operation in challenging rural areas of developing countries. Ultrasound scanners have become more portable and durable over the years and are relatively cheap compared to other diagnostic imaging methods. Therefore, they are more affordable and can be used in mobile clinics and as point-of-care ultrasound. Several studies have shown that introducing diagnostic ultrasound into clinics in rural areas reduces the length of stay and can change the treatment and surgical plans [33–35] and also has potential to improve the rate of maternal and fetal mortality [36].

1.2 Aims of study

Doppler imaging is highly useful as qualitative and quantitative analysis tool for detection of abnormal blood flow and it is the primary imaging modality used in obstetrics [37]. Currently, the user has to switch between the imaging modes to maintain the quality of blood velocity estimation or to increase the frame rate. This is especially challenging for the inexperienced user. The user is not updated with the current sample volume location when the examination is done in only PW-Doppler mode. On the other hand, quality of the CFI and the estimated spectrogram is deteriorated when the different modes are displayed simultaneously. However, practising diagnostic ultrasound can potentially be simplified if the advanced signal processing techniques are applied to data acquired with conventional scanning methods.

The aim of this study has been to develop and evaluate methods that can increase the quality of mean velocity estimations in CFI and further extend the use of CFI into more quantitative spectral-Doppler analysis. The objective is to provide improved quantitative analysis by using conventional CFI scanning, i.e. restricted to few temporal samples, to approach an automated method for extracting relevant Doppler indices from velocity spectra. The overall aim is to help to increase the efficiency of work flow and the quantitative abilities of ultrasound systems, with a particular focus on the low/mid-end range systems, in order to enable the use of diagnostic ultrasound for inexperienced users.

Conventionally, a time sharing approach is used for data acquisition and display

of two (duplex scanning) or three (triplex scanning) modes simultaneously, meaning that data acquisition for each mode is interleaved. Focused transmissions with different transmit and receive settings are employed for each type of acquisition. Each transmission is further optimized for the information to be extracted. A trade-off here is the data acquisition rate which affects the frame rate, the quality and the span of velocity estimation as well as the size of the region of interest (ROI).

Data adaptive spectral estimators have been applied to medical ultrasound for velocity spectrum estimation and have been shown to achieve high spectral resolution and suppression of side lobes using fewer samples compared to conventional techniques. In this work, we utilize these advantages to extract more information from the data acquired with conventional CFI scanning schemes. The overall aims of this study can be summarized as follows:

- Investigate whether modern data adaptive signal processing techniques can be used to improve the mean velocity estimation in CFI
- Investigate whether data adaptive spectral estimators can be used to provide useful spectral information from conventional color-Doppler acquisitions
- Investigate whether automatic maximum envelope extraction can be achieved based on the spectral information from conventional CFI to extract quantitative indices.

1.3 Previous work

Adaptive spectral estimators are utilized in this work for velocity spectrum estimation. They have previously been used in radar and sonar applications and have been shown to improve the spectral resolution and contrast compared to the conventional Welch method. Allam and Greenleaf [38] showed that the estimation of direction-of-arrival (DOA) in radar and velocity measurements using PW-Doppler in ultrasound has similarities and later demonstrated that high resolution techniques can potentially be used in Doppler ultrasound by using the minimum variance (MV) [39], also referred to as power spectral Capon (PSC), and the multiple signal classification (MUSIC) [40] estimators [41]. Received signals in DOA problem can be modelled as narrowband signals, meaning that the echo signals from the targets can be represented by a single frequency component. However, in PW-Doppler, the echo signal is wideband due to factors such as the limited observation time, resulting in band of frequencies. Allam and Greenleaf also discussed several wide-to-narrow-band conversion methods which can be used prior to velocity spectrum estimation with narrowband estimators, such as the Capon estimator.

More recently, Gran et al. [42] adapted the Capon and the amplitude and phase estimation (APES) methods to spectral Doppler estimation in medical ultrasound which were termed as blood PSC (BPSC) and blood APES (BAPES). The methods were evaluated by utilizing *slow time* (refers to sampling in time from pulse to pulse) and *fast time* (refers to sampling in depth for each pulse) averaging and through

simulation and *in vivo* experiment. It was concluded that the adaptive spectral estimators could outperform the Welch estimator for short observation windows. A more detailed *in vivo* validation research was later done and confirmed the previous observations [43].

Gudmundson et al. [44] introduced two iterative data adaptive spectral estimators, blood iterative adaptive approach (BIAA) and blood sparse learning via iterative minimization (BSLIM) into ultrasound blood velocity estimation. The methods showed better performance than the conventional Welch method as well as the more advanced BAPES and BPSC methods. In addition, the potential for spectral estimation in more than one sample volume location and using sparse data without restrictions on the sampling pattern were demonstrated.

The BIAA and the BAPES methods were further evaluated for their use in multigate spectral Doppler analysis by Ricci [45]. The number of spatial averaging locations along the fast time was limited to increase the spatial resolution. The methods could produce high frequency resolution spectra compared to the Welch method using fewer samples. It was concluded that the time resolution of the spectrograms as well as the number of locations where spectral profiles are displayed simultaneously could be increased. Also, the high clutter suppression capabilities of the methods were confirmed through a flow phantom experiment by estimating spectra without prior clutter filtering.

Ekroll et al. [46] used the spectral estimation methods BPSC, BAPES, MUSIC and a projection-based version of the Capon estimator by utilizing only 2-D spatial averaging (along the lateral and fast time dimensions), i.e., no slow time averaging. It was shown that the high frequency resolution spectral estimates, especially for low velocities, could be obtained using observation window lengths equal to ensemble lengths used in conventional CFI. Moreover, superior clutter suppression was demonstrated *in vivo* with vascular and cardiac imaging examples. The Capon estimator was later evaluated in this setting for obtaining spectral estimates from the spatial locations anywhere on the color flow image with plane wave acquisitions and showed promising results [47].

The previous work and observations made led to the idea of utilizing the adaptive spectral Doppler methods to improve the quanitative abilities of conventional CFI, i.e., packet based data acquisition with focused transmissions, as described further in the thesis.

1.4 Thesis outline

The thesis is organized as follows: Section 1.5 summarizes the contributions presented in this thesis. A more detailed discussion of the results and the connection of the separate chapters towards the overall aim are given in Section 1.6. This chapter concludes with a list of publications and written and oral contributions to international conferences. Chapter 2 gives an overview of the methods that can help the reader to better understand the work and to make the thesis more self-contained. Finally, chapters 3-6 present the technical papers that were the outcome of this work.

1.5 Summary of Contributions

In this section the aims are elaborated in connection to contributions presented in this thesis and the methods that are used to achieve these aims are briefly presented.

1.5.1 Improving estimation of mean velocities for CFI in time-shared systems

Interleaved transmissions for B-mode imaging and Doppler modes employed in duplex and triplex scanning schemes reduces the amount of data available for velocity estimation. The size of the ROI and the ensemble length in CFI is limited to 8-16 samples to achieve acceptable frame rates. Clutter filtering with such ensemble lengths is a challenge in CFI. As a result, the employed filters typically have broad transition regions where the low blood velocities are also attenuated. This causes overestimation of the mean velocities or signal loss and dropouts in the low blood velocity and transverse flow regions. It has previously been shown [43, 46] that data adaptive spectral estimators are able to suppress clutter and associated side lobes and provide high spectral resolution using observation window (OW) lengths equal to typical ensemble lengths used in CFI.

In Chapter 3, the data adaptive spectral estimation methods Capon and blood iterative adaptive approach (BIAA) were investigated for estimation of mean blood velocities. Clutter filtering is performed by removing parts of the power spectral density (PSD) considered as clutter and the mean velocity is estimated directly in the frequency domain using the altered PSDs. The PSDs were estimated with different OW lengths and the results were compared to polynomial regression filtering with suitable filter orders. CFI datasets were simulated with different packet sizes and signal to noise ratio (SNR) to obtain estimator statistics. Flow phantom, common carotid artery (CCA) and jugular vein acquisitions were performed to evaluate the proposed methods further.

It was found that the adaptive spectral estimation methods could reduce the bias and variance of low blood velocity estimates. The Capon estimator could reduce the bias substantially in the transition region compared to a conventional filter, and improved velocity estimations were obtained from the regions close to the artery walls where low blood velocities are present. Currently, filter cut-off velocities were chosen manually by inspecting the estimated spectra and the clutter velocities can be highly varying throughout the cardiac cycle, for instance in cardiac imaging. Therefore, further work should include developing an adaptive algorithm that sets the cut-off velocity automatically.

*This work is described in the paper "*Adaptive Spectral Estimation Methods in Color Flow Imaging*", published in IEEE Transactions on Ultrasonics, Ferroelectrics and Frequency Control, and presented here in its final form. The candidate was the main contributor to all aspects of the work, except for the data acquisition, for which, Dr. Tonje Dobrowen Fredriksen and Lars Mølgaard Saxhaug are gratefully acknowledged.*

1.5.2 A method to estimate maximum velocities for quantitative Doppler analysis

Color flow imaging displays the mean velocities for all spatial points in the ROI combined with the anatomical information from B-mode. It is useful for detection of abnormal flow and it can be used to navigate for PW-Doppler sample volume placement. However, CFI is not used quantitatively due to factors such as angle dependency, limited frame rate and lack of robustness. Diagnostic velocity measurements and Doppler indices are obtained using the maximum velocity traces from PW-Doppler. In PW-Doppler, narrow band ultrasound pulses are transmitted and the time samples are extracted at the depth of interest. The dimensions of the sample volume where the signal used for velocity spectrum estimation is sampled depend on the characteristics of the transmit pulse. The scatterers are observed in the sample volume for a limited amount of time. In addition, the angle between the flow direction and pulse transmission can limit this time interval even further. This results in a limited observation time and therefore a broadening of the estimated spectrum. Delineation of spectrograms consisting of spectra with significant broadening can result in overestimation of maximum velocities.

Several methods have been proposed to estimate the maximum velocity in presence of spectral broadening. However, extraction of the spectral envelope is not a straight forward step after maximum velocity estimation. Spectral envelopes that are constructed solely on the estimated values may contain erroneous estimates. Therefore, additional constraints have to be introduced to assess the accuracy of the estimated maximum velocity.

In Chapter 4, a method is proposed which is a combination of two existing maximum velocity estimation methods, the Signal Noise Slope Intersection (SNSI) [48] and an altered version of the Geometric Method (GM) [49], to improve the estimation of maximum velocities. After the maximum velocities are estimated with the proposed method, the estimates were classified as *valid* or *invalid* and the spectral envelope is constructed with the valid estimates and further used for calculation of Doppler indices. Simulations were performed to assess the performance of the proposed method with varying SNR. The proposed method was compared to several existing maximum velocity estimation methods using simulated data sets, string phantom and *in vivo* acquisitions.

It was shown that improvement was achieved using the combined approach. The proposed method could yield maximum velocity estimations with low variance and smooth spectral envelopes. Low sensitivity to SNR and low variance in the Doppler index estimation suggested that the method could potentially be used for automatic clinical index calculation.

*This work is described in the paper "*Adaptive Spectral Envelope Estimation for Doppler Ultrasound*", published in IEEE Transactions on Ultrasonics, Ferroelectrics and Frequency Control, and presented here in its final form. The candidate contributed to the algorithm development, simulations of data sets and writing.*

1.5.3 Extending the use of CFI to quantitative Doppler analysis

Restrictions on data amount imposed by the time-sharing approach in triplex scanning mode often result in deterioration of time and/or frequency resolution of PW-Doppler spectrogram. Therefore, once the sample volume is selected, it is recommended that the scanner is set to only PW-Doppler mode to maintain a high quality. However, the probe or the patient movement can easily result in change of sample volume location and loss of Doppler signal.

In Chapter 5, the Capon spectral estimator was used to estimate the spectrograms using CFI data sets. This approach can provide triplex display from a duplex acquisition. The Capon estimated spectrograms were evaluated in terms of spectral broadening by performing string phantom experiments, where the string velocity, beam-to-flow angle and the OW length were altered to inspect the broadening effect with different scenarios. In addition, the significance of this effect on the calculation of Doppler indices was investigated. Further, *in vivo* acquisitions from the umbilical artery, carotid artery and aorta were performed. Results from using the data adaptive approach and conventional CFI acquisition are compared to spectrograms estimated by a commercial scanner in only PW-Doppler mode.

The results showed that smooth maximum velocity envelopes could be achieved on the spectra estimated using packet data by only utilizing 2-D spatial averaging. Similar Doppler index values were achieved using the high quality PW-Doppler spectrograms and the CFI Capon estimated spectra. Maximum velocities could be extracted without significant performance degradation using the Capon estimator. The ROI had to be restricted to obtain frame rates around 100 Hz, however, similar quantitative result could be achieved by downsampling the envelope to 52 Hz for an umbilical artery recording.

*This work resulted in the paper "*Quantitative Doppler Analysis using Conventional Color Flow Imaging Acquisitions*", submitted to IEEE Transactions on Ultrasonics, Ferroelectrics and Frequency Control, and presented here in its current form. The candidate was the main contributor to all aspects of the work, except for the data acquisition, for which MD Eva Tegnander, Dr. Tonje Dobrowen Fredriksen, Lars Mølgaard Saxhaug and Morten Smedsrud Wigen are gratefully acknowledged.*

1.5.4 Decreasing OW length and spectral broadening

As mentioned in section 1.5.2, the spectral broadening due to limited observation time of the scatterers, causes overestimation in maximum velocity measurements. In 1995, a method called velocity matched spectrum analysis [50] was proposed to alleviate the broadening problem by tracking the scatterers in space to increase the observation time. However, the tracking was performed only in radial direction which limited the achievable reduction in spectral broadening. Parallel beamforming made it possible to further develop this method into a 2-D tracking method to further increase the observation window and reduce the spectral broadening. The 2-D tracking Doppler

method [51] requires OW lengths of around 30 time samples to achieve acceptable frequency resolution. As the time samples are extracted by tracking the scatterers, the tracking length increases with increased scatterer velocity. In the case of flow fields with high acceleration or complex flow patterns, the stationary assumption will often be violated for such tracking lengths.

In Chapter 6, an estimator was proposed that combined the 2-D tracking Doppler and the power spectral Capon estimator to reduce the spectral broadening as well as the time window that is needed to achieve this reduction. The proposed method was compared to the 2-D tracking Doppler, the Capon and the Welch's estimators using *in vivo* acquisition from the CCA and flow phantom experiments. It was shown that the proposed method could achieve a 66% decrease in spectral broadening compared to the 2-D tracking Doppler method using OW length of 16 samples.

*This work is described in the paper "*Data Adaptive 2-D Tracking Doppler*", published in 2016 IEEE International Ultrasonics Symposium (IUS), and presented here in its published form. The candidate was the main contributor to all aspects of the work, except for the data acquisition, for which Dr. Tonje Dobrowen Fredriksen is gratefully acknowledged.*

1.6 Discussion

This work investigated the possibility of increasing the applicability of packet based Doppler imaging, for improved quantitative analysis and efficient work flow, in particular for inexperienced users. The focus has been to allow for operation on low/mid-end ultrasound systems however the same advantages are valid for high-end scanners. The proposed methods were evaluated through simulations and phantom experiments and the clinical feasibility was investigated through *in vivo* recordings with clinical ultrasound scanners.

Improving the estimation of mean velocities in color flow imaging

One of the main objectives of this work was to improve the imaging possibilities with conventional scanning schemes; thus, all proposed methods were evaluated using conventional color flow imaging ensemble lengths. In Chapter 3, it was investigated whether improved spectral resolution and side lobe suppression provided by adaptive spectral estimators could expand the velocity span estimated without bias in CFI. The Capon and the BIAA estimator could reduce the bias in the transition band of the polynomial regression filters. However, a higher standard deviation was observed for the BIAA method for short OW lengths and low SNR. The Capon estimator, however, could reduce the bias and standard deviation for low ensemble lengths and low SNR, e.g., packet size $8-16$ and 5 dB SNR, compared to the autocorrelation method with a suitable order polynomial regression filter. The clutter isolation is affected by the frequency resolution of the estimates. It was observed that very small packet sizes, e.g.

6, did not provide sufficient resolution for clutter isolation, especially in case of high clutter-to-blood-signal ratios. A broad range of velocities were corrupted which shows that the method is not applicable in this setting. High clutter-to-blood-signal ratio is also a problem for larger packet sizes, e.g. 12, due to increased side lobe levels, and results in increased cut-off velocity. However, the severity is not to the same extent and the method could be still applicable.

The short OW length resulting from the discontinuous acquisition hinders the possibility of temporal averaging to reduce spectral variance. As the acquisition schemes were packet based, employment of temporal averaging would reduce the frequency resolution. In its formulation, the APES method has temporal averaging to estimate the interference matrix which reduces the effective OW length. Therefore, the APES method was not investigated in this work. For the other methods, however, the temporal averaging was compensated by 2-D spatial averaging. The averaging region size must be chosen carefully: to avoid an ill conditioned covariance matrix, the size must not be too small; to adhere to stationary assumptions and to be applicable also for smaller vessels, it must not be too large. The need for spatial averaging increases with increased packet size in the proposed method in order to avoid ill-conditioned matrices. Also therefore it is not desired to keep the OW long. However, it was observed that, the performance improvement of the proposed method with the Capon estimator is marginal above the conventionally used packet sizes, e.g., > 16. Therefore the aforementioned trade-off did not affect the mean velocity estimation significantly for its intended use.

A drawback of this method is that the cut-off of the filter was chosen manually. However, this can be seen as a common problem with conventional filters as the filter order is chosen manually as well. In addition, improvement with the Capon estimator is seen in the presence of low blood velocities. The conventional and the proposed methods provided similar results for large packet sizes and high SNR, e.g., packet size 16 and 20 dB SNR.

Spectral estimation using color flow imaging data

Chapter 5 presented a method that estimates velocity spectra using CFI data to avoid additional data acquisition for PW-Doppler, and further provide future opportunities for simultaneous display of multiple spectra. It was previously suggested that spectral estimation with the Capon estimator in this setting could yield estimates with sufficient quality [47]. This work investigated the effect of beam-to-flow angle, OW length and the limitations brought by different data acquisition settings employed in CFI.

The estimator could decrease broadening and yield comparable results to the conventional Welch's method with longer OW length (64) for low velocities, e.g., 20 cm/s. However, the gain is lost when the correlation length of the signal is decreased, which was the case for high velocities and large beam-to-flow angles. In this case, Welch's method outperformed the Capon estimator (OW length 16), e.g. for 60 cm/s and 60°. In addition, Welch's method provided spectrograms with better contrast. What could be achieved with Welch's method with short OW lengths was also investigated. The need for prior clutter filtering reduces the effective OW length

even further and the method provided maximum velocity estimates with significant bias. This shows that the concept is only possible using more advanced spectral estimators.

The short transmit pulses employed in CFI increases the bandwidth of the pulse and results in increased spectral broadening when used for power spectrum estimation. However, the *in vivo* results recorded from the uterine artery, aorta and common carotid artery showed that the Capon estimator could yield spectra which showed similar properties with the continuous PW-Doppler spectra estimated on the commercial scanner. Comparable peak velocities could be achieved; however, the estimations had higher variance. Results suggest that the Capon estimator can be used for spectral estimation with conventional CFI scanning schemes without significant performance loss. However, a research using different flow patterns is needed before a generalization of the results can be made.

Advantages of providing the user with an improved triplex mode ultrasound where quantitative analysis can be done on arbitrary spatial locations simultaneously are potentially many. Providing spectrograms simultaneously can support more detailed analysis. For instance, in the case of stenosis, velocity spectra from different regions, e.g., pre-stenosis and mid-stenosis regions, can be compared. Another advantage is that the user does not have to switch between modes which is cumbersome and can be especially difficult for the inexperienced user. The analysis can be done retrospectively once the required seconds of data are recorded. Moreover, the Doppler indices such as resistivity or pulsatility index can be estimated automatically in all spatial points and can be provided to the user using color coding, i.e., for a specific Doppler index, the index values are color mapped and displayed on a B-mode image. This avoids the index value's dependence on the sample volume location and a spatially averaged index value can be acquired in addition to time averaging. As the maximum velocities are often used in diagnosis, maximum velocity or peak systolic velocity (PSV) maps can also be obtained and displayed as color mapped images.

It is difficult to assess the influence of the clutter filter by solely investigating the color flow image. Estimation of velocity spectra gives a visual feedback on the clutter filtering effect as well. It is easier to spot the clutter leakage from the filter or removal of the low velocity blood signals. Additionally, the spectrograms can more easily be baseline shifted in order to avoid aliasing in the color flow image.

It is known, and also shown in this work, that the beam-to-flow angle affects the spectral broadening and can cause severe overestimation of maximum velocities. Therefore the user has to be careful when interpreting the results as the beam-to-flow angles may be different for different locations in a 2-D color flow image, and a direct comparison of the spectrograms may lead to inaccurate measurement. To get reliable results, the user must ensure a beam-to-flow angle smaller than 60°.

Spectral envelope extraction with CFI data

Quantitative analysis done with PW-Doppler usually requires delineation of spectrograms. Maximum velocity estimation as observed by the naked eye ignores the effect of spectral broadening and can be affected by the dynamic range and gain settings

on the scanner. Chapter 4 investigated the performance of a proposed algorithm that aims to estimate the maximum velocities robustly and eliminate false detections to provide smooth and reproducible spectral envelopes.

Combining the Signal Noise Slope Intersection (SNSI) and an altered version of the Geometric Method (GM) produced lower variance envelopes than either of the methods separately. This was due to the replacement of predefined values employed in the SNSI method with the dynamically estimated values, similar to estimations included in the GM, and further discarding the false and low quality detections.

First, in Chapter 4, the method was evaluated on the spectrograms generated with the fast Fourier transform (FFT) algorithm with relatively long (64) OW length. String phantom, simulation and *in vivo* results showed low sensitivity to SNR and variance in the power spectrum. This was also supported by the results of the Doppler index calculation. It shows that the algorithm can potentially be used for automated measurement of clinical indices, e.g., pulsatility index.

In the following work presented in Chapter 5, the algorithm was used on the spectrograms generated with the power spectral Capon estimator with short the OW lengths, i.e., 8-16 samples as typically used in CFI. The algorithm could provide smooth spectral envelopes with relatively low time resolution spectrograms. Even though the main focus of the work was on how the Capon estimator performed with short OW lengths in terms of broadening, it has also shown how the envelope estimator works in more challenging scenarios.

One of the challenges of this approach is the lower frame rate of the CFI mode. The frame rate directly determines the time resolution of the estimated spectrograms. Depending on the depth and the dimensions of the ROI, the attainable frame rates can be as low as 20 Hz in conventional CFI. The multi-line acquisition approach was used in *in vivo* recordings in order to increase the frame rate in this work. The acquisition started with a large image in order to choose specifically the main interest region and later the ROI box was narrowed down. This was done to increase the frame rate. Frame rates over 100 Hz could be obtained for depths around 12 cm. Based on these data, it was investigated whether it was possible to decrease the frame rate and maintain the quantitative analysis quality. It was seen that the frame rate could be reduced to half (52 Hz) without affecting the qualitative results significantly for normal umbilical artery flow, e.g., PSV and PI. However decreasing the frame rate further resulted in more severe underestimation of peak velocities and the low temporal resolution caused block-like artefacts in the spectrogram. These observations are valid for a specific velocity profile and need further evaluation with different flow profiles for generalization. Flow profiles with higher accelerations may cause a faster deterioration in the analysis performance. An approach to increase the time resolution of spectrograms and spectral envelope could be stitching bins from different heart cycles. For instance, detected PSV and end diastolic velocity (EDV) can be used for aligning the spectral bins and a combined spectrogram can be generated with multiple heart cycles using with low time resolution spectrograms. However, this requires a stable heart rate and fixed relative position of the probe and the patient.

Decreasing the spectral broadening using short OWs

With both conventional PW-Doppler and the adaptive spectral estimation methods, the spectral broadening is inevitable, especially for large beam-to-flow angles and high blood velocities. Both the velocity matched spectrum and the 2-D tracking Doppler methods require relatively long (around 30 samples) OWs for improved frequency resolution. The tracking Capon method proposed in Chapter 6 could decrease the spectral broadening and the OW length needed for this reduction. This was achieved by filtering the time samples with a narrow band, data adaptive filter with center frequency around zero as opposed to summation of the time samples as done in 2-D tracking Doppler. This approach has been used in the power spectral Capon with filters with different center frequencies. However the improvement was seen mostly for low velocities since the observation length of the scatterers is limited. Decreased spectral broadening can facilitate better measurement by improving delineation of maximum velocities.

Decreasing the number of time samples also decreases the tracking length in space. Long OWs may violate the assumption of stationarity in space and time which increases the spectral broadening. Reduced OW length can make this method feasible with a conventional CFI acquisition where an MLA scheme is employed to cover a sufficiently large area to perform tracking in 2-D. It was shown that a tracking length of 0.8 cm was adequate to track scatterers up to 2 m/s when the PRF was 4 kHz. This was approximately half the length needed for the 2-D tracking Doppler to achieve similar results. This would be the needed lateral length when the beam-to-flow angle is 90°. Even shorter lateral lengths can be used to track high velocities in case of smaller beam-to-flow angles, reducing the required number of parallel acquisition lines. The tracking length in time was 16 samples which is within the limits of conventional CFI packet size.

Applicability of the proposed methods

In Chapter 3, the estimator proposed for mean velocity estimation requires estimation of spectra for each pixel in the color flow image. Real-time implementation of such a system is not feasible yet for a low-cost ultrasound scanner, especially for large ROIs. The same applies for the simultaneous display of spectrograms from different locations. The power spectral Capon estimator is more computationally demanding than the conventional Welch and the autocorrelation methods. This is due to the matrix inversion employed in the estimation. The BIAA is even more computationally demanding as it is an iterative algorithm requiring several matrix inversions for each output estimate. Offline post-processing may be a short-term solution, with retrospective analysis of the Doppler data providing a familiar work flow for the sonographer. The user can be provided with the conventionally generated color flow image for data acquisition and the user can record the required duration of data for analysis. A system where the methods proposed in chapters 3, 4 and 5 are used together for qualitative and quantitative analysis would require estimation of spectrograms only once at each location. The estimated spectra can be used

for mean velocity estimation, spectral estimation and display of maximum velocity and automatic Doppler index value maps. To achieve sufficient frame rates, all the proposed methods in this work can utilize broad beams and multi-line acquisition. Hardware and processing power required for beamforming all channels simultaneously is now becoming standard on high-end systems, but not yet in low-cost systems. The beamforming demands can be alleviated by using limited number of parallel receive lines.

1.7 Concluding remarks and future work

This work aimed at providing methods to increase the quality and quantitative abilities of conventional CFI. This thesis work has contributed to the research in adaptive spectral estimators in medical ultrasound by providing more insight into how data adaptive spectral estimators (Capon, BIAA) would work with short OW lengths for qualitative and quantitative Doppler analysis.

It was shown that the power spectral Capon estimator could improve the estimation of low blood velocities in CFI. In addition, the estimator could provide spectral estimates with sufficient frequency resolution and side lobe suppression using packet based data acquisitions. The estimates were used for quantitative assessment of blood flow and it was shown that useful quantitative parameters, such as PSV and EDVs, could be extracted.

The proposed methods are computationally more demanding than the conventional estimation methods. However, increasing processing power of the processing units can make the real time implementation of these methods feasible on low-cost scanners in the future. They could potentially provide a more efficient work flow and be used for automation of the measurements, and to overcome the intra/inter-observer variability of the measurements, especially for inexperienced users.

The proposed mean velocity estimation method was only evaluated using continuous plane wave acquisitions in order to use the same acquisitions with different OW lengths. The method should be assessed further with clinically acquired CFI data to investigate the impact of CFI transmit settings in mean velocity estimation. Maximum velocity estimation using CFI data needs further evaluation using different types of flow conditions. Eventually, a system where the proposed quantitative and qualitative analysis methods are implemented should be tested clinically, and also then with inexperienced users and students who are being introduced to medical ultrasound. Further research should be made in order to investigate the pros and cons of such a system and whether it can affect the diagnostic ultrasound learning curve positively.

A maximum velocity and spectral envelope estimation method was proposed and was shown to work with relatively low time resolution spectrograms and with different spectral estimation methods. It had low sensitivity to SNR and variance in the Doppler index calculation was low. The results suggest that it can potentially be used in a clinical setting for automatic envelope extraction and index calculation.

The tracking Capon method was able to alleviate the spectral broadening in PW-Doppler systems and could improve frequency resolution and decrease the OW length.

This potentially increases the applicability of tracking-based methods, such as in fields with complex flow patterns. The ultimate goal of the work is to implement the method using CFI data recorded with a limited number of acquisition lines. Therefore, a feasibility study should be performed with clinically recorded CFI data with different applications, including flow fields with high velocities.

Even though it is suggested here that the methods can help to provide automatic measurements, further steps have to be taken for this to be realized. The cut-off velocity of the proposed threshold filter used with the Capon estimator must be set adaptive to the clutter characteristics for full automation. An automatic baseline shift method must to be employed in the spectral envelope estimation method to avoid aliasing in the spectrograms. Finally, further work should include a method that can estimate the beam-to-flow angle automatically for the tracking Capon method.

1.8 Publication list

In addition to published and unpublished manuscripts included in this thesis, written and oral contributions have been made to international conferences. Below, a list of the material to which the candidate has been a contributor to is presented.

Papers included in the thesis

1. **Yücel Karabiyik**, Ingvild Kinn Ekroll, Sturla H. Eik-Nes, Jørgen Avdal, and Lasse Løvstakken. "Adaptive Spectral Estimation Methods in Color Flow Imaging", *IEEE transactions on ultrasonics, ferroelectrics, and frequency control 63, no. 11 (2016): 1839-1851.*

2. Aditi Kathpalia, **Yücel Karabiyik**, Sturla H. Eik-Nes, Eva Tegnander, Ingvild Kinn Ekroll, Gabriel Kiss, and Hans Torp. "Adaptive Spectral Envelope Estimation for Doppler Ultrasound", *IEEE transactions on ultrasonics, ferroelectrics, and frequency control 63, no. 11 (2016): 1825-1838.*

3. **Yücel Karabiyik**, Ingvild Kinn Ekroll, Sturla Eik-Nes, and Lasse Løvstakken. "Quantitative Doppler Analysis using Conventional Color Flow Imaging Acquisitions.", submitted for review to *IEEE transactions on ultrasonics, ferroelectrics, and frequency control.*

4. **Yücel Karabiyik**, Jørgen Avdal, Ingvild Kinn Ekroll, Hans Torp and Lasse Løvstakken. "Adaptive Spectral Estimation Methods in Color Flow Imaging", *Ultrasonics Symposium (IUS), 2016 IEEE International, pp. 1-4. IEEE, 2016.*

Conference proceedings

1. Aditi Kathpalia, **Yücel Karabiyik**, Bente Simensen, Eva Tegnander, Sturla Eik-Nes, Hans Torp, Ingvild Kinn Ekroll, and Gabriel Kiss. "A robust Doppler spectral envelope detection technique for automated blood flow measurements.", *Ultrasonics Symposium (IUS), 2015 IEEE International, pp. 1-4. IEEE, 2015.*

2. **Yücel Karabiyik**, Jørgen Avdal, Ingvild Kinn Ekroll, Hans Torp and Lasse Løvstakken. "Data Adaptive 2-D Tracking Doppler", *Ultrasonics Symposium (IUS), 2016 IEEE International, pp. 1-4. IEEE, 2016.*

Presentations and posters

1. **Yücel Karabiyik**, Ingvild Kinn Ekroll, Sturla H. Eik-Nes, Jørgen Avdal, Hans Torp, and Lasse Løvstakken. "Adaptive signal processing for vector velocity imaging", *Artimino Conference on Medical Ultrasound Technology, 2015*

2. **Yücel Karabiyik**, Ingvild Kinn Ekroll, Sturla H. Eik-Nes, Jørgen Avdal, Hans Torp, and Lasse Løvstakken. "Adaptive Spectral Estimation Methods in Color Flow Imaging", *2015 IEEE International Ultrasonics Symposium*

3. Aditi Kathpalia, **Yücel Karabiyik**, Bente Simensen, Eva Tegnander, Sturla Eik-Nes, Hans Torp, Ingvild Kinn Ekroll, and Gabriel Kiss. "A robust Doppler spectral envelope detection technique for automated blood flow measurements.", *2015 IEEE International Ultrasonics Symposium*

4. **Yücel Karabiyik**, Jørgen Avdal, Ingvild Kinn Ekroll, Hans Torp and Lasse Løvstakken. "Data Adaptive 2-D Tracking Doppler", *2016 IEEE International Ultrasonics Symposium*

References

[1] T. L. Szabo, *Diagnostic ultrasound imaging: inside out*. Academic Press, 2004.

[2] L. A. French, J. J. Wild, and D. Neal, "Detection of cerebral tumors by ultrasonic pulses. Pilot studies on postmortem material," *Cancer*, vol. 3, no. 4, pp. 705–708, 1950.

[3] J. J. Wild, "The use of ultrasonic pulses for the measurement of biologic tissues and the detection of tissue density changes," *Surgery*, 1950.

[4] J. Wild and J. M. Reid, "The effects of biological tissues on 15-mc pulsed ultrasound," *The Journal of the Acoustical Society of America*, vol. 25, no. 2, pp. 270–280, 1953.

[5] W. D. O'Brien Jr, "Assessing the risks for modern diagnostic ultrasound imaging," *Japanese journal of applied physics*, vol. 37, no. 5S, p. 2781, 1998.

[6] J. J. Wild and J. M. Reid, "Application of echo-ranging techniques to the determination of structure of biological tissues.," *Science (New York, NY)*, vol. 115, no. 2983, pp. 226–230, 1952.

[7] J. H. Holmes, D. H. Howry, G. J. Posakony, and C. R. Cushman, "The ultrasonic visualization of soft tissue structures in the human body," *Transactions of the American Clinical and Climatological Association*, vol. 66, p. 208, 1955.

[8] I. Edler and C. H. Hertz, "The use of ultrasonic reflectoscope for the continuous recording of the movements of heart walls.," *Clinical physiology and functional imaging*, vol. 24, no. 3, pp. 118–136, 2004.

[9] S. Singh and A. Goyal, "The origin of echocardiography," *Tex Heart Inst J*, vol. 34, no. 4, pp. 431–438, 2007.

[10] S. Satomura, "Ultrasonic Doppler method for the inspection of cardiac functions," *The Journal of the Acoustical Society of America*, vol. 29, no. 11, pp. 1181–1185, 1957.

[11] B. Sigel, "A brief history of Doppler ultrasound in the diagnosis of peripheral vascular disease," *Ultrasound in medicine & biology*, vol. 24, no. 2, pp. 169–176, 1998.

[12] I. Donald, J. Macvicar, and T. Brown, "Investigation of abdominal masses by pulsed ultrasound," *The Lancet*, vol. 271, no. 7032, pp. 1188–1195, 1958.

[13] P. N. Wells, "Milestones in cardiac ultrasound: echoes from the past," *The International Journal of Cardiac Imaging*, vol. 9, pp. 3–9, 1993.

[14] K. Namekawa, "Real time blood flow imaging system utilizing auto-correlation techniques," *Ultrasound Med. Biol., Suppl.*, vol. 2, p. 203, 1983.

[15] C. Kasai, K. Namekawa, A. Koyano, R. Omoto, *et al.*, "Real-time two-dimensional blood flow imaging using an autocorrelation technique," *IEEE Trans. Sonics Ultrason*, vol. 32, no. 3, pp. 458–464, 1985.

[16] P. Munk and J. A. Jensen, "A new approach for the estimation of the axial velocity using ultrasound," *Ultrasonics*, vol. 37, no. 10, pp. 661–665, 2000.

[17] J. Bercoff, G. Montaldo, T. Loupas, D. Savery, F. Mézière, M. Fink, and M. Tanter, "Ultrafast compound Doppler imaging: Providing full blood flow characterization," *IEEE transactions on ultrasonics, ferroelectrics, and frequency control*, vol. 58, no. 1, 2011.

[18] B. Delannoy, R. Torguet, C. Bruneel, E. Bridoux, J. Rouvaen, and H. Lasota, "Acoustical image reconstruction in parallel-processing analog electronic systems," *Journal of Applied Physics*, vol. 50, no. 5, pp. 3153–3159, 1979.

[19] M. Couade, M. Pernot, M. Tanter, E. Messas, A. Bel, M. Ba, A.-A. Hagège, and M. Fink, "Ultrafast imaging of the heart using circular wave synthetic imaging with phased arrays," in *Ultrasonics Symposium (IUS), 2009 IEEE International*, pp. 515–518, IEEE, 2009.

[20] J. A. Jensen, S. I. Nikolov, K. L. Gammelmark, and M. H. Pedersen, "Synthetic aperture ultrasound imaging," *Ultrasonics*, vol. 44, pp. e5–e15, 2006.

[21] L. Bohs, B. Geiman, M. Anderson, S. Gebhart, and G. Trahey, "Speckle tracking for multi-dimensional flow estimation," *Ultrasonics*, vol. 38, no. 1, pp. 369–375, 2000.

[22] A. Pastorelli, G. Torricelli, M. Scabia, E. Biagi, and L. Masotti, "A real-time 2-D vector Doppler system for clinical experimentation," *IEEE Transactions on Medical Imaging*, vol. 27, pp. 1515–1524, Oct 2008.

[23] B. Dunmire, K. Beach, K. Labs, M. Plett, and D. Strandness, "Cross-beam vector Doppler ultrasound for angle-independent velocity measurements," *Ultrasound in medicine & biology*, vol. 26, no. 8, pp. 1213–1235, 2000.

[24] T. Misaridis and J. A. Jensen, "Use of modulated excitation signals in medical ultrasound. Part I: Basic concepts and expected benefits," *IEEE transactions on ultrasonics, ferroelectrics, and frequency control*, vol. 52, no. 2, pp. 177–191, 2005.

[25] M. Tanter and M. Fink, "Ultrafast imaging in biomedical ultrasound," *IEEE transactions on ultrasonics, ferroelectrics, and frequency control*, vol. 61, no. 1, pp. 102–119, 2014.

[26] Unicef *et al.*, "Trends in maternal mortality: 1990 to 2013," *World Bank Publications*, 2014.

[27] R. Horton and U. Samarasekera, "Stillbirths: ending an epidemic of grief," *The Lancet*, vol. 387, no. 10018, pp. 515–516, 2016.

[28] I. UNFPA, "WHO: The state of the worlds midwifery 2014: A universal pathway. a women's right to health," *United Nations Population Fund, New York*, 2014.

[29] S. Sippel, K. Muruganandan, A. Levine, and S. Shah, "Review article: use of ultrasound in the developing world," *International journal of emergency medicine*, vol. 4, no. 1, p. 72, 2011.

[30] W. H. Organization *et al.*, "Training in diagnostic ultrasound: essentials, principles and standards: report of a WHO study group," 1998.

[31] M. Messawa, E. Maajeni, M. H. Daghistani, A. Ayaz, and M. U. Farooq, "The role of Doppler ultrasound in high risk pregnancy: A comparative study," *Nigerian medical journal: journal of the Nigeria Medical Association*, vol. 53, no. 3, p. 116, 2012.

[32] L. Say, D. Chou, A. Gemmill, Ö. Tunçalp, A.-B. Moller, J. Daniels, A. M. Gülmezoglu, M. Temmerman, and L. Alkema, "Global causes of maternal death: a WHO systematic analysis," *The Lancet Global Health*, vol. 2, no. 6, pp. e323–e333, 2014.

[33] S. P. Shah, H. Epino, G. Bukhman, I. Umulisa, J. Dushimiyimana, A. Reichman, and V. E. Noble, "Impact of the introduction of ultrasound services in a limited resource setting: rural Rwanda 2008," *BMC international health and human rights*, vol. 9, no. 1, p. 4, 2009.

[34] S. Kotlyar, C. L. Moore, *et al.*, "Assessing the utility of ultrasound in Liberia," *Journal of emergencies, trauma, and shock*, vol. 1, no. 1, p. 10, 2008.

[35] M. Blaivas, W. Kuhn, B. Reynolds, and L. Brannam, "Change in differential diagnosis and patient management with the use of portable ultrasound in a remote setting," *Wilderness & environmental medicine*, vol. 16, no. 1, pp. 38–41, 2005.

[36] K. Stanton and L. Mwanri, "Global maternal and child health outcomes: the role of obstetric ultrasound in low resource settings," *World Journal of Preventive Medicine*, vol. 1, no. 3, pp. 22–29, 2013.

[37] C. B. Benson and P. M. Doubilet, "The history of imaging in obstetrics," *Radiology*, vol. 273, no. 2S, pp. S92–S110, 2014.

[38] M. E. Allam and J. F. Greenleaf, "Isomorphism between pulsed-wave Doppler ultrasound and direction-of-arrival estimation. I. Basic principles," *IEEE transactions on ultrasonics, ferroelectrics, and frequency control*, vol. 43, no. 5, pp. 911–922, 1996.

[39] J. Capon, "High-resolution frequency-wavenumber spectrum analysis," *Proceedings of the IEEE*, vol. 57, no. 8, pp. 1408–1418, 1969.

[40] R. Schmidt, "Multiple emitter location and signal parameter estimation," *IEEE transactions on antennas and propagation*, vol. 34, no. 3, pp. 276–280, 1986.

[41] M. E. Allam, R. R. Kinnick, and J. F. Greenleaf, "Isomorphism between pulsed-wave Doppler ultrasound and direction-of-arrival estimation. II. Experimental results," *IEEE transactions on ultrasonics, ferroelectrics, and frequency control*, vol. 43, no. 5, pp. 923–935, 1996.

[42] F. Gran, A. Jakobsson, and J. A. Jensen, "Adaptive spectral Doppler estimation," *IEEE transactions on ultrasonics, ferroelectrics, and frequency control*, vol. 56, no. 4, 2009.

[43] K. L. Hansen, F. Gran, M. M. Pedersen, I. K. Holfort, J. A. Jensen, and M. B. Nielsen, "In-vivo validation of fast spectral velocity estimation techniques," *Ultrasonics*, vol. 50, no. 1, pp. 52–59, 2010.

[44] E. Gudmundson, A. Jakobsson, J. A. Jensen, and P. Stoica, "Blood velocity estimation using ultrasound and spectral iterative adaptive approaches," *Signal Processing*, vol. 91, no. 5, pp. 1275–1283, 2011.

[45] S. Ricci, "Adaptive spectral estimators for fast flow-profile detection," *IEEE transactions on ultrasonics, ferroelectrics, and frequency control*, vol. 60, no. 2, pp. 421–427, 2013.

[46] I. K. Ekroll, H. Torp, and L. Lovstakken, "Spectral Doppler estimation utilizing 2-D spatial information and adaptive signal processing," *IEEE transactions on ultrasonics, ferroelectrics, and frequency control*, vol. 59, no. 6, pp. 1182–1192, 2012.

[47] I. K. Ekroll, T. Dahl, H. Torp, and L. Løvstakken, "Combined vector velocity and spectral Doppler imaging for improved imaging of complex blood flow in the carotid arteries," *Ultrasound in medicine & biology*, vol. 40, no. 7, pp. 1629–1640, 2014.

[48] A. Steinman, J. Tavakkoli, J. Myers, R. Cobbold, and K. Johnston, "A new approach for determining maximum frequency in clinical Doppler ultrasound spectral estimates," in *Engineering in Medicine and Biology Society, 2000. Proceedings of the 22nd Annual International Conference of the IEEE*, vol. 4, pp. 2640–2643, IEEE, 2000.

[49] K. Marasek and A. Nowicki, "Comparison of the performance of three maximum Doppler frequency estimators coupled with different spectral estimation methods," *Ultrasound in medicine & biology*, vol. 20, no. 7, pp. 629–638, 1994.

[50] H. Torp and K. Kristoffersen, "Velocity matched spectrum analysis: A new method for suppressing velocity ambiguity in pulsed-wave Doppler," *Ultrasound in medicine & biology*, vol. 21, no. 7, pp. 937–944, 1995.

[51] T. D. Fredriksen, I. K. Ekroll, L. Lovstakken, and H. Torp, "2-D tracking Doppler: a new method to limit spectral broadening in pulsed wave Doppler," *IEEE transactions on ultrasonics, ferroelectrics, and frequency control*, vol. 60, no. 9, pp. 1896–1905, 2013.

Chapter 2

Background

This chapter provides the background material that consists of brief presentation of the methods that have been used throughout this work or methods that will give the foundation for better understanding this work. Please refer to [1–6] and the references given in each section for more thorough description of the methods. In addition, a small discussion on importance of CFI and PW-Doppler in diagnosis is given at the end of this chapter.

2.1 Medical ultrasound imaging

Sound waves are mechanical waves that are transmitted through pressure changes in a medium. The compressibility and density differences between different mediums cause reflection or scattering when the wave travels. Transducers with piezoelectric elements convert the applied electrical signals into ultrasound waves for transmission and the echoes received by the transducer are converted to electrical signals by expansion and contraction of the elements. The time difference between the transmission of a wave and receiving the backscattered echo can be used for determination of the distances of interfaces between different mediums from the transducer using the following relation

$$z = \frac{ct}{2}, \tag{2.1}$$

where t is the time difference and c is the speed of sound and assumed to be constant. This technique is referred to as echo ranging or pulse-echo technique.

Today, most commercial ultrasound scanners employ array of transducers for transmission of ultrasound waves [4]. This is done to achieve focusing and steering of ultrasound waves by creating time delays between each element and applying different weighting. The sound waves are attenuated by the medium depending on the frequency of the wave and the medium properties. High frequency ultrasound waves are attenuated more and therefore the depth of penetration is limited. Focusing increases the intensity of the ultrasound wave at the focus and deeper structures can be imaged. The steering of the waves to different directions increases the field of view (FOV) and objects outside the transducer aperture extents can be imaged [7].

2.2 Data acquisition

In conventional ultrasound scanners, the image generation is done by transmitting focused ultrasound waves and generating one line of the image per transmit. This approach has advantages such as high signal-to-noise ratio (SNR) and good resolution, however, the attainable frame rates is limited by the number of lines needed to form the image and the propagation velocity of the ultrasound wave. Alternative approaches have been proposed to increase the frame rate at the expense of SNR and resolution loss such as synthetic aperture [8,9], diverging wave [10,11] and plane wave imaging [12–14]. Here, the focused transmissions, multi line acquisition (MLA) and plane wave imaging schemes are presented briefly as they are utilized in this work.

2.2.1 Line-by-line acquisition

In this approach, focused transmissions are used for generation of each line in the image. The transmit and receive lines are aligned to increase the SNR and resolution. Focusing of the beam is usually obtained by applying different delay times for each element of the transducer, however it may also be obtained by placing the elements in curve or using an acoustic lens [15]. Depending on the application and the transducer type, the beam can be steered to different directions or a group of transducer elements (sub-aperture) can be used to construct the image line-by-line.

The transmit beam characteristics are dependent on the transmit aperture size, the transmit frequency, the pulse length, the focusing depth and the medium properties. The axial resolution is proportional to the pulse length where pulse length is given by

$$L_p = N_{cycles}\lambda, \tag{2.2}$$

where N_{cycles} is the number of cycles that the transmit signal contains and λ is the wavelength. The lateral resolution is determined by the beam width which defined as

$$D_f = F\lambda/D = F_{\#}\lambda. \tag{2.3}$$

D_f is the effective boundaries of the ultrasound beam at the focus, which is the distance from the beam axis to a -3 dB drop in pressure amplitude, F is the focus distance from the transducer, D is the size of the aperture used and $F_{\#}$ is the ratio of the focus depth to aperture size and referred to as F-number. When both transmit and receive focusing is applied, the two-way $F_{\#}$ is given by

$$F_{\#txrx} = (1/F_{\#tx} + 1/F_{\#rx})^{-1}, \tag{2.4}$$

where $F_{\#tx}$ and $F_{\#rx}$ are the F-numbers on transmit and receive respectively.

2.2.2 Parallel beamforming

Parallel beamforming approaches employ broader transmit beams than that are used in focused imaging. Several image lines can be generated per transmit due to the fact that a larger region is insonified. Multi line acquisition (MLA) approach usually employs

slightly defocused transmits and several receive lines are processed in parallel [13]. Currently, most commercial scanners provide 4 to 16 MLA with hardware beamforming while some research platforms provide more channels to be processed in parallel with software implementation. As the number of transmit beams is reduced in this approach, the frame rate and/or FOV can be increased. This is particularly needed for 3-D imaging as substantially more transmits are needed to acquire volumetric data [16].

In plane wave imaging, an unfocused beam is transmitted ($F \rightarrow \infty$) insonifying the whole ROI and all receive lines are generated in parallel [17]. As one image is generated for each transmit, the frame rates in kHz range can be obtained. The methods that are based on this approach are often referred to as ultrasfast ultrasound imaging. Both MLA and plane wave imaging methods come with the disadvantage of reduced resolution and SNR. It is possible to increase both by having overlapped transmissions and do coherent compounding [18] or using synthetic transmit beams [19]. Even though compounding increases the number of transmits for each image generation, the frame rate can still be substantially higher than line-by-line acquisition with acceptable image quality.

In addition to disadvantages stated above, the MLA method can introduce artefacts such as block-like effects [20] and bias when used for velocity estimation [21] and compounding of plane wave images also acts like low pass filtering and creates bias in velocity estimation [22].

Figure 2.1 shows an example of three imaging schemes where different number of receive lines generated for each transmit.

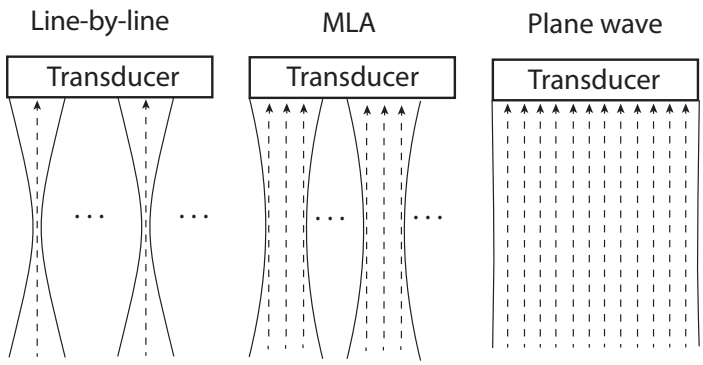

Figure 2.1: An example of receive lines generated with line-by-line imaging, MLA and plane wave imaging schemes. More receive lines can be generated for each transmit using parallel receive beamforming.

2.3 Color flow imaging

Medical ultrasound is one of the imaging modalities that is used widely for blood flow imaging. The mean blood velocities can be displayed in 2-D or 3-D along with the anatomy of the region being displayed as well as the spectrum of blood velocities in a spatial location in the ROI. The mean velocity inspection is usually done qualitatively for inspection of abnormal flow due to pathology, e.g., jet flow pattern caused by heart valve leakage.

Color flow imaging (CFI) displays mean velocities in the ROI combined with the anatomical information. Conventionally, packet based acquisitions are done for color flow image generation [23]. A number of consecutive pulses are transmitted for each line in the image with a given pulse repetition frequency (PRF). The time samples are extracted by sampling the returned echoes at spatial points within the ROI. Fig. 2.2 shows an example of data acquisition for CFI. The columns represent the transmit beams (b) which are sampled at different depths (r). Several emissions are performed for each beam location (along n) and the number of transmits is referred to as *packet size*.

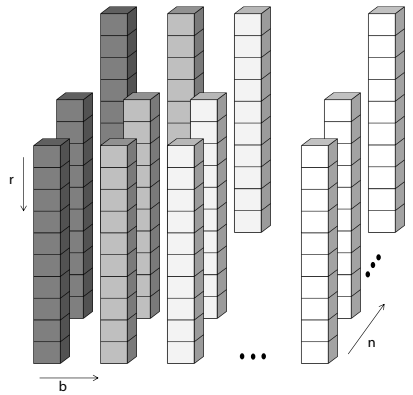

Figure 2.2: An example CFI data set. Each column represents a transmit beam (b) which are sampled at different depths (r). Several beams are transmitted for the same location (along n).

2.3.1 The autocorrelation estimator

Mean velocities are conventionally estimated by using the autocorrelation estimator [24]. The method estimates the mean velocity from the phase shifts between consecutive samples, i.e., lag 1. Let $x_{r,b}(n)$ denote time sample at location b in the lateral direction and r in the radial direction and emission n, after complex demodulation. The autocorrelation estimator with averaging in lateral and axial

dimensions is given by

$$\hat{R}(1) = \frac{1}{RB(N-1)} \sum_{r=1}^{R} \sum_{b=1}^{B} \sum_{n=1}^{N-1} x_{r,b}(n) x_{r,b}^{*}(n+1), \tag{2.5}$$

where $(.)^*$ denotes the complex conjugate, R and B are the number of spatial points utilized for spatial averaging in radial and lateral directions respectively, and N is the packet size or ensemble length. These terms are used interchangeably in this work. The mean velocity is then found by

$$\bar{v} = \frac{\angle \hat{R}(1) PRFc}{4\pi f_0}. \tag{2.6}$$

where f_0 is the transmit center frequency. Fig. 2.3 shows a color flow image from an obstetric acquisition. Anatomical structures such as uterine wall, placenta and fetal abdomen and extremities can be seen from the B-mode image while the mean blood velocity information within the umbilical artery is displayed using colors. The mean velocity estimates are done within the ROI where the boundaries are shown with the green curves. The colorbar in the top left corner shows the relation between the colors and velocity information.

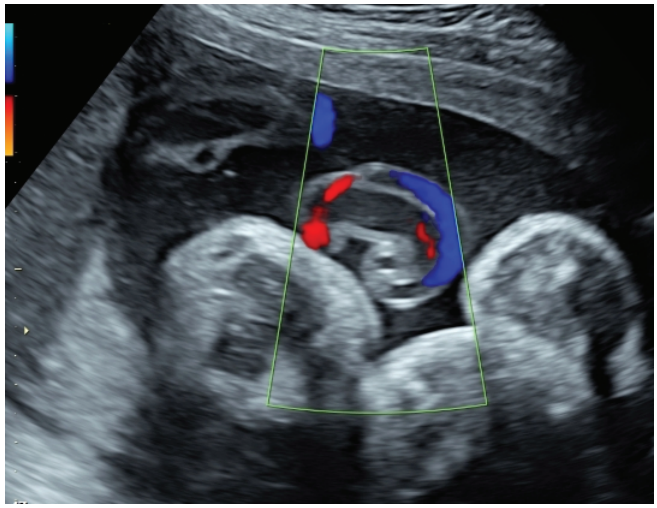

Figure 2.3: An example color flow image where anatomical structures can be seen in the B-mode image and the mean velocities are color mapped and overlaid on the B-mode image.

2.4 Spectral Doppler

Spectral Doppler displays the spectrum of velocities available in the location of interest. For this, a point in space is observed for a certain time interval to extract quantitative

information. In this section only PW-Doppler will be presented as it was utilized in this work for spectral estimation. Conventionally in PW-Doppler, focused pulses are transmitted in one direction with a certain PRF and the received echoes are sampled at the location of interest to extract time samples. The pulse length is relatively long to increase the sample volume size in order to observe scatterers in a larger region and increase the observation time and the SNR. The pulse length is around 10 cycles although it can be up to 40, while this is around 3 cycles for CFI [25]. The frequency resolution of the estimates depends heavily on the observation time. However, the observation time is limited by the non-stationary nature of the flow dynamics. The blood velocity is assumed to be stationary through the observation window (OW) length. This time interval is usually around 10 ms for arterial circulation while it can be around 5 ms for fetus imaging due to higher heart rates [26], however OW lengths less than 2 ms might be required to resolve details in the flow structure [27]. Therefore, short time frequency analysis is done on the extracted data and estimated frequency spectra are stacked together and displayed as 2-D sonograms with velocity on the vertical axis and time on the horizontal axis. These plots are also referred to as spectrograms.

The spectrograms are usually estimated using the Welch estimator [28]. It is a discrete Fourier transform (DFT) based method that can be implemented efficiently using the fast Fourier transform (FFT). The observation window is divided into sub-segments for temporal averaging to reduce the variance and each sub-segment is multiplied with a windowing/apodization function to reduce the side lobes. However, the observation window length required for robust and high frequency resolution estimates is relatively long, i.e., 64-128 time samples every 5 to 10 ms [29]. Therefore, the quality may degrade when used in duplex or triplex scanning modes due to time sharing. In addition, rapid changes in the flow may be obscured due to long observation windows, in other words, low time resolution. The assumption that the data is periodic outside the window is a limitation of DFT based methods as this assumption is not realistic [29, 30]. Therefore, estimating the spectra based on finite OW length results in spectral leakage and smoothing of the spectrum.

The fact that the spectral estimation is done on a windowed part of the signal is not the only contributor to the broadening of the spectrum in PW-Doppler. The ultrasound beam has limited sample volume dimensions depending on the pulse transmit parameters. A single scatterer passing through the sample volume can result in a spectrum containing band of velocities due to intrinsic spectral broadening. The broadening in the spectrum may be due to [31, 32]

- inhomogeneity of the ultrasound field resulting in amplitude fluctuations in the returned signal
- changes in the insonation angle throughout the sample volume
- change of scatterer velocities within the observation time or the velocity gradients within the sample volume
- finite duration of the scatterer observation time due to limited sample volume dimensions (transit time effect)

Advanced spectral estimation techniques

There exist many methods for spectral estimation which can provide improved spectra using fewer time samples than needed for Welch's method. A set of estimators which model the acquired data and estimate a set of parameters were shown to provide improved frequency resolution spectra using fewer time samples. The methods such as autoregressive (AR), moving average (MA), autoregressive moving average (ARMA) fall into this category and they are referred to as parametric spectral estimators [33–36]. The modelling approach eliminates the need for window functions and the assumption that the autocorrelation sequence is zero outside the window and these estimators have better statistical stability for short segments of signal. The disadvantages of these methods are that they are computationally more expensive and need a priori information to model the data.

Another approach to spectral estimation is generating filters for estimation of power for each frequency. These methods are referred to as filter bank methods. As the name implies, the methods are referred to as the data adaptive spectral estimation methods when the filters are data dependent. It is assumed that the power of the signal is constant over the passband of the filter and that the filter has gain one in the passband region and zero in the stop band region [5]. As the data is windowed with a finite length window, the generated filter orders are limited by the window length. Filters with sharp transition region have long impulse responses and as a result cannot be attained with short OW lengths. However, data adaptive methods design filters on different criteria to suppress the effect of interfering high power frequency components on the frequency of interest, i.e., passband region, and decrease the spectral leakage.

The velocity matched spectrum analysis method was proposed alleviate the transit time effect by tracking the scatterers [37]. The method can provide spectra with improved frequency resolution and lower side lobe levels and suppresses the velocity ambiguity in PW-Doppler. Focused transmissions are used in this method for data acquisition. Therefore, the tracking region is bounded by the transmit beam dimensions and the improvement is achieved for small beam-to-flow angles where the scatterers are tracked along the beam direction. In order to overcome this limitation, the extension of this method was proposed where the scatterers are observed in a 2-D region [38]. A plane wave acquisition scheme was used to evaluate the method and 4 fold reduction in spectral broadening was achieved for 0.82 m/s velocity compared to the Welch method. The tracking methods work well with flow fields where the flow is stationary in space and time within the observation region and time as well as in absence of out-of-plane movement. These assumptions are difficult to meet, especially when the tracking lengths are long.

Data adaptive filter-bank spectral estimators

This set of estimators generate narrow band, band pass filters for each frequency component to be estimated. The idea is to estimate the power spectrum using finite impulse response (FIR) filters that are designed specifically for the data to be filtered in order to generate high resolution spectra [6]. These methods are initially implemented for radar and later applied to medical ultrasound. The power spectral

Capon, the amplitude and phase estimation (APES) method and the blood iterative adaptive approach (BIAA) have been applied to spectral estimation in PW-Doppler successfully and were shown to outperform the Welch method [39–41]. These methods employ general linear estimators for each frequency estimate. The signal $x_{r,b}(n)$ can be modelled as sum of signals within a grid of velocities as [39, 42]

$$x_{r,b}(n) = \sum_{k=1}^{K} \alpha_{r,b}(k) e^{-j2\pi f_k n} + e_{r,b}(n), \tag{2.7}$$

where f_k is the normalized frequency with respect to PRF, $\alpha_{r,b}(k)$ is the complex amplitude of the signal at frequency f_k and $e_{r,b}(n)$ is zero mean complex white Gaussian noise with variance σ^2. The FIR filter, $\mathbf{h}$, generated for spectral estimation can be given as

$$h = [h_1 h_2 \cdots h_N]^T. \tag{2.8}$$

The filter output for frequency f_k can be written as

$$\hat{\alpha}_{r,b}(f_k) = \mathbf{h}_{f_k}^{\mathrm{H}} \mathbf{x}_{r,b}, \tag{2.9}$$

where $\mathbf{h}_{f_k}$ filter designed for estimation for frequency f_k and $\hat{\alpha}_{r,b}$ is the amplitude estimate, $\mathbf{x}_{r,b}$ is the ensemble with length N which can be expressed as $\mathbf{x}_{r,b} = [x_{r,b}(1)\ x_{r,b}(2)\ \cdots\ x_{r,b}(N)]^T$ and $(.)^{\mathrm{H}}$ represents the Hermitian transpose. The filters are designed to pass the frequency of interest undistorted which can be stated as

$$\mathbf{h}_{f_k}^{\mathrm{H}} \mathbf{a}_{f_k} = 1 \tag{2.10}$$

where $\mathbf{a}_{f_k} = [1\ e^{i2\pi f_k}\ \cdots\ e^{i2\pi f_k (N-1)}]^T$ is the Fourier vector. In addition, the Capon estimator minimizes the output power while the APES and the BIAA estimators minimize the power of the frequency components other than the frequency of interest. These formulations lead to a constrained minimization problem which can be stated as

$$\min_{\mathbf{h}_{f_k}} \quad \mathbf{h}_{f_k}^{\mathrm{H}} \mathbf{R} \mathbf{h}_{f_k} \quad s.t. \quad \mathbf{h}_{f_k}^{\mathrm{H}} \mathbf{a}_{f_k} = 1 \tag{2.11}$$

where $\mathbf{R}$ is the data covariance matrix for the Capon and the BIAA estimators whereas it is the covariance matrix of interfering signals and the thermal noise for the APES estimator. This minimization problem can be solved analytically by using Lagrange multipliers approach [43]. Let $O_F(\mathbf{h}_{f_k}, \gamma)$ represent the objective function

$$O_F(\mathbf{h}_{f_k}, \gamma) = \mathbf{h}_{f_k}^{\mathrm{H}} \mathbf{R} \mathbf{h}_{f_k} - \gamma(\mathbf{h}_{f_k}^{\mathrm{H}} \mathbf{a}_{f_k} - 1), \tag{2.12}$$

where γ is the Lagrange multiplier. The minimization of the objective function can be obtained by setting the gradient of $O_F(\mathbf{h}_{f_k}, \gamma)$ with respect to $\mathbf{h}_{f_k}^{\mathrm{H}}$ to zero

$$\nabla_{\mathbf{h}_{f_k}^{\mathrm{H}}} O_F(\mathbf{h}_{f_k}, \gamma) = \mathbf{R} \mathbf{h}_{f_k} - \gamma \mathbf{a}_{f_k} = 0. \tag{2.13}$$

Therefore,

$$\mathbf{h}_{f_k} = \gamma \mathbf{R}^{-1} \mathbf{a}_{f_k} \tag{2.14}$$

Later, the derivative of $O_F(\mathbf{h}_{f_k}, \gamma)$ with respect to γ is set to zero in order to find the value of the Lagrange multiplier

$$\frac{\partial O_F(\mathbf{h}_{f_k}, \gamma)}{\partial \gamma} = 1 - \mathbf{h}_{f_k}^{\mathrm{H}} \mathbf{a}_{f_k} \tag{2.15}$$

Substituting (2.14) into (2.15) and solving for γ yields:

$$\gamma = \frac{1}{\mathbf{a}_{f_k}^{\mathrm{H}} \mathbf{R}^{-1} \mathbf{a}_{f_k}} \tag{2.16}$$

Finally, substituting (2.16) into (2.14) gives:

$$\mathbf{h}_{f_k} = \frac{\mathbf{R}^{-1} \mathbf{a}_{f_k}}{\mathbf{a}_{f_k}^{\mathrm{H}} \mathbf{R}^{-1} \mathbf{a}_{f_k}} \tag{2.17}$$

The covariance matrix, $\mathbf{R}$ is estimated differently for each method. The following sections present the construction of covariance matrices and the estimation approaches for the previously mentioned three adaptive spectral estimators.

2.4.1 Power spectral Capon

The Capon estimator designs adaptive filters based on the criteria that the filter minimizes the output power and passes the frequency of interest undistorted which is represented by (2.10) [5, 44, 45]. The filter output power can be shown as

$$E[\mathbf{h}_{f_k}^{\mathrm{H}} \mathbf{x}_{r,b}^{*} \mathbf{x}_{r,b}^{T} \mathbf{h}_{f_k}] = \mathbf{h}_{f_k}^{\mathrm{H}} \mathbf{R}_{Capon} \mathbf{h}_{f_k}, \tag{2.18}$$

This minimization problem leads to the solution given by (2.17). $\mathbf{R}_{Capon}$ is the sample covariance matrix and estimated as

$$\hat{\mathbf{R}}_{Capon} = \hat{\mathbf{R}}_x = \frac{1}{RB} \sum_{r=1}^{R} \sum_{b=1}^{B} \mathbf{x}_{r,b} \mathbf{x}_{r,b}^{\mathrm{H}}. \tag{2.19}$$

In order to increase the robustness of the estimation and avoid ill conditioned covariance matrices, the temporal or/and spatial averaging can be used for estimation of the covariance matrix. The time averaging can be achieved by subdividing the OW into several ensembles and the spatial averaging can be achieved by extraction of data from the neighbouring spatial points. The spatial points can be chosen along the beam for the focused data acquisition while a 2-D region can be used for averaging when parallel beamforming techniques are employed. Only 2-D averaging is utilized in (2.19) and also in this work. This is done in order to estimate the spectra on full ensemble length and keep the frequency resolution high. Finally, the estimator can be found by substituting (2.17) into (2.18)

$$\hat{P}_{Capon}(f_k) = \frac{1}{\mathbf{a}_{f_k}^{\mathrm{H}} \hat{\mathbf{R}}_{Capon}^{-1} \mathbf{a}_{f_k}}. \tag{2.20}$$

2.4.2 The APES power spectral estimator

The APES power spectral estimator suppresses the interference from frequency components other than the frequency of interest and the thermal noise [39, 46]. This can be also formulated as the signal filtered in a way such that the filtered signal resembles a sinusoid as closely as possible in a least squares sense. The minimization problem is given by

$$\min_{\mathbf{h}_{f_k}} \quad \mathbf{h}_{f_k}^{\mathrm{H}} \mathbf{Q} \mathbf{h}_{f_k} \tag{2.21}$$

where $\mathbf{Q}$ is referred to as the *noise and interference covariance matrix*. The solution to this minimization problem with the constraint in (2.10) is given by (2.17). In this approach, the ensemble is subdivided into smaller segments for time averaging in order to enhance the signal of interest and average out the interferences. The covariance matrix can be estimated as

$$\hat{\mathbf{Q}} = \hat{\mathbf{R}}_x - \sum_{r=1}^{R} \sum_{b=1}^{B} g_{r,b}(f_k) g_{r,b}^{\mathrm{H}}(f_k) \tag{2.22}$$

where

$$\mathbf{g}_{r,b}(f_k) = \frac{1}{L} \sum_{l=1}^{L} \tilde{\mathbf{x}}_{r,b}(l) e^{-i f_k (l-1)}. \tag{2.23}$$

The number of sub-segments is L and $\tilde{\mathbf{x}}_{r,b}$ represent a sub-segment

$$\tilde{\mathbf{x}}_{r,b}(l) = [x_{r,b}(l) \; x_{r,b}(l+1) \; \cdots \; x_{r,b}(l+M-1)]^T, \tag{2.24}$$

where M is the sub-segment length and filter order. If sub-segment length is N, i.e., $M = N$, then the OW length must be $N + L - 1$. If OW length is limited which is often the case in this work, the sub-segment length must be shorter than N and $N = L + M - 1$. In such case, the frequency resolution of the estimates degrades. The filter coefficients are given following (2.17) as

$$\mathbf{h}_{f_k} = \frac{Q^{-1} \mathbf{a}_{f_k}}{\mathbf{a}_{f_k}^{\mathrm{H}} Q^{-1} \mathbf{a}_{f_k}} \tag{2.25}$$

Finally the estimator can be given by

$$\hat{P}_{APES}(f_k) = \frac{1}{RB} \sum_{r=1}^{R} \sum_{b=1}^{B} \left| \mathbf{h}_{f_k} g_{r,b}(f_k) \right|^2. \tag{2.26}$$

2.4.3 Blood iterative adaptive approach

The BIAA method [40, 47] has similarities with both the Capon and the APES estimators. The problem formulation is similar to that of Capon where the filter minimizes the output from all frequencies except for the frequency of interest which is passed undistorted. Let the covariance matrix $\mathbf{Q}_{f_k}$ represent the interference covariance matrix, i.e., interference from frequency components other than f_k. It can be defined as

$$\mathbf{Q}_{f_k} = \mathbf{R}_{BIAA} - |\alpha(f_k)|^2 \mathbf{a}_{f_k}\mathbf{a}_{f_k}^{\mathrm{H}} \tag{2.27}$$

The minimization problem given here can be represented by (2.10) and (2.21) as given in the APES section. However, the definition of both the interference and the covariance matrices are different than the APES method. The covariance matrix is expressed as

$$\mathbf{R}_{BIAA} = \sum_{k=1}^{K} |\alpha(f_k)|^2 \mathbf{a}_{f_k}\mathbf{a}_{f_k}^{\mathrm{H}} + \hat{\sigma}^2\mathbf{I}, \tag{2.28}$$

where $\mathbf{I}$ is the $N \times N$ identity matrix and $\hat{\sigma}^2$ is the variance for each sample and can be estimated as

$$\hat{\sigma}^2 = \left| \frac{\mathbf{v}_n^{\mathrm{H}}\mathbf{R}_{BIAA}^{-1}\mathbf{x}}{\mathbf{v}_n^{\mathrm{H}}\mathbf{R}_{BIAA}^{-1}\mathbf{v}_n} \right|, \tag{2.29}$$

where $\mathbf{v}_n$ is the nth column of $\mathbf{I}$. Spatial averaging can be used to estimate the covariance matrix in order to increase the robustness of the estimates. Therefore one can form the covariance matrix and the variance as follows

$$\hat{\mathbf{R}}_{BIAA} = \frac{1}{RB}\sum_{r=1}^{R}\sum_{b=1}^{B}\hat{\mathbf{R}}_{BIAA}^{r,b} \quad \textit{and} \quad \hat{\sigma}^2 = \frac{1}{RBN}\sum_{r=1}^{R}\sum_{b=1}^{B}\sum_{n=1}^{N}\hat{\sigma}_{r,b,n}^2, \tag{2.30}$$

where $\hat{\mathbf{R}}_{BIAA}^{r,b}$ is the covariance matrix estimate at location (r, b). As the filter passes the frequency of interest undistorted, it can be seen from (2.27) that the minimization of the interference covariance matrix is equal to minimization of the covariance matrix $\mathbf{R}_{BIAA}$ and it has the solution given in (2.17). Finally the estimator is given by

$$\hat{\alpha}_{r,b}(f_k) = \mathbf{h}_{f_k}^{\mathrm{H}}\mathbf{x}_{r,b} = \frac{\mathbf{a}_{f_k}^{\mathrm{H}}\hat{\mathbf{R}}_{BIAA}^{-1}\mathbf{x}_{r,b}}{\mathbf{a}_{f_k}^{\mathrm{H}}\hat{\mathbf{R}}_{BIAA}^{-1}\mathbf{a}_{f_k}} \tag{2.31}$$

As can be seen, the covariance matrix and the amplitude estimates are interdependent which makes the BIAA an iterative algorithm. Initialization of the algorithm can be done by setting the amplitude estimates as the Fourier transform of the data for each frequency and the variance can be set to a small number, e.g, 10^{-9} [40]. The iterations continue until a termination criterion is met. Finally the power estimate is

$$\hat{P}_{BIAA}(f_k) = \frac{1}{RB}\sum_{r=1}^{R}\sum_{b=1}^{B} \mid \hat{\alpha}_{r,b}(f_k) \mid^2 . \tag{2.32}$$

2.5 Clutter filtering

The echoes from stationary or slowly moving tissue are received due to the placement of the sample volume, sidelobes of the beam and reverberation [48], and the strength varies with the location of the sample volume. The echo from the tissue is typically 40-80 dB higher than the echo from the blood. This can corrupt the mean velocity and power estimation in CFI or create leakage and obscure the blood velocities in PW-Doppler. However, blood velocities have higher velocities than that of tissue for most applications in ultrasound. Therefore, the clutter signal can be filtered out by using a temporal high pass filter. Depending on the length of the signal to be filtered and the application, different types of filter can be chosen.

2.5.1 Infinite impulse response filters

The output of infinite impulse response (IIR) filters depend on the present and past input samples as well as the past output samples. The filter can be defined by the difference equation

$$y(n) = -\sum_{i=1}^{I} a_i y(n-i) + \sum_{i=0}^{I} b_i x(n-i). \tag{2.33}$$

where a_i and b_i are the filter coefficients, $x(n)$ and $y(n)$ are input and output samples respectively, and I is the filter order. As the filter is recursive, the transient response affect its performance and may generate spurious frequency components [49]. Therefore, the transient response must be minimized. This is especially the case for CFI as the packet size is limited. The transient response depends on the filter type used as well as the initialization technique. Several methods have been proposed for minimizing the transient response [50, 51].

2.5.2 Finite impulse response filters

The FIR filters are time invariant filters that have finite duration impulse responses [52]. The filter can be described by convolution sum between the impulse response and input signal as

$$y(n) = \sum_{i=0}^{I} h(i)x(n-i), \tag{2.34}$$

where $\mathbf{h}$ is the impulse response with length I. The output of the FIR filter does not depend on previous output samples, i.e., no feedback required. The filter must be initialized before the output samples are valid. This reduces the number of samples

that can be used for velocity estimation and may cause higher variance in case of CFI and reduced frequency resolution when used before spectral estimation. In addition, the filter have a transition band which may attenuate low blood velocities.

2.5.3 Polynomial regression filters

In this method, the slowly varying clutter is approximated by set of polynomials which are determined by least squares fit and later subtracted from the signal. The Legendre polynomials have previously been used for this purpose [52, 53]. An efficient matrix implementation of this filter can be found in Section 3.2.3. This set of filters do not require initialization which leaves more time samples for velocity estimation. These filters generally have narrower transition regions compared to FIR and IIR filters with the same order. However, the IIR filters can achieve similar performance depending on the chosen initialization method [52].

2.5.4 Adaptive clutter filtering

The filters listed above do not take the characteristics of the clutter to be filtered into account. These filters have cut-off velocities that depend on the chosen filter order and filter type. Filters that are dependent on the signal characteristics are referred to as adaptive filters.

Several clutter filters have been proposed that are adapted to the tissue motion [54,55]. Thomas et al. [56], proposed an adaptive filter that estimates the Doppler shift of the clutter and shifts the signal to zero frequency by complex multiplication. After this, the clutter is removed by using DC removal. In other words, the mean of the signal is subtracted from the signal after multiplication. The advantage of this method is that a narrow band filter can be created without decreasing the number of samples for blood velocity estimation. Another type of adaptive filter which is similar to polynomial regression filters is eigenvector regression filter. In polynomial regression filtering, the cut-off frequency is adjusted by changing the filter order while in eigenvector regression filtering, the filter order defines the number of largest eigenvectors representing clutter to be removed from the signal. A more elaborate description and comparison of these filters can be found in [57].

2.6 Diagnostic value of CFI and PW-Doppler

Computed tomography, magnetic resonance imaging and ultrasound are used for flow detection in medical imaging. Even though all methods have their advantages and limitations, the ultrasound Doppler imaging is used widely for diagnosis for being cost-effective, portable and real-time. Doppler ultrasound can be used for applications such as evaluation of cardiac systolic and diastolic function, diagnosis of stenosis in arteries, detections of regions with abnormal flow or assessment of fetus growth in obstetrics.

In general, PW-Doppler is used for estimation of maximum velocities, such as PSV and EDV, through delineation of spectrograms. These parameters can be used

for determination of degree of stenosis [58], estimation of resistivity and pulsatility indices [59], cardiac output and pressure gradients [60]. As mentioned previously, PW-Doppler has the limitation of intrinsic broadening which can result in overestimation of maximum velocities. In addition, the method is angle dependent. The beam-to-flow angle has to be determined in order to calculate the true velocity. Large beam-to-flow angles causes higher degree of broadening making it difficult to delineate the spectrogram. An example of this can be seen in Fig. 2.4. The estimated spectrograms with small (left panel) and large (right panel) beam-to-flow angle from the same CCA. Increased spectral broadening obscures the maximum velocity and causes overestimation, especially for high velocities. Therefore, it is a common practice obtain spectrograms with beam-to-flow angles smaller than 60° to minimize spectral broadening. However, inter-/intra-observer variability can still result in significant bias.

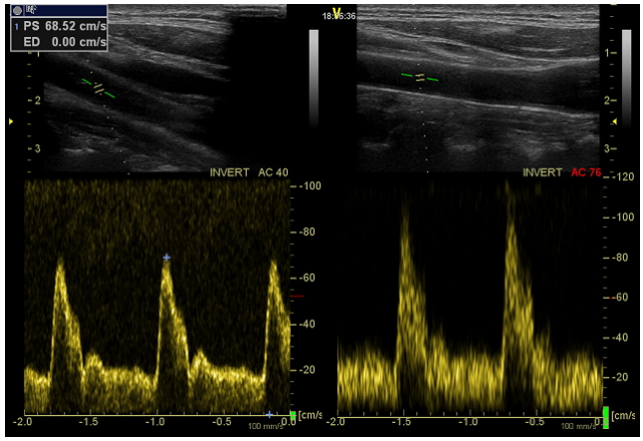

Figure 2.4: The effect of beam-to-flow angle on PW-Doppler. The spectrogram on the left is generated with a small beam-to-flow angle while the right one is estimated with the data recorded with a large beam-to-flow angle. Large beam-to-flow angles result in increased spectral broadening and potentially overestimation of maximum blood velocities.

On the other hand, CFI is a semi-quantitative tool that is useful for demonstration of turbulence, acceleration and backward flow [61]. It gives an overall flow dynamics in the ROI and it is used for detection of regions with blood flow. This is highly useful for sample volume placement in PW-Doppler. However, conventional CFI method also has the limitation of angle dependency as the velocity component along the beam is estimated. It is is heavily affected by the clutter filtering and can result in overestimation or underestimation of velocities [62]. More recent mean velocity estimation approaches, such as vector Doppler [63], have been proposed for quantitative analysis [64]. The vector Doppler approach can visualize 2-D velocity vectors and display estimated true velocity without manual angle correction. The method was applied to stenosis screening in carotid artery recently and it was reported

that the method can be of great value in determination of risk and diagnosis of stenosis. However, similar to the conventional CFI, estimates are affected by the clutter filtering and it is difficult to evaluate the extend of this effect visually. Therefore, a system which can provide both the spectral estimations and the mean velocities estimated from these spectra can be of use to assess the clutter filter distortions and provide more quantitative analysis. In other words, PW-Doppler and CFI should be seen as complimentary to each other rather than substitute.

References

[1] B. Angelsen, *Ultrasound imaging: waves, signals, and signal processing*. Trondheim: Emantec AS, 2000.

[2] J. A. Jensen, *Estimation of blood velocities using ultrasound: a signal processing approach*. Cambridge University Press, 1996.

[3] R. S. Cobbold, *Foundations of biomedical ultrasound*. 2007.

[4] T. L. Szabo, *Diagnostic ultrasound imaging: inside out*. Academic Press, 2004.

[5] P. Stoica, R. L. Moses, *et al.*, *Spectral analysis of signals*, vol. 452. Pearson Prentice Hall Upper Saddle River, NJ, 2005.

[6] J. Proakis and D. Manolakis, *Digital Signal Processing*. Prentice Hall international editions, Pearson Prentice Hall, 2007.

[7] J. Somer, "Electronic sector scanning for ultrasonic diagnosis," *Ultrasonics*, vol. 6, no. 3, pp. 153–159, 1968.

[8] M. Karaman, P.-C. Li, and M. O'Donnell, "Synthetic aperture imaging for small scale systems," *IEEE transactions on ultrasonics, ferroelectrics, and frequency control*, vol. 42, no. 3, pp. 429–442, 1995.

[9] J. A. Jensen, S. I. Nikolov, K. L. Gammelmark, and M. H. Pedersen, "Synthetic aperture ultrasound imaging," *Ultrasonics*, vol. 44, pp. e5–e15, 2006.

[10] M. Couade, M. Pernot, M. Tanter, E. Messas, A. Bel, M. Ba, A.-A. Hagège, and M. Fink, "Ultrafast imaging of the heart using circular wave synthetic imaging with phased arrays," in *Ultrasonics Symposium (IUS), 2009 IEEE International*, pp. 515–518, IEEE, 2009.

[11] C. Papadacci, M. Pernot, M. Couade, M. Fink, and M. Tanter, "High-contrast ultrafast imaging of the heart," *IEEE transactions on ultrasonics, ferroelectrics, and frequency control*, vol. 61, no. 2, pp. 288–301, 2014.

[12] C. Bruneel, R. Torguet, K. Rouvaen, E. Bridoux, and B. Nongaillard, "Ultrafast echotomographic system using optical processing of ultrasonic signals," *Applied Physics Letters*, vol. 30, no. 8, pp. 371–373, 1977.

[13] B. Delannoy, R. Torguet, C. Bruneel, E. Bridoux, J. Rouvaen, and H. Lasota, "Acoustical image reconstruction in parallel-processing analog electronic systems," *Journal of Applied Physics*, vol. 50, no. 5, pp. 3153–3159, 1979.

[14] D. P. Shattuck, M. D. Weinshenker, S. W. Smith, and O. T. von Ramm, "Explososcan: A parallel processing technique for high speed ultrasound imaging with linear phased arrays," *The Journal of the Acoustical Society of America*, vol. 75, no. 4, pp. 1273–1282, 1984.

[15] W. R. Hedrick, D. L. Hykes, and D. E. Starchman, "Ultrasound physics and instrumentation," 2005.

[16] O. T. Von Ramm, S. W. Smith, and H. G. Pavy, "High-speed ultrasound volumetric imaging system. II. Parallel processing and image display," *IEEE transactions on ultrasonics, ferroelectrics, and frequency control*, vol. 38, no. 2, pp. 109–115, 1991.

[17] J. Bercoff, *Ultrafast ultrasound imaging*. INTECH Open Access Publisher, 2011.

[18] G. Montaldo, M. Tanter, J. Bercoff, N. Benech, and M. Fink, "Coherent plane-wave compounding for very high frame rate ultrasonography and transient elastography," *IEEE transactions on ultrasonics, ferroelectrics, and frequency control*, vol. 56, no. 3, pp. 489–506, 2009.

[19] T. Hergum, T. Bjastad, K. Kristoffersen, and H. Torp, "Parallel beamforming using synthetic transmit beams," *IEEE transactions on ultrasonics, ferroelectrics, and frequency control*, vol. 54, no. 2, pp. 271–280, 2007.

[20] T. Bjastad, S. A. Aase, and H. Torp, "The impact of aberration on high frame rate cardiac B-mode imaging," *IEEE Transactions on Ultrasonics Ferroelectrics and Frequency Control*, vol. 54, no. 1, p. 32, 2007.

[21] T. Hergum, T. G. Bjastad, L. Lovstakken, K. Kristoffersen, and H. Torp, "Reducing color flow artifacts caused by parallel beamforming," *IEEE transactions on ultrasonics, ferroelectrics, and frequency control*, vol. 57, no. 4, pp. 830–838, 2010.

[22] I. K. Ekroll, M. M. Voormolen, O. K.-V. Standal, J. M. Rau, and L. Lovstakken, "Coherent compounding in Doppler imaging," *IEEE transactions on ultrasonics, ferroelectrics, and frequency control*, vol. 62, no. 9, pp. 1634–1643, 2015.

[23] J. A. Kisslo, D. B. Adams, and R. N. Belkin, *Doppler color flow imaging*. Churchill Livingstone New York, 1988.

[24] C. Kasai, K. Namekawa, A. Koyano, R. Omoto, *et al.*, "Real-time two-dimensional blood flow imaging using an autocorrelation technique," *IEEE Trans. Sonics Ultrason*, vol. 32, no. 3, pp. 458–464, 1985.

[25] H. F. Routh, "Doppler ultrasound," *IEEE engineering in medicine and biology magazine*, vol. 15, no. 6, pp. 31–40, 1996.

[26] D. Maulik and I. Zalud, *Doppler ultrasound in obstetrics and gynecology*. Springer, 2005.

[27] H. Talhami and R. Kitney, "Maximum likelihood frequency tracking of the audio pulsed Doppler ultrasound signal using a Kalman filter," *Ultrasound in medicine & biology*, vol. 14, no. 7, pp. 599–609, 1988.

[28] P. Welch, "The use of fast Fourier transform for the estimation of power spectra: a method based on time averaging over short, modified periodograms," *IEEE Transactions on audio and electroacoustics*, vol. 15, no. 2, pp. 70–73, 1967.

[29] F. Schlindwein and D. Evans, "Autoregressive spectral analysis as an alternative to fast Fourier transform analysis of Doppler ultrasound signals," *Diagnostic vascular ultrasound*, vol. 8, pp. 74–84, 1992.

[30] E. D. Übeylı and I. Güler, "Spectral analysis of internal carotid arterial Doppler signals using FFT, AR, MA, and ARMA methods," *Computers in biology and medicine*, vol. 34, no. 4, pp. 293–306, 2004.

[31] P. Hoskins, "Ultrasound techniques for measurement of blood flow and tissue motion," *Biorheology*, vol. 39, no. 4, pp. 451–460, 2002.

[32] P. J. Fish, "Nonstationarity broadening in pulsed Doppler spectrum measurements," *Ultrasound in medicine & biology*, vol. 17, no. 2, pp. 147–155, 1991.

[33] S. M. Kay and S. L. Marple, "Spectrum analysis a modern perspective," *Proceedings of the IEEE*, vol. 69, no. 11, pp. 1380–1419, 1981.

[34] J. A. Cadzow, "Spectral estimation: An overdetermined rational model equation approach," *Proceedings of the IEEE*, vol. 70, no. 9, pp. 907–939, 1982.

[35] P. Vaitkus, R. Cobbold, and K. Johnston, "A comparative study and assessment of Doppler ultrasound spectral estimation techniques part II: methods and results," *Ultrasound in medicine & biology*, vol. 14, no. 8, pp. 673–688, 1988.

[36] P. Vaitkus and R. Cobbold, "A comparative study and assessment of doppler ultrasound spectral estimation techniques part I: Estimation methods," *Ultrasound in Medicine and Biology*, vol. 14, no. 8, pp. 661–672, 1988.

[37] H. Torp and K. Kristoffersen, "Velocity matched spectrum analysis: A new method for suppressing velocity ambiguity in pulsed-wave Doppler," *Ultrasound in medicine & biology*, vol. 21, no. 7, pp. 937–944, 1995.

[38] T. D. Fredriksen, I. K. Ekroll, L. Lovstakken, and H. Torp, "2-D tracking Doppler: a new method to limit spectral broadening in pulsed wave Doppler," *IEEE transactions on ultrasonics, ferroelectrics, and frequency control*, vol. 60, no. 9, pp. 1896–1905, 2013.

[39] F. Gran, A. Jakobsson, and J. A. Jensen, "Adaptive spectral Doppler estimation," *IEEE transactions on ultrasonics, ferroelectrics, and frequency control*, vol. 56, no. 4, 2009.

[40] E. Gudmundson, A. Jakobsson, J. A. Jensen, and P. Stoica, "Blood velocity estimation using ultrasound and spectral iterative adaptive approaches," *Signal Processing*, vol. 91, no. 5, pp. 1275–1283, 2011.

[41] K. L. Hansen, F. Gran, M. M. Pedersen, I. K. Holfort, J. A. Jensen, and M. B. Nielsen, "In-vivo validation of fast spectral velocity estimation techniques," *Ultrasonics*, vol. 50, no. 1, pp. 52–59, 2010.

[42] S. Ricci, "Adaptive spectral estimators for fast flow-profile detection," *IEEE transactions on ultrasonics, ferroelectrics, and frequency control*, vol. 60, no. 2, pp. 421–427, 2013.

[43] J. S. Arora, "Introduction to optimum design," 1989.

[44] J. Capon, "High-resolution frequency-wavenumber spectrum analysis," *Proceedings of the IEEE*, vol. 57, no. 8, pp. 1408–1418, 1969.

[45] P. Stoica, A. Jakobsson, and J. Li, "Matched-filter bank interpretation of some spectral estimators," *Signal Processing*, vol. 66, no. 1, pp. 45–59, 1998.

[46] J. Li and P. Stoica, "An adaptive filtering approach to spectral estimation and SAR imaging," *IEEE Transactions on Signal Processing*, vol. 44, no. 6, pp. 1469–1484, 1996.

[47] T. Yardibi, J. Li, P. Stoica, M. Xue, and A. B. Baggeroer, "Source localization and sensing: A nonparametric iterative adaptive approach based on weighted least squares," *IEEE Transactions on Aerospace and Electronic Systems*, vol. 46, no. 1, 2010.

[48] J. J. Dahl and N. M. Sheth, "Reverberation clutter from subcutaneous tissue layers: Simulation and in vivo demonstrations," *Ultrasound in medicine & biology*, vol. 40, no. 4, pp. 714–726, 2014.

[49] A. P. Kadi and T. Loupas, "On the performance of regression and step-initialized IIR clutter filters for color Doppler systems in diagnostic medical ultrasound," *IEEE transactions on ultrasonics, ferroelectrics, and frequency control*, vol. 42, no. 5, pp. 927–937, 1995.

[50] E. S. Chornoboy, "Initialization for improved IIR filter performance," *IEEE transactions on signal processing*, vol. 40, no. 3, pp. 543–550, 1992.

[51] R. Fletcher and D. W. Burlage, "An initialization technique for improved MTI performance in phased array radars," *Proceedings of the IEEE*, vol. 60, no. 12, pp. 1551–1552, 1972.

[52] S. Bjaerum, H. Torp, and K. Kristoffersen, "Clutter filter design for ultrasound color flow imaging," *IEEE transactions on ultrasonics, ferroelectrics, and frequency control*, vol. 49, no. 2, pp. 204–216, 2002.

[53] H. Torp, "Clutter rejection filters in color flow imaging: A theoretical approach," *ieee transactions on ultrasonics, ferroelectrics, and frequency control*, vol. 44, no. 2, pp. 417–424, 1997.

[54] Y. M. Yoo, R. Managuli, and Y. Kim, "Adaptive clutter filtering for ultrasound color flow imaging," *Ultrasound in medicine & biology*, vol. 29, no. 9, pp. 1311–1320, 2003.

[55] C. M. Gallippi and G. E. Trahey, "Adaptive clutter filtering via blind source separation for two-dimensional ultrasonic blood velocity measurement," *Ultrasonic imaging*, vol. 24, no. 4, pp. 193–214, 2002.

[56] L. Thomas and A. Hall, "An improved wall filter for flow imaging of low velocity flow," in *Ultrasonics Symposium, 1994. Proceedings., 1994 IEEE*, vol. 3, pp. 1701–1704, IEEE, 1994.

[57] S. Bjaerum, H. Torp, and K. Kristoffersen, "Clutter filters adapted to tissue motion in ultrasound color flow imaging," *IEEE transactions on ultrasonics, ferroelectrics, and frequency control*, vol. 49, no. 6, pp. 693–704, 2002.

[58] W. Blackshear, D. Phillips, P. Chikos, J. Harley, B. Thiele, and D. Strandness, "Carotid artery velocity patterns in normal and stenotic vessels.," *Stroke*, vol. 11, no. 1, pp. 67–71, 1980.

[59] F. Dallaire, C. Slorach, W. Hui, T. Sarkola, M. K. Friedberg, T. J. Bradley, E. Jaeggi, A. Dragulescu, R. L. Har, D. Z. Cherney, *et al.*, "Reference values for pulse wave Doppler and tissue Doppler imaging in pediatric echocardiography," *Circulation: Cardiovascular Imaging*, vol. 8, no. 2, p. e002167, 2015.

[60] A. Maslow, M. E. Comunale, J. M. Haering, and J. Watkins, "Pulsed wave Doppler measurement of cardiac output from the right ventricular outflow tract," *Anesthesia & Analgesia*, vol. 83, no. 3, pp. 466–471, 1996.

[61] J. De Bray, F. Galland, P. Lhoste, S. Nicolau, F. Dubas, J. Emile, and J. Pillet, "Colour Doppler and duplex sonography and angiography of the carotid artery bifurcations," *Neuroradiology*, vol. 37, no. 3, pp. 219–224, 1995.

[62] B. Griewing, C. Morgenstern, F. Driesner, G. Kallwellis, M. Walker, and C. Kessler, "Cerebrovascular disease assessed by color-flow and power Doppler ultrasonography," *Stroke*, vol. 27, no. 1, pp. 95–100, 1996.

[63] A. Pastorelli, G. Torricelli, M. Scabia, E. Biagi, and L. Masotti, "A real-time 2-D vector Doppler system for clinical experimentation," *IEEE transactions on medical imaging*, vol. 27, no. 10, pp. 1515–1524, 2008.

[64] P. Tortoli, M. Lenge, D. Righi, G. Ciuti, H. Liebgott, and S. Ricci, "Comparison of carotid artery blood velocity measurements by vector and standard Doppler approaches," *Ultrasound in medicine & biology*, vol. 41, no. 5, pp. 1354–1362, 2015.

Chapter 3

Adaptive Spectral Estimation Methods in Color Flow Imaging

Yücel Karabiyik[1], Ingvild Kinn Ekroll[1,3], Sturla Eik-Nes[2], Jørgen Avdal[1], and Lasse Løvstakken[1]

[1] Dept. of Circulation and Medical Imaging, NTNU, Norway

[2] National Center for Fetal Medicine, St. Olavs University Hospital, Norway

[3] St. Olavs Hospital, Trondheim University Hospital, Norway

Clutter rejection for color flow imaging (CFI) remains a challenge due to either limited amount of temporal samples available or non-stationary tissue clutter. This is particularly the case for interleaved CFI and B-mode acquisitions. Low velocity blood signal is attenuated along with the clutter due to the long transition band of the available clutter filters, causing regions of biased mean velocity estimates or signal dropouts. This work investigates how adaptive spectral estimation methods, the Capon and BIAA, can be used to estimate the mean velocity in CFI without prior clutter filtering. The approach is based on confining the clutter signal in a narrow spectral region around the zero Doppler frequency while keeping the spectral side lobes below the blood signal level, allowing for the clutter signal to be removed by thresholding in the frequency domain. The proposed methods are evaluated using computer simulations, flow phantom experiments and *in-vivo* recordings from the common carotid and jugular vein of healthy volunteers. Capon and BIAA methods could estimate low blood velocities which are normally attenuated by polynomial regression filters, and may potentially give better estimation of mean velocities for CFI at a higher computational cost. The Capon method decreased the bias by 81% in the transition band of the used polynomial regression filter for small packet size (N=8) and low SNR (5 dB). Flow phantom and *in-vivo* results demonstrate that the Capon method can provide color flow images and flow profiles with lower variance and bias especially in the regions close to the artery walls.

3.1 Introduction

Color flow imaging (CFI) is used for displaying the mean blood velocity in a spatial region and is highly useful for detection of regions of abnormal blood flow. In a focused imaging setup, CFI and B-mode acquisitions are typically interleaved, only allowing a small number (8-16) of Doppler pulses to be fired in a given beam direction. A fixed

pulse repetition frequency (PRF) is used and after sampling the signal at all depths of interest, the mean Doppler frequency is commonly estimated using the autocorrelation technique [1].

The sampled data contain echoes from moving blood and stationary or near stationary tissue clutter which can be 40-60 dB stronger than the signal from blood. Therefore, the clutter signal must be attenuated prior to mean blood velocity estimation to minimize mean velocity bias, and avoid false detection (flashing artifacts) of blood in tissue regions of the image. Clutter rejection filtering for CFI applications is a major challenge due to the limited number of samples available for processing and velocity estimation. Several types of filters have been investigated. Finite impulse response (FIR) filters have wider transition bands and need more samples for initialization than infinite impulse response (IIR) and polynomial regression filters [2]. Polynomial regression and IIR filters can have similar frequency responses when an appropriate initialization technique is chosen for the IIR filter [2]. Regardless, the gradual filter transition region leads to attenuation and overestimation of low blood velocities or signal dropouts.

In this work, a frequency domain approach to clutter filtering and mean velocity estimation is proposed. Provided that the clutter signal is confined in a limited region in the Doppler power spectrum and does not interfere with the blood signal, clutter rejection can be done using a frequency threshold, and mean velocity estimation can further be done using the frequency domain autocorrelation method [3]. Improvement over the traditional time-domain clutter filter is achieved when the clutter can be confined sufficiently in the stop band region, reducing transition region effects of the traditional clutter filter.

The ability to confine the clutter signal within the stop band is determined by the frequency resolution and side lobe levels of the power spectrum estimator. Using the Welch [4] approach as in conventional PW-Doppler will not work well due to the relatively poor frequency resolution and high side lobe levels, and especially when restricted to using very few temporal samples as in CFI. However, several power spectral density (PSD) estimators have been shown to provide such desired characteristics in different settings. Parametric estimation methods [5–8] have been shown to provide superior resolution but are computationally complex and need correct determination of model parameters. Data adaptive filter-bank methods originally developed for radar applications have been adapted and applied for ultrasound imaging. For instance, the Capon minimum variance [5,9] and the amplitude and phase estimation (APES) [10, 11] methods have been shown to produce improved frequency resolution and reduce spectral leakage compared to Welch's method [12]. An iterative adaptive approach (IAA) [13] was shown to improve power spectrum estimation further for ultrasound PW-Doppler signals, which termed blood IAA (BIAA) [14].

In this work we investigate whether the classical Capon and more recent BIAA approach can provide sufficient spectral resolution and side lobe suppression to confine and remove tissue clutter signal and associated side lobes, as well as their use in subsequent mean velocity estimation in CFI. The methods have shown promise for improving the frequency resolution in PW-Doppler [10, 14], and we recently observed that the high spectral resolution and side lobe suppression of the Capon approach

could make traditional clutter filtering superfluous in PW-Doppler when the tissue clutter was sufficiently narrow band [15].

The main motivation of this work is to improve the detection and estimation of low flow velocities, which is important for imaging small peripheral vessels, e.g. tumor vessels [16], but also for the estimation of vascular wall shear stress [17], or for accurate estimation of volume flow in general.

The paper is organized as follows. In Section 4.3 the PSD estimators and polynomial regression filters are presented. The mean velocity estimation methods and the signal model used in the simulations are explained. Section 4.4 presents the simulation, *in-vivo* and flow phantom experiment results. The improvements and the disadvantages of the methods are discussed in Section 4.5. Finally, concluding remarks are given in Section 3.5.

3.2 Methods

The CFI data set consists of time series acquired at several radial and lateral spatial points. Following the data model presented in [10] and its interpretation in [18], the data model is extended to represent a signal from a 2-D spatial region. After demodulation, the signal from depth r in radial, beam b in lateral direction and emission n can be modeled as the sum of contributions from each frequency as

$$x_{r,b}(n) = \sum_{k=1}^{K} \alpha_{r,b}(k) e^{-j2\pi f_k n} + e_{r,b}(n), \tag{3.1}$$

where f_k is the normalized frequency with respect to PRF, $\alpha_{r,b}(k)$ is the complex amplitude of the signal at frequency f_k and $e_{r,b}(n)$ is zero mean complex white Gaussian noise with variance σ^2.

3.2.1 PSD Estimators

The Welch's Method

An ensemble that is acquired at depth r, beam b and with N temporal samples where N is commonly referred to as packet size, can be expressed as $\mathbf{x}_{r,b} = [x_{r,b}(1)\ x_{r,b}(2)\ \cdots\ x_{r,b}(N)]^T$. The ensemble is subdivided into smaller segments for temporal averaging to decrease the variance. Let l denote the index for the sub-segments $\tilde{\mathbf{x}}_{r,b}$

$$\tilde{\mathbf{x}}_{r,b}(l) = [x_{r,b}(l)\ x_{r,b}(l+1)\ \cdots\ x_{r,b}(l+M-1)]^T, \tag{3.2}$$

where M is the length of the sub-segment.

Including the spatial averaging in radial and lateral directions, the Welch PSD estimator is expressed as

$$\hat{\mathbf{P}}_{Welch}(f_k) = \frac{1}{RBL}\sum_{r=1}^{R}\sum_{b=1}^{B}\sum_{l=1}^{L}\left|\sum_{m=0}^{M-1}\mathbf{w}(m)x_{r,b}(l+m)e^{-i2\pi f_k m}\right|^2, \quad (3.3)$$

where $\mathbf{w}$ is a window function, L is the number of sub-segments and $M = N-L+1$. The Welch estimate is equivalent to the following when the window function is chosen as a rectangular window

$$\begin{aligned}\hat{\mathbf{P}}_{Welch}(f_k) &= \frac{1}{RBL}\sum_{r=1}^{R}\sum_{b=1}^{B}\sum_{l=1}^{L}\left|\mathbf{a}_{f_k}^{\mathrm{H}}\tilde{\mathbf{x}}_{r,b}(l)\right|^2 \\ &= \frac{1}{RBL}\sum_{r=1}^{R}\sum_{b=1}^{B}\sum_{l=1}^{L}\mathbf{a}_{f_k}^{\mathrm{H}}\tilde{\mathbf{x}}_{r,b}(l)\tilde{\mathbf{x}}_{r,b}^{\mathrm{H}}(l)\mathbf{a}_{f_k} \\ &= \mathbf{a}_{f_k}^{\mathrm{H}}\hat{\mathbf{R}}_{Welch}\mathbf{a}_{f_k},\end{aligned} \quad (3.4)$$

where $(.)^{\mathrm{H}}$ represents the Hermitian transpose, $\mathbf{a}_{f_k} = [1\ e^{i2\pi f_k}\ \cdots\ e^{i2\pi f_k(M-1)}]^T$ is the Fourier vector and the covariance matrix $\hat{\mathbf{R}}_{Welch}$ is

$$\hat{\mathbf{R}}_{Welch} = \frac{1}{RBL}\sum_{r=1}^{R}\sum_{b=1}^{B}\sum_{l=1}^{L}\tilde{\mathbf{x}}_{r,b}(l)\tilde{\mathbf{x}}_{r,b}^{\mathrm{H}}(l). \quad (3.5)$$

Subdividing the ensemble for temporal averaging decreases the variance of the PSD estimation in exchange for decreased spectral resolution. The PSD estimation is modified by multiplying each sub-segment with a window function to reduce spectral side lobes. A Hamming windows is commonly used for this purpose.

Power Spectral Capon

The Capon estimator is a data adaptive spectral estimation method which can be interpreted as a filter bank approach where the power of each frequency in the spectrum is estimated by filtering the data with an optimized filter, $\mathbf{h}_{f_k}$, designed to pass the frequency of interest, f_k, undistorted while minimizing the output power of the filter. The filter output power can be written as [5]

$$E[\mathbf{h}_{f_k}^{\mathrm{H}}\mathbf{x}_{r,b}^{*}\mathbf{x}_{r,b}^{T}\mathbf{h}_{f_k}] = \mathbf{h}_{f_k}^{\mathrm{H}}\mathbf{R}_{Capon}\mathbf{h}_{f_k}, \quad (3.6)$$

where $(.)^*$ denotes the complex conjugate and $\mathbf{R}_{Capon}$ is the data covariance matrix and can be estimated as

$$\hat{\mathbf{R}}_{Capon} = \frac{1}{RB}\sum_{r=1}^{R}\sum_{b=1}^{B}\mathbf{x}_{r,b}\mathbf{x}_{r,b}^{\mathrm{H}}. \quad (3.7)$$

Minimization of (3.6) is done subject to $\mathbf{h}_{f_k}^{\mathrm{H}}\mathbf{a}_{f_k} = 1$, where $\mathbf{a}_{f_k}$ represents the Fourier vector with length N. This can be shown to give [5]

$$\mathbf{h}_{f_k} = \frac{\hat{\mathbf{R}}_{Capon}^{-1}\mathbf{a}_{f_k}}{\mathbf{a}_{f_k}^{\mathrm{H}}\hat{\mathbf{R}}_{Capon}^{-1}\mathbf{a}_{f_k}}. \tag{3.8}$$

Thus, the filter output power in (3.6) is found as

$$\hat{\mathbf{P}}_{Capon}(f_k) = \frac{1}{\mathbf{a}_{f_k}^{\mathrm{H}}\hat{\mathbf{R}}_{Capon}^{-1}\mathbf{a}_{f_k}}. \tag{3.9}$$

BIAA

Similar to the Capon method, estimation of each spectral component is done by a general linear estimator [14]

$$\hat{\alpha}_{r,b}(f_k) = \mathbf{h}_{f_k}^{\mathrm{H}}\mathbf{x}_{r,b}. \tag{3.10}$$

Filter coefficients $\mathbf{h}_{f_k}$ are designed to minimize the output amplitudes of frequencies other than the frequency of interest f_k and passing the component with f_k undistorted. Same as the Capon estimator, the minimizer is found as

$$\mathbf{h}_{f_k} = \frac{\mathbf{R}_{BIAA}^{-1}\mathbf{a}_{f_k}}{\mathbf{a}_{f_k}^{\mathrm{H}}\mathbf{R}_{BIAA}^{-1}\mathbf{a}_{f_k}}. \tag{3.11}$$

An estimate of the data covariance matrix $\mathbf{R}_{BIAA}$ is defined as

$$\hat{\mathbf{R}}_{BIAA} = \frac{1}{RB}\sum_{r=1}^{R}\sum_{b=1}^{B}\hat{\mathbf{R}}_{BIAA}^{r,b} = \frac{1}{RB}\mathbf{A}\left[\sum_{r=1}^{R}\sum_{b=1}^{B}\mathbf{P}_{r,b}\right]\mathbf{A}^{\mathrm{H}} + \hat{\sigma}^2\mathbf{I}. \tag{3.12}$$

$\mathbf{P}_{r,b}$ is a diagonal matrix that has $\mid \hat{\alpha}_{r,b}(1) \mid^2 \cdots \mid \hat{\alpha}_{r,b}(K) \mid^2$ as its diagonal elements, $\mathbf{A} = [\mathbf{a}_{f_1} \cdots \mathbf{a}_{f_K}]$ and $\mathbf{I}$ is the $N \times N$ identity matrix. An estimate of the amplitude at f_k can be found by inserting (3.11) into (3.10)

$$\hat{\alpha}_{r,b}(f_k) = \mathbf{h}_{f_k}^{\mathrm{H}}\mathbf{x}_{r,b} = \frac{\mathbf{a}_{f_k}^{\mathrm{H}}\hat{\mathbf{R}}_{BIAA}^{-1}\mathbf{x}_{r,b}}{\mathbf{a}_{f_k}^{\mathrm{H}}\hat{\mathbf{R}}_{BIAA}^{-1}\mathbf{a}_{f_k}}. \tag{3.13}$$

Variance at each range, beam and emission can be estimated with

$$\hat{\sigma}_{r,b,n}^2 = \left|\frac{\mathbf{v}_n^{\mathrm{H}}\mathbf{R}_{BIAA}^{-1}\mathbf{x}_{r,b}}{\mathbf{v}_n^{\mathrm{H}}\mathbf{R}_{BIAA}^{-1}\mathbf{v}_n}\right|, \tag{3.14}$$

where $\mathbf{v}_n$ is the nth column of $\mathbf{I}$ and the noise variance can be calculated as

$$\hat{\sigma}^2 = \frac{1}{RBN} \sum_{r=1}^{R} \sum_{b=1}^{B} \sum_{n=1}^{N} \hat{\sigma}^2_{r,b,n}. \tag{3.15}$$

BIAA is an iterative algorithm as $\mathbf{R}_{BIAA}$ and α_{f_k} are interdependent. The initialization of the algorithm can be done by choosing $\hat{\alpha}_{r,b}(f_k) = \frac{\mathbf{a}^{\mathrm{H}}_{f_k} \mathbf{x}_{r,b}}{N}$ and $\hat{\sigma}^2_{BIAA} = 10^{-9}$ as the initial estimates of the amplitudes at different frequencies and the noise variance respectively [14]. $\mathbf{R}_{BIAA}$ is found by using the initial estimates and then used for estimation of new $\hat{\alpha}_{r,b}(f_k)$ and $\hat{\sigma}^2$. Iterations continue until a termination criterion is met. Finally, the power spectrum is found as

$$\hat{\mathbf{P}}_{BIAA}(f_k) = \mid \hat{\alpha}_{r,b}(f_k) \mid^2 . \tag{3.16}$$

The algorithm is terminated when the mean difference of the estimates between two consecutive iterations is less than 1%. This is the same termination condition used in [18].

Comparison of PSD estimators

Fig. 3.1 shows an example of the side lobe levels and resolution of the described PSD estimation methods. Fig. 3.1(a) shows the estimated PSDs of a signal which includes a single frequency component at zero frequency in complex white Gaussian noise. The signal in Fig. 3.1(b) consists of a band of frequencies in complex white Gaussian noise that have zero mean and $0.01 \times PRF$ bandwidth, which is more representative of ultrasound imaging scenario. The ensemble length $N = 12$ and the SNR is 10 dB. The window function used for Welch's method is a Hamming window and $L = 1$.

3.2.2 Mean Velocity Estimators

Autocorrelation method

The complex correlation function with lag one in the temporal direction is used to estimate the mean velocity [1].

$$\hat{R}(1) = \frac{1}{RB(N-1)} \sum_{r=1}^{R} \sum_{b=1}^{B} \sum_{n=1}^{N-1} x_{r,b}(n) x^*_{r,b}(n+1). \tag{3.17}$$

The mean velocity is then found by

$$\bar{v} = \frac{\angle \hat{R}(1) PRF c}{4\pi f_0}, \tag{3.18}$$

where f_0 is the transmit center frequency and c is the speed of sound in blood. The autocorrelation estimator is unbiased under certain conditions such as absence of frequency dependent attenuation [19].

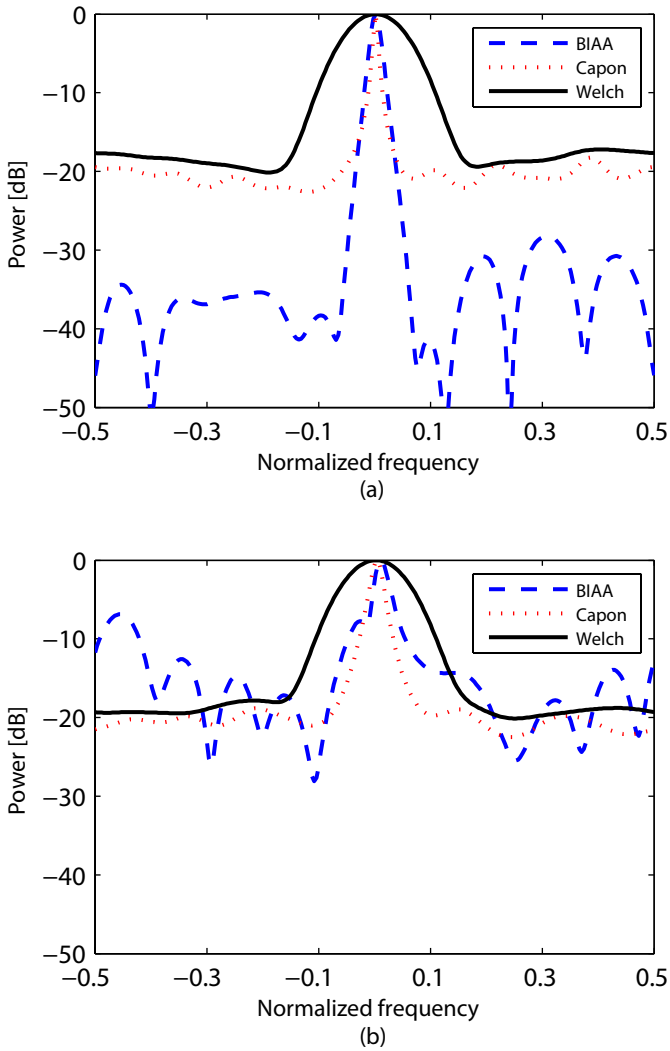

Figure 3.1: PSDs of signals including (a) a single frequency at zero frequency in complex white Gaussian noise (b) band of frequencies with zero mean and $0.01 \times PRF$ bandwidth in complex white Gaussian noise estimated with the Welch's method, Capon and BIAA. $N = 12$

Mean velocity estimation using estimated PSDs

The autocorrelation function with lag one is used for estimation of mean velocities. As the autocorrelation function and the power spectrum are Fourier pairs through the Wiener-Khinchin relation, the autocorrelation function with lag one can be expressed as [3]

$$\hat{R}(1) = \frac{1}{2\pi} \int_{-\pi}^{\pi} \hat{\mathbf{P}}(\omega) e^{i\omega} d\omega, \tag{3.19}$$

where ω is the normalized angular frequency and $\hat{\mathbf{P}}$ is the PSD estimated with a spectral estimator. $R(1)$ is estimated from the PSD after removal of the clutter components, and the mean velocity is found using equation (3.18).

3.2.3 Clutter Filtering

Polynomial regression filters with suitable orders are used for filtering the data used for the autocorrelation method. The clutter is estimated by calculating the least square fitting of the input signal to a set of polynomials, and subtracted from the input signal. The filter can be represented as [2]

$$\mathbf{H} = \mathbf{I} - \sum_{z=0}^{Z} \mathbf{c}_z \mathbf{c}_z^H, \tag{3.20}$$

where $\mathbf{H}$ is the filter matrix and $\mathbf{c}_z$ is a set of basis vectors, such as the Legendre polynomials [2, 20], spanning the Z dimensional clutter space. The filter output will have the form $\mathbf{y} = \mathbf{H}\mathbf{x}_{r,b}$. The order of a polynomial regression filter is defined as Z. The filter orders were chosen manually to give sufficient clutter attenuation for varying packet sizes.

Clutter removal of the data used for estimation of mean velocities using the BIAA and the Capon methods is performed by removing the power spectrum components in a region defined by the frequency f_t

$$\hat{\mathbf{P}}_m(f_k) = \begin{cases} 0, & -f_t \leq f_k \leq f_t \\ \hat{\mathbf{P}}(f_k), & \text{otherwise} \end{cases},$$

where $\hat{\mathbf{P}}_m$ is the modified PSD after clutter removal. Even though this can be seen as an ideal high-pass filter i.e., it has no transition region and eliminates the frequencies below a certain frequency while passing the higher frequencies undistorted, it may introduce errors due the limitations of the PSD estimators such as resolution, bias [21] and high side lobe levels due to strong clutter signal. This filter will be referred to as *threshold filter* and f_t will be referred to as the cut-off frequency of the threshold filter. The variable f_t is set empirically by visually investigating the PSD spectra. It is chosen as the minimum frequency component in the power spectrum which does not include the clutter signal.

Table 3.1: Signal model

Parameter	
Blood signal mean frequency, f_k	0 to 0.5 × PRF
Clutter signal mean frequency	0.005 × PRF
Blood signal RMS bandwidth	$0.1 f_k$
Clutter signal RMS bandwidth	0.0055 × PRF
Blood signal SNR [dB]	5 & 20
Clutter signal SNR [dB]	40

3.2.4 Signal Model and Simulation Setup

Simulated data sets used for evaluation of the methods were generated with a signal model similar to the model presented in [2]. The Doppler spectrum is a sum of three independent components: blood, clutter and noise signals. The simulated blood and clutter signal power spectra are modelled with Gaussian shapes that have mean frequencies and bandwidths given in Table 4.1. The blood signal was generated by calculating the Fourier transform of complex white Gaussian noise of length $512 \times N$ and multiplying it with the power spectrum of the blood signal. The clutter signal was generated following the same steps and added to the blood signal. The resulting signal was transformed to the time domain and complex white Gaussian noise was added yielding a defined SNR. N samples were extracted from this generated time signal to form one ensemble. Fig. 3.2 shows one of the simulated Doppler spectra. The same approach was repeated 262 144 times for each blood velocity. The ensembles were later merged into groups of size 32 ensembles to mimic spatial averaging giving 8192 mean velocity estimations for each mean frequency. The bandwidth of the blood signal changes with the mean velocity of the blood to simulate the transit time effect. Simulations were performed for 64 mean frequencies spaced regularly between 0 and 0.5 normalized velocity with respect to PRF. This was repeated for packet sizes 8, 16 and 32 and for blood SNR values 5 and 20 dB.

3.2.5 Data Acquisition and Processing

The methods were further evaluated using *in-vivo* acquisitions from carotid artery, jugular vein and flow phantom experiment. The data were acquired using plane wave acquisitions to be able to generate results for small and large packet sizes. Table 6.1 summarizes the acquisition parameters for both *in-vivo* and flow phantom recordings. The flow phantom and carotid artery acquisitions were performed using a SonixMDP ultrasound system (Ultrasonix, Richmond, BC, Canada) with a 5 MHz linear probe. The acquisition scheme used was a plane wave transmission steered straight down at 4 kHz PRF.

A flow phantom (Model 524 Peripheral Vascular Doppler Flow Phantom, ATS laboratories, Bridgeport, CT, USA) consisting of a tissue mimicking material

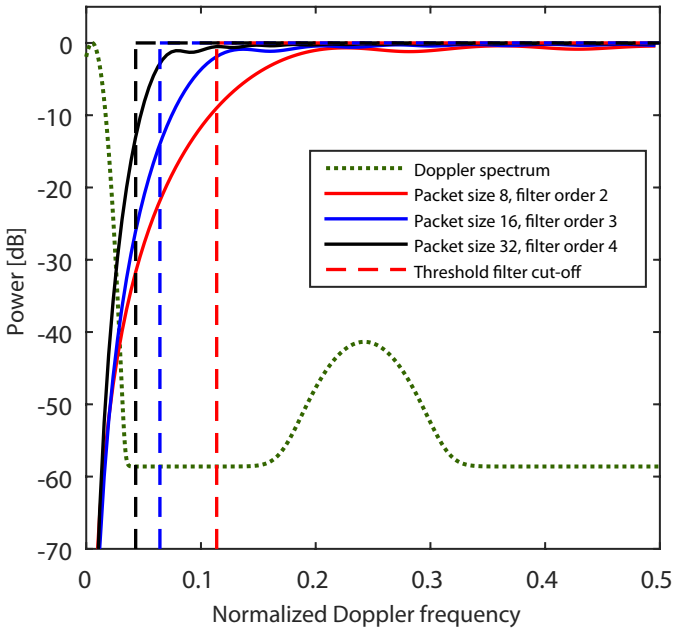

Figure 3.2: An example of simulated theoretical Doppler spectrum and the regression filter frequency responses along with the corresponding threshold filter cut-off frequencies (f_t) used in the simulations. The frequency responses and the threshold filter cut-offs for the same packet size are plotted in same color. The blood signal SNR and the clutter signal SNR are 5 and 40 dB respectively.

Table 3.2: Acquisition setup and processing

Parameter	flow phantom	carotid artery	jugular vein
Center frequency [MHz]	5	5	6.25
Pulse periods	2.5	2.5	2.5
PRF [kHz]	4	4	6
F-number	1.4	1.4	1.4
Packet size, N	8	12	12
Number of frequency points, K	256	256	256
Regression filter order	1	2	2
Threshold filter cut-off [cm/s]	3.9	4.3	5.3

surrounding a 6 mm inner diameter straight tube which simulates a vessel was used for the recording. The PhysioPulse 100 flow system (Shelley Medical Image Technologies,

London, ON, Canada), pumping blood mimicking fluid, was connected to the flow phantom to form a flow loop. The system was set to give 1 Hz sinusoidal flow.

A Verasonics ultrasound system (Verasonics Inc., Redmond, WA, USA) used for a combined jugular vein and carotid artery data acquisition. L11-4V linear probe with a plane wave acquisition scheme is used for the recording. The system was set to generate straight down steered plane waves at 6 kHz PRF.

The *in-vivo* data sets were acquired on the common carotid artery of a healthy 28 years old female volunteer and jugular vein and common carotid artery of a healthy 30 years old male volunteer. The jugular vein recording was performed in Trendelenburg position in order to get decreased velocity flow in the vein.

The PSD estimations were done on 256 frequency points. Spatial averaging region for each mean velocity estimation was chosen to be 8×8 lateral and radial spatial samples ($R = 8, B = 8$). This corresponds to 0.5mm $\times$ 1.2mm, 0.9mm $\times$ 0.9mm and 1.3mm $\times$ 1.2mm spatial region for carotid artery, jugular vein and flow phantom recordings respectively. $R = 8, B = 8$ was chosen to ensure well conditioned covariance matrices and low variance for the velocity estimates for all recordings.

3.3 Results

Performance analysis was done for the three methods using computer simulations for different packet size and blood SNR scenarios. The flow phantom and *in-vivo* acquisitions were used for comparison of the Capon, BIAA and the autocorrelation methods for relatively small packet sizes. The simulation results along with the factors that affect the estimation quality in the proposed methods are given in this section.

3.3.1 Simulations

The simulations were performed for 8, 16 and 32 ensemble lengths and 5 and 20 dB blood SNRs while the clutter signal SNR is 40 dB for all cases. The SNR is defined as the total signal power to total noise power ratio for both clutter and blood signals. Simulated data sets were generated with the presented signal model and the mean velocity estimations were performed as described in section 3.2.2.

The polynomial regression filter frequency response is dependent on the filter order and the ensemble length. Therefore, the filter order is changed with the ensemble length to keep the stop band approximately the same. Fig. 3.2 shows the polynomial regression filter frequency responses and threshold filter cut-off frequencies used for each ensemble length. The threshold filter cut-off frequencies depend on the resolution of the spectral estimators for different ensemble lengths. For ensemble lengths of 8, 16 and 32, the f_t intersects the corresponding filter frequency responses at -9, -14 and -13 dB attenuation respectively.

The BIAA algorithm was terminated after 8 iterations on average and the maximum number of iterations required was 13.

Fig. 3.3 shows the bias and the standard deviation as a function of mean blood frequency normalized with respect to PRF when $N = 8$ and the blood SNR 5 dB. Mean

velocity estimation using the BIAA spectrum has the largest standard deviation among the three mean velocity estimation methods. The Capon and the autocorrelation methods have similar performance for high velocities. However, the autocorrelation method has larger positive bias for lower velocities due to the signal loss in the stop and the transition band of the polynomial regression filter.

The vertical dashed lines show the cut-off frequencies used for the adaptive spectral estimation methods. Also, the regression filter frequency responses are added to the figures to indicate the transition and the passband region of these filters for better interpretation of the results. The shaded areas in the figures indicate the region between the threshold filter cut-off and -3 dB cut-off frequency of the regression filter. In this region, there is a clear reduction in bias by utilizing Capon or BIAA mean velocity estimation methods compared to the autocorrelation method. In the same region, the standard deviation is low and similar for the Capon and autocorrelation method, whereas it is substantially larger for the BIAA method.

Fig. 3.4 shows the simulation results for $N = 8$ and 20 dB blood SNR. All methods have lower bias and standard deviation compared to the 5 dB SNR case. In addition, the difference in bias between the adaptive spectral estimation methods and the autocorrelation method decreases when the SNR is increased. Standard deviation of BIAA method improves considerably while it still has the largest standard deviation compared to other methods. As in the 5 dB case, the difference in bias between the adaptive spectral estimation and the autocorrelation methods is highest for velocities in the transition region of the polynomial regression filter.

Fig. 3.5 shows the bias and standard deviation for $N = 16$ and blood SNR 5 dB. The region where there is difference in bias between the methods decreases with increasing packet size as the transition region of the polynomial regression filters become narrower. Also f_t can be set to a lower value. This is due to the improved resolution of spectral estimation methods with increasing ensemble length. Compared to $N = 8$ and SNR 5 dB, it can be seen that the standard deviation of the methods decreases with the increased ensemble length.

Increasing the blood signal SNR while keeping $N = 16$ improves the estimates further. As can be seen in Fig. 3.6, the methods have similar standard deviation and bias for low and high velocities.

Tables 5.3 and 3.4 summarize the simulation results for the 4 kHz PRF, 5 MHz center frequency and $c = 1540$m/s imaging scenario. The mean absolute standard deviation and the mean absolute bias are calculated between the threshold filter cut-off frequency and -3 dB cut-off frequency of the regression filter which corresponds to the shaded area in the figures 3.3 - 3.6. As can be seen from the tables, all methods have similar performance for high blood SNR and ensemble lengths.

Fig. 3.7 and Fig. 3.8 provide insight into two factors that limit the ability of spectral estimation methods to separate clutter and blood signals. Fig. 3.7 depicts the PSDs estimated with the Capon estimator where $N = 8$ and $N = 16$. The spectral resolution of the Capon estimator deteriorates when the packet size is decreased from 16 to 8 samples. The increased spectral width of the clutter and blood signals at 8 samples makes separation of the clutter difficult, and different threshold values (f_t) are required to avoid bias in mean velocity estimates.

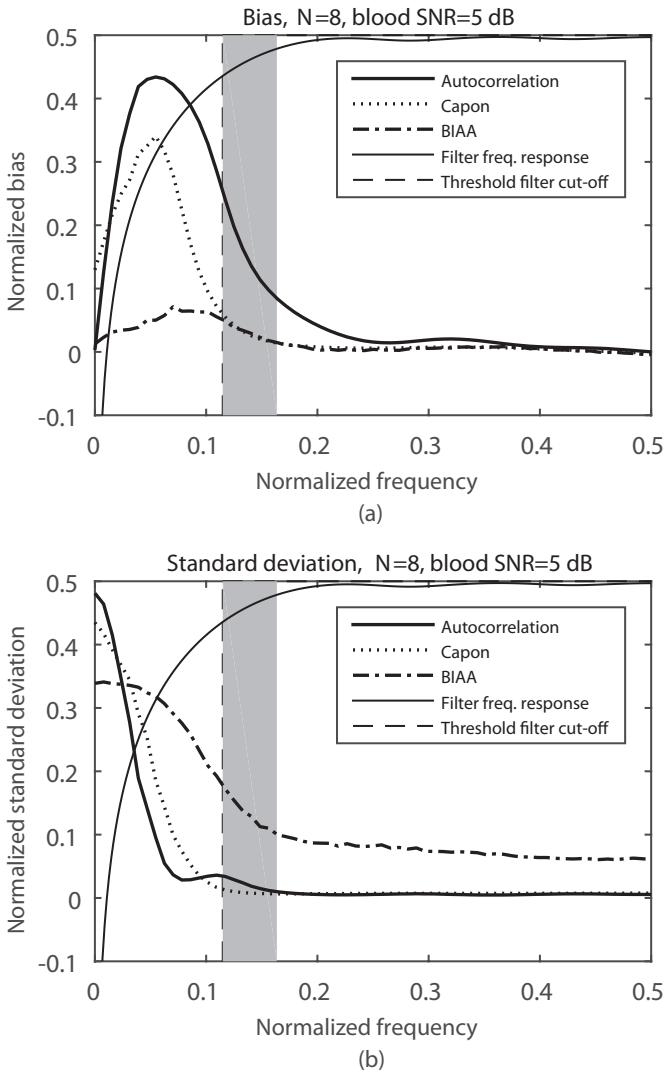

Figure 3.3: a) Bias and b) standard deviation of the methods for packet size $N = 8$ and 5 dB blood SNR. The shaded area corresponds to the spectral region between the threshold filter cut-off and -3 dB cut-off frequency of the regression filter.

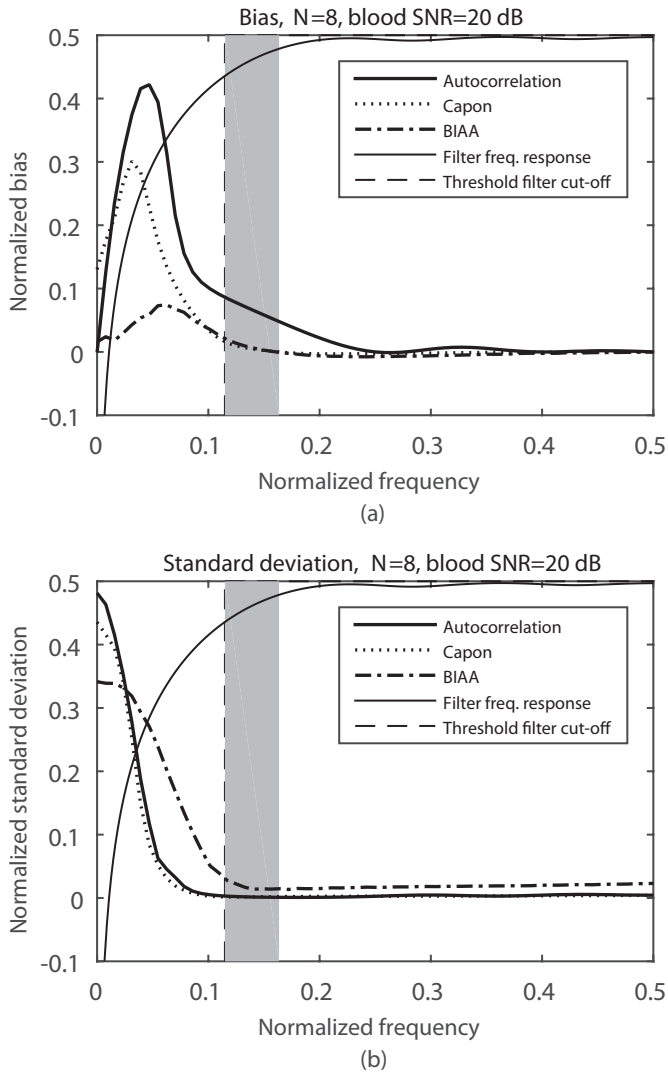

Figure 3.4: a) Bias and b) standard deviation of the methods for packet size $N = 8$ and 20 dB blood SNR. The shaded area corresponds to the spectral region between the threshold filter cut-off and -3 dB cut-off frequency of the regression filter.

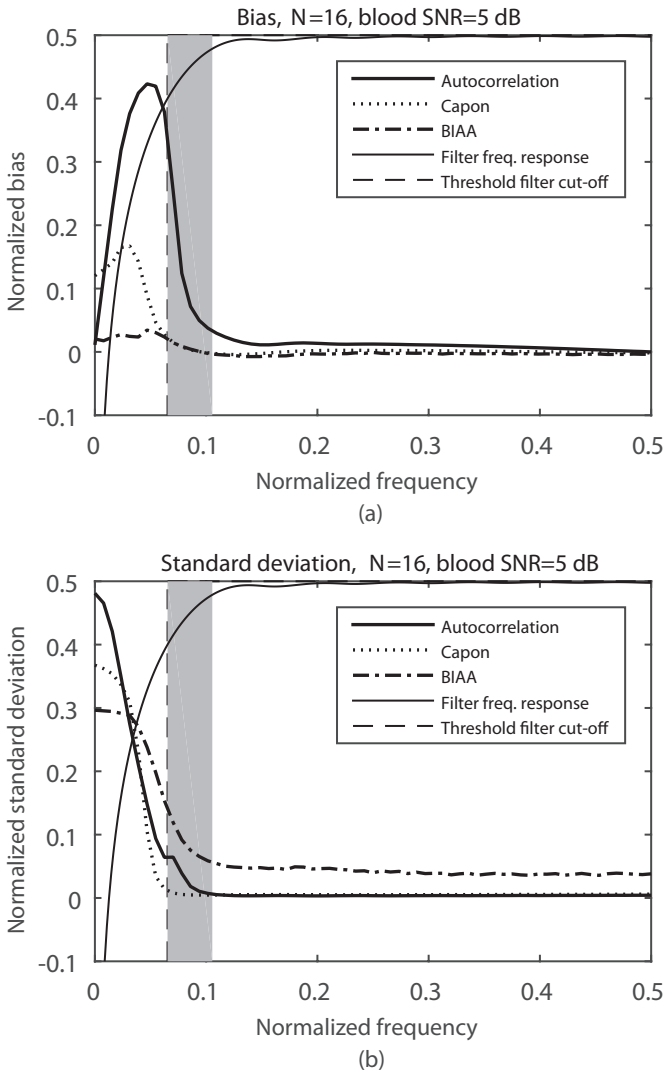

Figure 3.5: a) Bias and b) standard deviation of the methods for packet size $N = 16$ and 5 dB blood SNR. The shaded area corresponds to the spectral region between the threshold filter cut-off and -3 dB cut-off frequency of the regression filter.

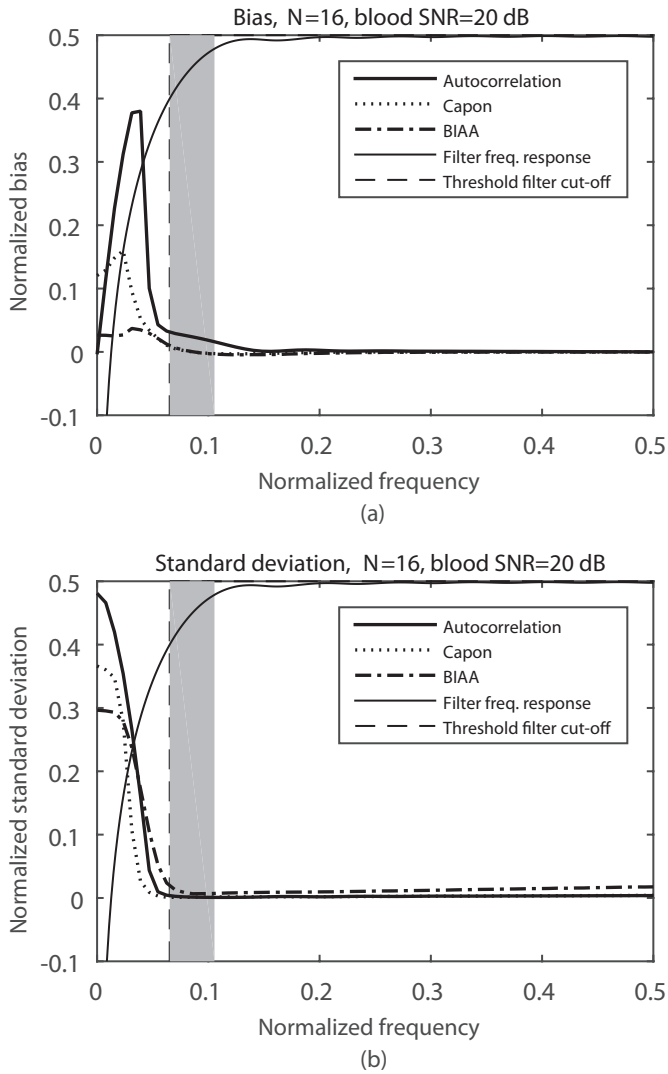

Figure 3.6: a) Bias and b) standard deviation of the methods for packet size $N = 16$ and 20 dB blood SNR. The shaded area corresponds to the spectral region between the threshold filter cut-off and -3 dB cut-off frequency of the regression filter.

Table 3.3: Mean absolute bias [cm/s]

SNR \ Ensemble length	8	16	32
5 dB	A: 8.1 B: 1.6 C: 1.5	A: 3.8 B: 0.3 C: 0.2	A: 0.9 B: 0.1 C: 0.1
20 dB	A: 3.8 B: 0.4 C: 0.3	A: 1.2 B: 0.14 C: 0.11	A: 0.4 B: 0.07 C: 0.06

Table 3.4: Mean absolute standard deviation [cm/s]

SNR \ Ensemble length	8	16	32
5 dB	A: 1.1 B: 7.6 C: 0.5	A: 0.9 B: 4.2 C: 0.3	A: 0.3 B: 2.4 C: 1.5
20 dB	A: 0.09 B: 0.1 C: 0.1	A: 0.07 B: 0.05 C: 0.08	A: 0.04 B: 0.23 C: 0.17

A: Autocorrelation, B: BIAA, C: Capon

Fig. 3.8 shows three Capon PSDs estimated where $N = 12$. The blood and clutter signal parameters are the same as in Fig. 3.7 except that the clutter SNR is varying between 20 and 60 dB. A similar effect to that of the packet size can be seen here. The separation of the clutter and the blood signal deteriorates with increasing clutter-to-blood power ratio due to the increased side lobe levels. This narrows the velocity span where the blood signal velocity can be estimated without clutter bias.

3.3.2 In-vivo

The common carotid artery and the combined jugular vein and carotid artery acquisitions were used for further evaluation of the methods. Fig. 3.9 shows color flow images and spectra generated using $N = 12$ and polynomial regression filter order 2 for the autocorrelation method. The threshold filter cut-off was set to 5.3 cm/s and intersects the frequency response of the regression filter at -10 dB attenuation.

In figures 3.9,3.11 and 3.13, periodograms are estimated with Capon and BIAA estimators from sample volumes shown as rectangles in the corresponding color flow

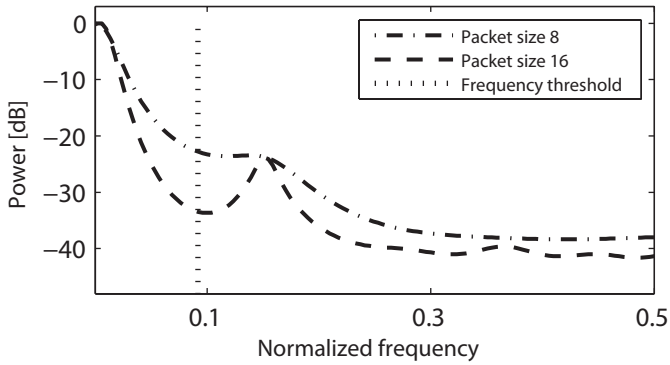

Figure 3.7: Capon PSD estimates with packet size 8 and 16. The signal consists of 5 dB SNR blood signal at $0.15 \times PRF$ center frequency and $0.01 \times PRF$ bandwidth and 30 dB SNR clutter signal at zero center frequency and $0.01 \times PRF$ bandwidth in complex white Gaussian noise.

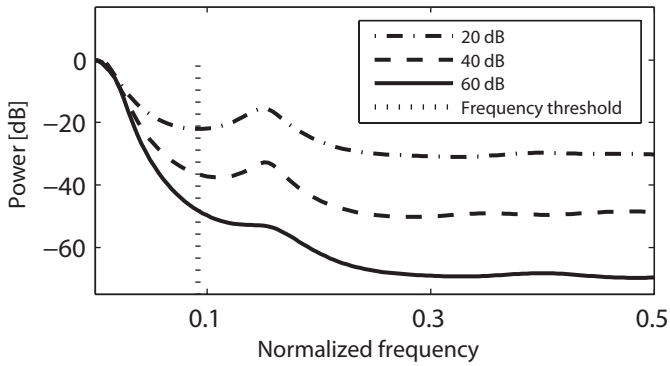

Figure 3.8: PSD estimates with the Capon estimator with $N = 12$. The signal consists of 5 dB SNR blood signal at $0.15 \times PRF$ center frequency and $0.01 \times PRF$ bandwidth and clutter signal at zero center frequency, $0.01 \times PRF$ bandwidth and varying SNR between 20 - 60 dB in complex white Gaussian noise.

images. The sample volumes have the same dimensions as the averaging area used for the corresponding velocity profile estimation and color flow image generation. Vertical lines on the periodograms indicate the time instants at which the color flow images are generated.

The filter used for the autocorrelation method removes low velocity blood signals close to the walls of the vein causing signal dropouts. The Capon and the autocorrelation methods yield similar mean velocity estimates with similar variance for the carotid artery. The BIAA method has higher variance in both carotid artery

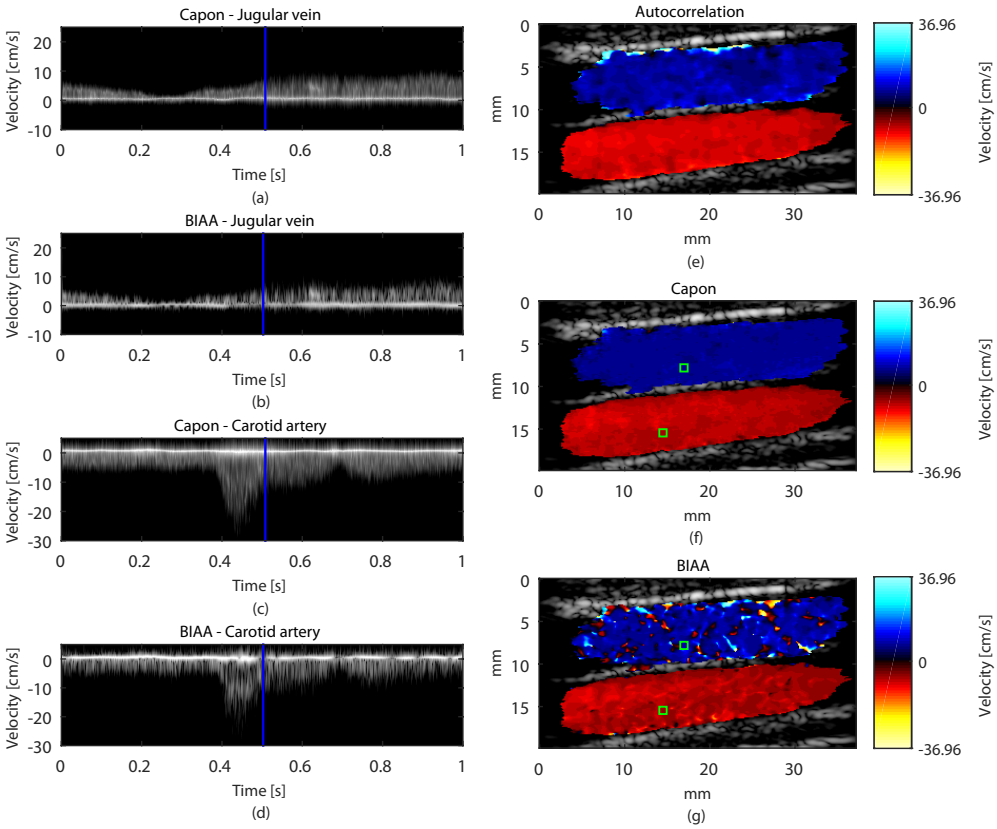

Figure 3.9: Example periodograms estimated with Capon from jugular vein (a) and carotid artery (c) and BIAA from jugular vein (b) and carotid artery (d). The dynamic range used is 50 dB. Color flow images are generated from the vein and artery using the autocorrelation method with polynomial regression filter (e) and proposed Capon (f) and BIAA (g) methods. The vertical lines in periodograms show the time instant where the color flow images are generated and the rectangles in color flow images corresponds to the sample volumes where the PSDs in periodograms are estimated from. $N = 12$.

and jugular vein compared to other methods. The variance is higher in the jugular vein due to presence of lower velocities.

Fig. 3.10 shows the flow profiles estimated with the three methods using the common carotid artery acquisition. In total, 109 velocity profiles were estimated along the artery where each of them had 62 points. The ensemble length was $N = 12$ and the regression filter order was 2. The threshold filter cut-off intersects the filter frequency response where the filter had -11 dB attenuation. In addition, an autocorrelation estimate with 32 packet size included in the estimations as a reference. The regression

filter order used for the reference velocity profile estimation was 5. The peak systolic velocity in the center of the artery was found to be around 35 cm/s without angle correction.

Fig. 3.10 shows that the autocorrelation method yields higher while BIAA yields lower velocity estimates around the center of the artery and close to the artery walls when compared to the reference velocity profile. The Capon method yields similar velocity estimates to the reference velocity profile. The difference is approximately 1 cm/s for the blood velocities in the center.

Similar to Fig. 3.9, Fig. 3.11 shows the color flow images generated using the autocorrelation, Capon and BIAA methods and the Capon and BIAA periodogram estimates. The packet size and the filters are the same as used in *in-vivo* velocity profile estimation. The color flow images show a part of the artery where the flow profiles are estimated. It can be seen that the autocorrelation method gives estimates with higher variance for the lower velocities around the artery walls compared to the Capon method. BIAA method has largest variance especially for low velocities and shows signal dropouts.

3.3.3 Flow phantom

Velocity profiles across the straight tube were estimated using the autocorrelation and the Capon methods. The packet size is 8 and polynomial regression filter order 1 is used. The filter frequency response and f_t intersects where the filter has -11 dB attenuation. In addition, an autocorrelation estimate with ensemble length 32 and filter order 3 is included as a reference.

Fig. 3.12 shows the mean and the standard deviation of the estimated flow profiles. 86 flow profiles were estimated along the phantom tube. There are 32 points in each velocity profile where each of them are estimated using 1.3mm $\times$ 1.2mm spatial averaging region in radial and lateral directions respectively. The methods give similar estimates for high velocities which are present in the middle of the tube. For lower velocities, the autocorrelation method with ensemble length 8 has larger standard deviation than the Capon method and the mean velocity difference to the reference velocity profile is smaller for the Capon method. The difference between the Capon and the autocorrelation method mean velocity estimates is around 4 cm/s around the tube walls. The Capon method gives similar estimates to the reference for low and high blood velocities.

Fig. 3.13(b) and 3.13(c) show the color flow images that are generated with the autocorrelation and the Capon method respectively. The same clutter filter parameters as used for the velocity profile estimation are used. As in Fig. 3.12, the methods give similar estimates in the center of the tube, whereas the Capon method improves the display of the lower velocities closer to the tube walls.

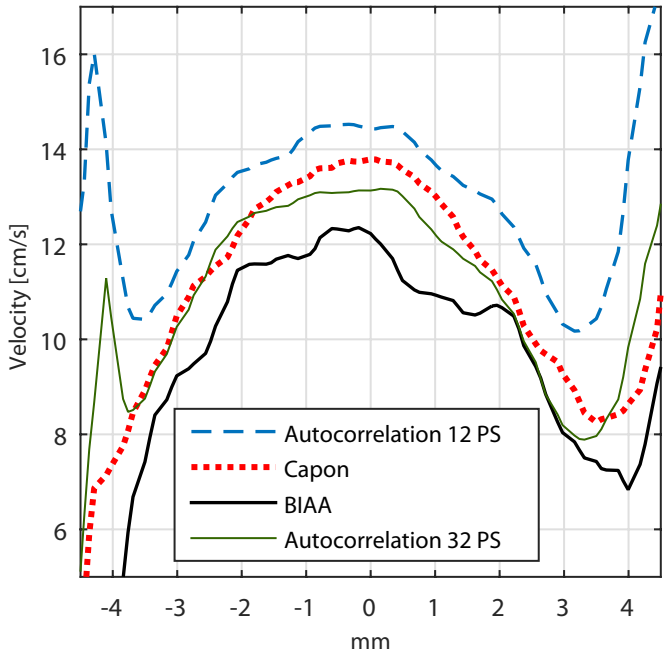

Figure 3.10: Estimated *in-vivo* velocity profiles using the autocorrelation method with packet sizes 12 and 32 and the Capon and BIAA methods with packet size 12.

3.4 Discussion

Two data adaptive spectral estimation methods, the BIAA and Capon, has been evaluated for improving the estimation of low blood velocities in CFI. While the adaptive spectral estimators have previously been examined for their use in PW-Doppler, their potential use for clutter rejection and mean velocity estimation in CFI was investigated in this work. In particular, the performance of the methods were evaluated using very short ensemble sizes used in conventional CFI, replacing temporal with spatial information to achieve required correlation matrix estimates. The methods were compared to the conventional autocorrelation method with polynomial regression filtering, using simulated data sets with different packet sizes and SNRs, as well as flow phantom and *in-vivo* acquisitions.

Results showed that the Capon method can isolate the clutter sufficiently even for very small packet sizes ($N = 8$) and the Capon and BIAA methods can provide improved mean velocity estimates over the autocorrelation method for lower velocities in terms of bias. All methods provide comparable estimates for large packet sizes and high SNR, e.g. $N = 16$, 20 dB SNR.

It was further demonstrated with *in-vivo* and flow phantom acquisitions that the Capon adaptive spectral estimator may improve estimation of low blood velocities close to the artery walls. It was shown that the bias is similar to that of autocorrelation

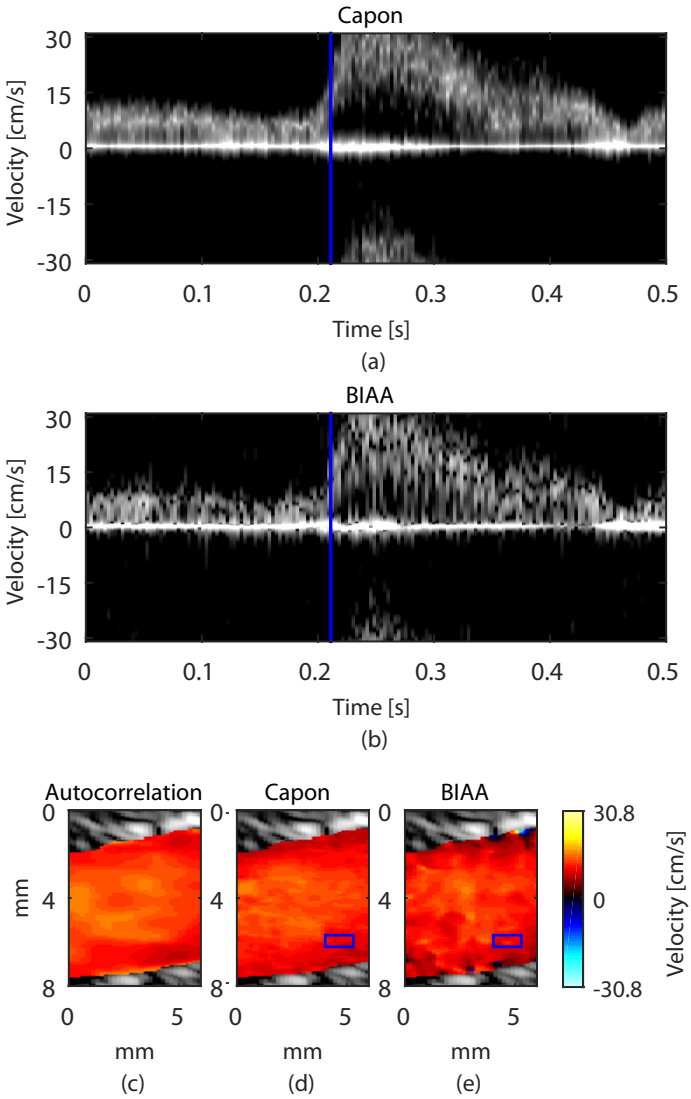

Figure 3.11: Example of periodograms estimated with the Capon (a) and the BIAA (b) estimators and displayed with 40 dB dynamic range. The autocorrelation (c), the Capon (d) and the BIAA (e) color flow images generated using *in-vivo* data. The vertical lines in (a) and (b) show the time instant where the color flow images are generated. The rectangles in the color flow images correspond to the sample volume where the PSDs in (a) and (b) are estimated from. $N = 12$.

method with 32 packet size. This can be useful for the applications where the low velocities are of importance, e.g. volume flow and shear stress estimation. The color

flow images generated with the Capon method display flow profiles with lower variance and bias compared to the autocorrelation method along the direction of the flow and across the tube and the artery.

Simulation results showed that BIAA and Capon estimators introduced similar bias for the velocities higher than the threshold filter cut-offs for different packet size and SNR scenarios. BIAA has been shown to give improved estimates of the power spectrum in terms of frequency resolution and side lobes [14], [18] and can achieve significantly lower side lobe level than the Capon method for single frequency estimates as shown in Fig. 3.1. However, the simulation results show that the BIAA suffers from high standard deviation for small packet sizes and low SNR when signals are not narrow band. However, it performs equally good for relatively larger packet sizes and blood SNR, e.g., $N = 16$, 20 dB SNR.

Blood and clutter bandwidth, velocity, SNR and the clutter-to-blood-signal power ratio are important factors that determine the improvement of adaptive spectral estimation methods over the conventional autocorrelation method. The adaptive methods outperform the conventional method when the blood signal is in the transition band of the polynomial regression filters. Suppression of clutter signals with high velocities and large bandwidth requires higher filter orders which alters the width of the transition band [22]. In addition, the polynomial regression filter introduces additional bias due to its non-zero phase response [20]. However, this effect accounts for relatively small part of the bias estimates given here. The performance of the adaptive spectral estimation methods on the other hand depends on the ability to separate the clutter and blood spectral content, and the sufficient suppression of clutter spectral side lobes below the blood spectral SNR. High clutter-to-blood-signal ratio deteriorates the clutter isolation as shown in Fig. 3.8 and can introduce negative bias to the estimates.

The clutter isolation is also affected by the packet size. Small packet size results in decreased frequency resolution and potentially biased estimates. The effect becomes more apparent for high clutter-to-blood-signal ratios. Too small packet sizes, e.g. smaller than 6, results in a situation where blood velocities can be estimated accurately only in a narrow velocity span. This shows that these methods are not suitable for CFI with very small packet sizes.

The methods were evaluated using plane wave acquisitions where the whole region of interest can be imaged with single transmission. The motivation for this was to be able to generate results for both low and high packet sizes from the same data. For a high-end system capable of software beamforming, one could also utilize plane wave acquisition which allows for high frame rates. Therefore, longer ensemble lengths can be attained without losing the temporal resolution [23]. However, these methods are limited to depths where desirable SNR can be obtained with plane waves and transducer geometry and setup allows for plane wave generation [15]. The low SNR problem can be alleviated using coherent compounding although this introduces additional bias to velocity estimates [24]. Alternatively, using slightly broader but focused transmit beams and 2-4 parallel receive beams [25] could also be used to achieve spatial averaging while keeping the SNR sufficient [15].

The data adaptive spectral estimation methods may require a larger spatial

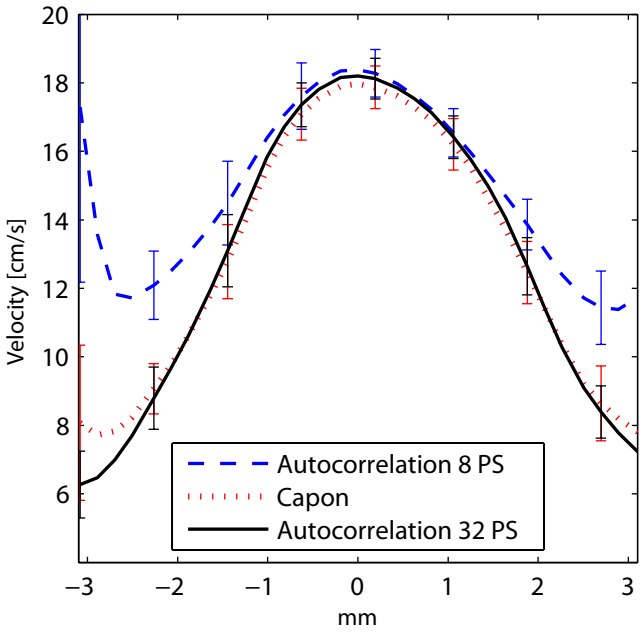

Figure 3.12: Estimated flow phantom velocity profiles using the autocorrelation method with 8 and 32 and the Capon method with 8 packet size.

averaging region than used for the autocorrelation method to give robust estimates depending on the packet size. Temporal averaging is not used in this work in order to keep the frequency resolution sufficient as small packet sizes in duplex acquisitions are of interest. This results in increased dependency on spatial averaging and reduces the resolution of the color flow images. Therefore, there is a trade-off between the spatial resolution of the images and the robustness of the mean velocity estimates. Using a small averaging region gives estimates with higher standard deviation. It has been observed that using number of spatial points equal to the packet size yields estimates with higher standard deviation compared to the autocorrelation method when spatial points are uncorrelated. The methods will require a larger averaging region to give robust estimates when there is correlation between the spatial points. Diagonal loading can be used for increasing the robustness of the Capon estimates [15] for small averaging regions. However, this reduces the frequency resolution, and the gain in estimator performance may be lost.

Another disadvantage of the adaptive methods is that they are much more computationally demanding. An overview of the computational complexity of the Capon and the BIAA spectral estimators is given in [10] and [26] respectively. The main factor that makes the methods computationally expensive is the matrix inversion operation. Therefore, the BIAA is more computationally expensive due to multiple iterations. Although efficient algorithms have been suggested for BIAA estimator

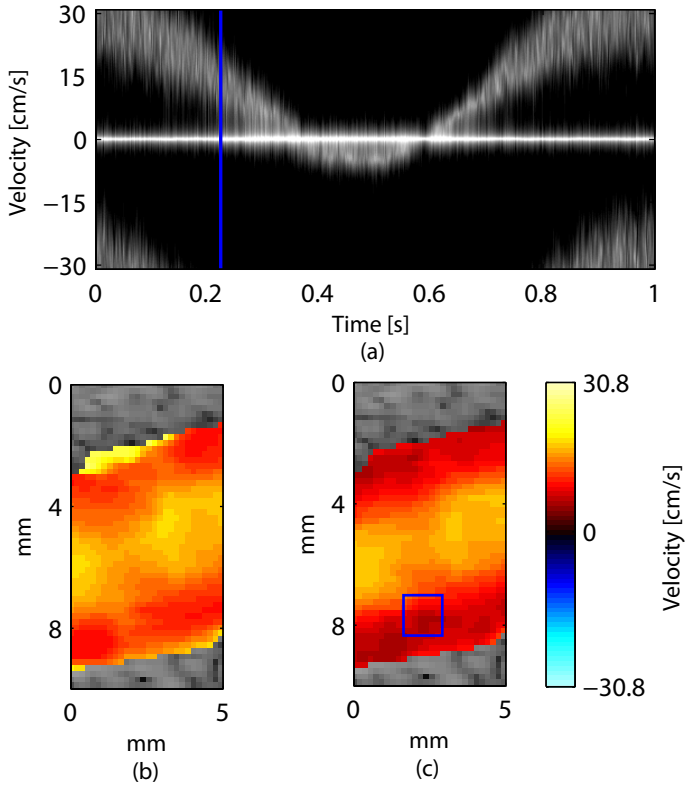

Figure 3.13: (a) An example of periodogram estimated with the Capon estimator and displayed with 40 dB dynamic range. The autocorrelation (b) and the Capon (c) color flow images generated using flow phantom data. The vertical line in (a) shows the time instant where the color flow images are generated and the rectangle in (c) corresponds to the sample volume where the PSDs in (a) are estimated from. $N = 8$.

in [26] and [27], the complexity is still not comparable to the autocorrelation method. In case the difference in performance is marginal, the autocorrelation estimator is preferred due to its simpler implementation and increased robustness for low SNR.

The cut-off frequencies of the threshold filter was chosen manually to minimize the clutter bias on the velocity estimates. An adaptive filtering scheme can be developed to set the cut-off frequency based on defined criteria to improve the velocity estimates and standardization of the filtering process to make it user independent.

The adaptive spectral estimation methods enable mean velocity estimation with small packet sizes as a result of their improved side lobe levels and frequency resolution. Another way of looking at this is that the PSDs can be estimated using color-Doppler data. This can be utilized to display the Doppler power spectrum anywhere on the color flow image to aid improvement of imaging workflow and ease of use. Another advantage of having the spectral content available would be to provide maximum

velocity maps in addition to mean velocity by extracting the maximum velocities from the estimated spectra [28]. Maximum velocities are used for diagnosis of diseases such as carotid artery stenosis [29] and estimation of Doppler indices such as pulsatility index [30].

3.5 Conclusions

The estimation of low blood velocities corrupted by clutter filters can be improved by using data adaptive spectral estimation methods for mean velocity estimation. It is shown that by utilizing these spectral estimators it is possible to achieve lower bias and standard deviation for velocity estimates in a region between the threshold filter cut-off and the passband of conventional clutter filters which can amount to 81% lower bias for 5 dB blood SNR and 8 packet size.

The Capon method improves the estimation of low blood velocities even for small packet sizes. Therefore, the Capon estimator can be considered as a candidate for improving low velocity estimation in interleaved B-mode and CFI acquisitions.

Acknowledgment

This work was supported by the UMOJA - Ultrasound for midwives in rural areas (Helse Midt-Norge HMF) project. The authors would like to thank Lars Mølgaard Saxhaug for the jugular vein data acquisition and Tonje D. Fredriksen for the acquisition of the flow phantom data.

References

[1] C. Kasai, K. Namekawa, A. Koyano, and R. Omoto, "Real-time two-dimensional blood flow imaging using an autocorrelation technique," *IEEE Trans. Sonics Ultrason*, vol. 32, no. 3, pp. 458–464, 1985.

[2] S. Bjaerum, H. Torp, and K. Kristoffersen, "Clutter filter design for ultrasound color flow imaging," *Ultrasonics, Ferroelectrics, and Frequency Control, IEEE Transactions on*, vol. 49, no. 2, pp. 204–216, 2002.

[3] J. A. Jensen, *Estimation of blood velocities using ultrasound: A signal processing approach*. Cambridge University Press, 1996.

[4] P. D. Welch, "The use of fast Fourier transform for the estimation of power spectra: A method based on time averaging over short, modified periodograms," *IEEE Transactions on audio and electroacoustics*, vol. 15, no. 2, pp. 70–73, 1967.

[5] P. Stoica and R. L. Moses, *Spectral analysis of signals*. Pearson/Prentice Hall Upper Saddle River, NJ, 2005.

[6] P. Vaitkus and R. Cobbold, "A comparative study and assessment of Doppler ultrasound spectral estimation techniques part I: Estimation methods," *Ultrasound in Medicine & Biology*, vol. 14, no. 8, pp. 661–672, 1988.

[7] P. Vaitkus, R. Cobbold, and K. Johnston, "A comparative study and assessment of doppler ultrasound spectral estimation techniques part II: Methods and results," *Ultrasound in medicine & biology*, vol. 14, no. 8, pp. 673–688, 1988.

[8] E. D. Übeylı and I. Güler, "Spectral analysis of internal carotid arterial Doppler signals using FFT, AR, MA, and ARMA methods," *Computers in biology and medicine*, vol. 34, no. 4, pp. 293–306, 2004.

[9] J. Capon, "High-resolution frequency-wavenumber spectrum analysis," *Proceedings of the IEEE*, vol. 57, no. 8, pp. 1408–1418, 1969.

[10] F. Gran, A. Jakobsson, and J. A. Jensen, "Adaptive spectral Doppler estimation," *Ultrasonics, Ferroelectrics, and Frequency Control, IEEE Transactions on*, vol. 56, no. 4, pp. 700–714, 2009.

[11] J. Li and P. Stoica, "An adaptive filtering approach to spectral estimation and SAR imaging," *Signal Processing, IEEE Transactions on*, vol. 44, no. 6, pp. 1469–1484, 1996.

[12] K. L. Hansen, F. Gran, M. M. Pedersen, I. K. Holfort, J. A. Jensen, and M. B. Nielsen, "In-vivo validation of fast spectral velocity estimation techniques," *Ultrasonics*, vol. 50, no. 1, pp. 52–59, 2010.

[13] T. Yardibi, J. Li, P. Stoica, M. Xue, and A. B. Baggeroer, "Source localization and sensing: A nonparametric iterative adaptive approach based on weighted least squares," *Aerospace and Electronic Systems, IEEE Transactions on*, vol. 46, no. 1, pp. 425–443, 2010.

[14] E. Gudmundson, A. Jakobsson, J. A. Jensen, and P. Stoica, "Blood velocity estimation using ultrasound and spectral iterative adaptive approaches," *Signal Processing*, vol. 91, no. 5, pp. 1275–1283, 2011.

[15] I. Ekroll, H. Torp, and L. Lvstakken, "Spectral Doppler estimation utilizing 2-D spatial information and adaptive signal processing," *Ultrasonics, Ferroelectrics, and Frequency Control, IEEE Transactions on*, vol. 59, pp. 1182–1192, June 2012.

[16] W.-J. Lee, J.-S. Chu, C.-S. Huang, M.-F. Chang, K.-J. Chang, and K.-M. Chen, "Breast cancer vascularity: color Doppler sonography and histopathology study," *Breast cancer research and treatment*, vol. 37, no. 3, pp. 291–298, 1996.

[17] P. J. Brands, A. P. Hoeks, L. Hofstra, and R. S. Reneman, "A noninvasive method to estimate wall shear rate using ultrasound," *Ultrasound in medicine & biology*, vol. 21, no. 2, pp. 171–185, 1995.

[18] S. Ricci, "Adaptive spectral estimators for fast flow-profile detection," *Ultrasonics, Ferroelectrics, and Frequency Control, IEEE Transactions on*, vol. 60, no. 2, pp. 421–427, 2013.

[19] K. W. Ferrara, V. R. Algazi, and J. Liu, "The effect of frequency dependent scattering and attenuation on the estimation of blood velocity using ultrasound," *Ultrasonics, Ferroelectrics, and Frequency Control, IEEE Transactions on*, vol. 39, no. 6, pp. 754–767, 1992.

[20] H. Torp, "Clutter rejection filters in color flow imaging: A theoretical approach," *Ultrasonics, Ferroelectrics, and Frequency Control, IEEE Transactions on*, vol. 44, no. 2, pp. 417–424, 1997.

[21] P. Stoica, A. Jakobsson, and J. Li, "Matched-filter bank interpretation of some spectral estimators," *Signal Processing*, vol. 66, no. 1, pp. 45–59, 1998.

[22] A. P. Kadi and T. Loupas, "On the performance of regression and step-initialized IIR clutter filters for color Doppler systems in diagnostic medical ultrasound," *Ultrasonics, Ferroelectrics, and Frequency Control, IEEE Transactions on*, vol. 42, no. 5, pp. 927–937, 1995.

[23] J. Bercoff, G. Montaldo, T. Loupas, D. Savery, F. Mézière, M. Fink, and M. Tanter, "Ultrafast compound Doppler imaging: providing full blood flow characterization," *Ultrasonics, Ferroelectrics, and Frequency Control, IEEE Transactions on*, vol. 58, no. 1, pp. 134–147, 2011.

[24] I. K. Ekroll, M. M. Voormolen, O. K. V. Standal, J. M. Rau, and L. Lovstakken, "Coherent compounding in Doppler imaging," *IEEE Transactions on Ultrasonics, Ferroelectrics, and Frequency Control*, vol. 62, pp. 1634–1643, Sept 2015.

[25] T. Hergum, T. G. Bjåstad, L. Løvstakken, K. Kristoffersen, and H. Torp, "Reducing color flow artifacts caused by parallel beamforming," in *Ultrasonics Symposium (IUS), 2009 IEEE International*, pp. 1367–1370, IEEE, 2009.

[26] A. Jakobsson, G.-O. Glentis, and E. Gudmundson, "Computationally efficient time-recursive IAA-based blood velocity estimation," *Signal Processing, IEEE Transactions on*, vol. 60, no. 7, pp. 3853–3858, 2012.

[27] G.-O. Glentis and A. Jakobsson, "Efficient implementation of iterative adaptive approach spectral estimation techniques," *Signal Processing, IEEE Transactions on*, vol. 59, no. 9, pp. 4154–4167, 2011.

[28] I. K. Ekroll, T. Dahl, H. Torp, and L. Løvstakken, "Combined vector velocity and spectral Doppler imaging for improved imaging of complex blood flow in the carotid arteries," *Ultrasound in medicine & biology*, vol. 40, no. 7, pp. 1629–1640, 2014.

[29] E. G. Grant, C. B. Benson, G. L. Moneta, A. V. Alexandrov, J. D. Baker, E. I. Bluth, B. A. Carroll, M. Eliasziw, J. Gocke, B. S. Hertzberg, *et al.*, "Carotid artery stenosis: Gray-scale and Doppler US diagnosissociety of radiologists in ultrasound consensus conference 1," *Radiology*, vol. 229, no. 2, pp. 340–346, 2003.

[30] K. Nicolaides, G. Rizzo, K. Hecher, and R. Ximenes, "Doppler in obstetrics," *London: The Fetal Medicine Foundation*, 2002.

Chapter 4

Adaptive Spectral Envelope Estimation for Doppler Ultrasound

Aditi Kathpalia[1] ,Yücel Karabiyik[1], Sturla Eik-Nes[1], Eva Tegnander[1], Ingvild Kinn Ekroll[1,2], Gabriel Kiss[1], Hans Torp[1],
[1] Dept. of Circulation and Medical Imaging, NTNU, Norway
[2] St. Olavs Hospital, Trondheim University Hospital, Norway

Estimation of accurate maximum velocities and spectral envelope in ultrasound Doppler blood flow spectrograms are both essential for clinical diagnostic purposes. However, obtaining accurate maximum velocity is not straightforward due to intrinsic spectral broadening and variance in the power spectrum estimate. The method proposed in this work for maximum velocity point detection has been developed by modifying an existing method — Signal Noise Slope Intersection (SNSI), incorporating in it steps from an altered version of another method called Geometric Method (GM). Adaptive noise estimation from the spectrogram ensures that a smooth spectral envelope is obtained post detection of these maximum velocity points. The method has been tested on simulated Doppler signal with scatterers possessing a parabolic flow velocity profile constant in time, steady and pulsatile string phantom recordings as well as *in vivo* recordings from uterine, umbilical, carotid and subclavian arteries. Results from simulation experiments indicate a bias of less than 2.5% in maximum velocities when estimated for a range of peak velocities, Doppler angles and SNR levels. Standard deviation in the envelope is low — less than 2% in case of experiments done by varying the peak velocity and Doppler angle for steady phantom and simulated flow; and also less than 2% in case of experiments done by varying SNR but keeping constant flow conditions for *in vivo* and simulated flow. Low variability in the envelope makes the prospect of using the envelope for automated blood flow measurements possible and is illustrated for the case of Pulsatility Index estimation in uterine and umbilical arteries.

4.1 Introduction

Blood flow assessment in relevant vessels using an ultrasound Doppler spectrogram is important in the diagnosis of various pathological conditions. Maximum velocity measurement representing the velocity of blood cells travelling with the highest velocity in the vessel is one of the most clinically significant measurements obtained from a

Doppler spectrogram. Maximum velocity as a function of time, often referred to as the maximum velocity envelope or spectral envelope is also used in a number of diagnostic applications.

In the case of carotid stenosis, peak systolic velocities (PSVs) observed using Doppler spectrogram are used to quantify the degree (percentage) of stenosis [1] and further for determining and using optimal PSV thresholds to establish the need for carotid endarterectomy [2]. Blood Flow volume assessment based on the calculation of time averaged maximum velocity and the vessel cross sectional area is essential in cerebral blood flow assessment [3], arteriovenous fistula inspection during hemodialysis [4], in techniques such as anaesthesia [5] and fetal outcome assessment [6].

In maternal-fetal examination, Doppler investigation of the uterine and umbilical arteries gives information on the perfusion of the utero-placental and feto-placental circulations. In case of pre-eclampsia and intra uterine growth restriction (IUGR), there is an increased resistance within the placenta, affecting the quality as well as the quantity of the blood perfusion through the organ. The calculation of Doppler indices which quantify the blood velocity in uterine/ umbilical arteries makes use of points on the spectral envelope [7]. Pulsatility Index (PI), alone or combined with early diastolic notching, has been found to be the most predictive uterine artery Doppler index in predicting pre-eclampsia and IUGR [8]. Along with peak systolic and end diastolic velocities, it takes into account the volume of blood flow during the cardiac cycle. With increasing use of ultrasound in low resource settings with lack of adequately trained users, an automated/semi-automated estimation of Doppler indices is becoming requisite.

In the most ideal case, a single blood velocity at any instance in time should give rise to a single Doppler frequency shift at that instance in the Doppler spectrogram as according to the Doppler equation. However, in practice, a single velocity may give rise to a range of frequencies resulting in a phenomenon called intrinsic spectral broadening [9]. Intrinsic spectral broadening has been physically interpreted as occurring due to a combination of transit time broadening [10] and geometrical broadening [11, 12]. The two phenomena were thought to be equivalent for a long time [13] but were later shown to be different by Guidi et al. [14], who came to the conclusion that the two phenomena at the focus are equivalent.

A number of methods have been proposed to estimate the single maximum frequency that, according to the classic Doppler equation, would correspond to maximum velocity in the absence of intrinsic spectral broadening. The earliest methods were heuristic threshold crossing methods which identified maximum frequency as a particular percentage of the spectral power / integrated spectral power at the tail end of the corresponding power spectrum / integrated power spectrum. These include the percentile method, D'Alessio's threshold crossing method, modified threshold crossing method and the hybrid method [15, 16]. However, as the threshold in these methods depends on the noise at the tail end of the spectrum, these are very sensitive to SNR [15–17].

The later methods, Geometric method (GM) [17], Modified Geometric Method (MGM) [18] and Signal Noise Slope Intersection (SNSI) [19] method have been shown to give better results [17, 19–21]. However, GM can perform well only when the

maximum analyzed frequency is optimally chosen and the IPS curve retains its typical characteristic shape while MGM is affected by the SNR and is more prone to maximum frequency overestimation in case of narrow band signals. Also, SNSI makes use of certain pre-defined parameters which are data dependent. These methods are discussed in detail in Section 4.2.

A recent method proposed by Vilkomerson et al. [22] and its extension by Ricci et al. [23,24] are based on modelling the Doppler power spectrum based on flow velocity profile and from that model, determining a relation for power spectral value at the maximum frequency point. Further, based on simulations and *in vitro* experiments, it is shown that the power value at which maximum frequency point occurs is a particular fraction of the peak spectral power in the spectrum. The Vilkomerson method is shown to give good results for the kind of model it is formulated from — uniformly insonated parabolic flow velocity profile. However, the extension by Ricci et al., for non-parabolic velocity profile and non-uniform insonation requires the use of a large sample volume and a wide beam profile achieved by non-focused beamforming. Velocity components with directions and amplitudes other than those of main blood flow can be easily included in the sample volume. These may contribute to the Doppler spectra and interfere with measurements [23].

The methods discussed above focus only on obtaining maximum velocity at a time point and do not touch the aspect of spectral envelope estimation. In addition, most of the methods have been tested on steady flow power spectra averaged over large ensemble lengths [19, 20, 22], or take the average of maximum velocities occurring at the same cardiac event over a number of cardiac cycles [23]. This is because they can be easily affected by the variance in the power spectrum.

Envelope extraction techniques have mainly focused on using image processing methods [25–27]. These techniques overcome the inter- and intraobserver variation and yield faster and reproducible results. However, they do not take intrinsic broadening into account and have been evaluated visually or by comparison to manual tracing of the Doppler spectrogram.

In this work, we present a technique for maximum velocity and spectral envelope estimation which is tested on simulated, string phantom and *in vivo* flow spectrograms. To evaluate the method, its performance is compared against existing methods, it is tested for its accuracy and precision in estimating maximum velocity by varying the peak velocity, Doppler angle and SNR level as well as the accuracy with which the obtained spectral envelope can be used to estimate Pulsatility Index in obstetric diagnostics.

The paper is organised as follows. In Section 4.2, a description of the algorithm for maximum velocity detection, envelope estimation and Pulsatility Index calculation is given. In Section 4.3, the signal model used in parabolic flow profile simulations is discussed along with *in vivo* and phantom data acquisition and processing. Section 4.4 delineates the results obtained from validation tests. The results, advantages and limitations of the method are discussed in Section 4.5. Finally, concluding remarks are given in Section 4.6.

4.2 Algorithm Description

4.2.1 Maximum Velocity Point Detection

The algorithm proposed for maximum velocity point detection is based on SNSI, modifying it based on an idea obtained from GM. This was done to overcome the limitations of SNSI. Both GM and SNSI compute maximum velocity based on the identification of maximum frequency. Maximum frequency, f_{max} is defined as the frequency that directly corresponds to the maximum velocity through the classic Doppler equation below, without needing any correction factors, and will be used in the same sense in this text.

$$v_{max} = f_{max} c / 2 f_0 \cos(\theta), \tag{4.1}$$

where f_0 is the center frequency of the transmitted ultrasound pulse, and c and θ represent the sound velocity and beam-to-flow angle respectively.

Geometric Method (GM): With this method, f_{max} is estimated as a point on the Integrated Power Spectrum (IPS) whose normal distance to a reference line is maximum. This reference line is a line joining two points on the IPS: the first corresponds to the frequency associated with peak spectral power and the second corresponds to the 'maximum analyzed frequency (f_H)'. GM can be implemented when the maximum frequency point is not too close to the finishing end of the power spectrum (f_H) and the IPS is relatively flat at higher frequencies close to the end of the spectrum. To obtain accurate results, the IPS should be close to its characteristic shape [17].

In case of *Modified Geometric Method (MGM)*, the reference line chosen is the line joining the first and the last points in the IPS, that is the points corresponding to frequencies 0 Hz and f_H respectively. This was done to get past the problem of marked fluctuations caused by noise spikes and variance of the spectral estimator in the location of frequency point that corresponds to peak spectral power. Results indicate that MGM is influenced by the level of SNR and spectral broadening and leads to overestimation of f_{max} in case of narrow band signals.

Signal Noise Slope Intersection (SNSI): With this method, IPS is divided into three regions: the signal region, the knee region and the noise region (Fig. 4.1). The slope of the points in the knee region is then modelled with two best fit lines: one in the signal region with a slope of m_S and one in the noise region with a slope of m_N.

$$m(x) = m_S x + m_N (1 - x), \tag{4.2}$$

where x is the fractional signal contribution to the slope and $(1-x)$ is the fractional noise contribution.

m_S is calculated as the slope of a linear least squares fit line between data points in the IPS corresponding to frequencies in the strong signal range. Strong signal is defined as the full-width at 70% of the signal peak in the power spectrum. f_S corresponds to the frequency point at the end of signal region. m_N is calculated as the slope of line joining the point on the IPS corresponding to maximum analyzed frequency point, f_H

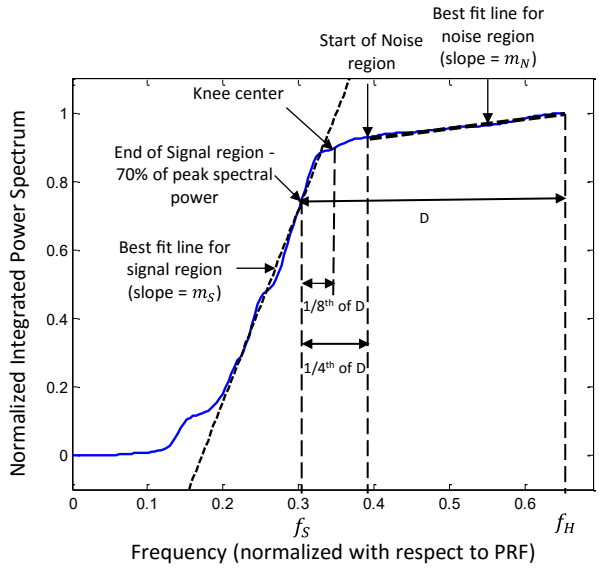

Figure 4.1: Location of end of signal region, knee center and noise start point in SNSI method.

and the start of noise region. Fig. 4.1 shows the location of the start of noise region, which is found as the point on IPS corresponding to frequency $f_S + D/4$, where D is the distance between f_S and f_H.

The value of x varies from 1 at the start of the knee region, on the signal side to 0 at the end of the knee region. In case of no intrinsic spectral broadening, f_{max} will occur at $x = 0$. However, when intrinsic spectral broadening is present, the spectrum extends beyond the true f_{max}. In SNSI, the point on IPS corresponding to the maximum frequency has been heuristically found to be the point where $x = 0.1$. This value is based on qualitative observations tested up to a Doppler angle of 60 degrees [19, 20].

SNSI has been shown to work well for a broad range of SNRs [19, 20]. However, this method uses a fixed fraction of the distance between f_S and f_H to determine the beginning of noise region. This may lead to inaccurate estimation of f_{max} where this assumption does not hold.

A more accurate way to locate the noise start point in IPS would be to identify the knee center (mid-point of the end of signal region and beginning of noise region) first based on GM, and make its location free from any pre-defined values. The method proposed in this work combines steps from altered GM and SNSI. The order in which the algorithm runs and locates f_{max} is depicted in Fig. 4.2 and enlisted in the steps below [28].

***Proposed Method*:**

Once the spectrogram has been corrected for any aliasing by baseline shifting

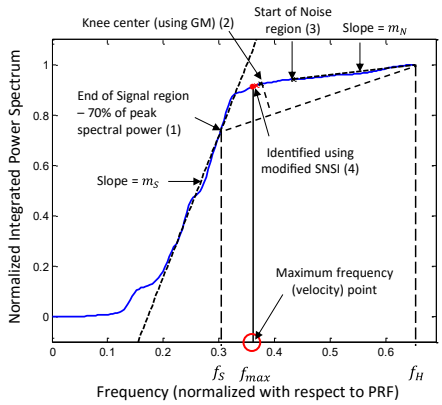

Figure 4.2: Maximum frequency point estimation using steps from GM and SNSI.

manually, the direction of flow is identified by calculating the mean frequency at that time point. IPS at that time point is then obtained by integrating the power spectrum values from 0 Hz to the maximum analyzed frequency, f_H, in the direction of flow.

1. The end of signal region (f_S) is identified as in SNSI method. This is the point corresponding to highest frequency value which falls in the strong signal range.

2. The knee center is identified based on an altered version of GM. It is located as the point on IPS which lies at maximum normal distance from the reference line joining points on IPS corresponding to f_S and f_H.

   The reference line used in this case is different from that used in GM or MGM. The requirement was the location of the center of the knee region (the transition region between signal and noise) and not the knee of the IPS, as in the earlier methods, which they ascribe as the f_{max}. Moreover, the location of the first point of the reference line being the point on IPS corresponding to f_S is advantageous in two ways — one, it is devoid of the fluctuations of the point corresponding to peak spectral power (which happens in case of GM) and two, it is not much influenced by the fact that higher noise contribution to the IPS in case of narrow band signals would lead to overestimation of the point being located (as happens in case of MGM).

3. As the frequency at knee center is equidistant from the frequencies corresponding to end of signal region and the start of noise region, the latter can be located once the former two points are identified.

4. The slope of signal region (m_S) and the slope of noise region (m_N) are computed as in the SNSI method and the SNSI equation (4.2) is used with $x = 0.1$ to estimate the slope of IPS at maximum frequency point. Finally, the algorithm looks for the point in the knee region at which the slope value is closest to the estimated slope value. The frequency corresponding to this point is f_{max}.

5. From the estimated f_{max}, maximum velocity (v_{max}) is computed using equation (4.1).

Note that the value of x corresponding to f_{max} in the knee region was kept 0.1, as empirically found for SNSI based maximum velocity estimation in case of clinically relevant Doppler angles [19, 20].

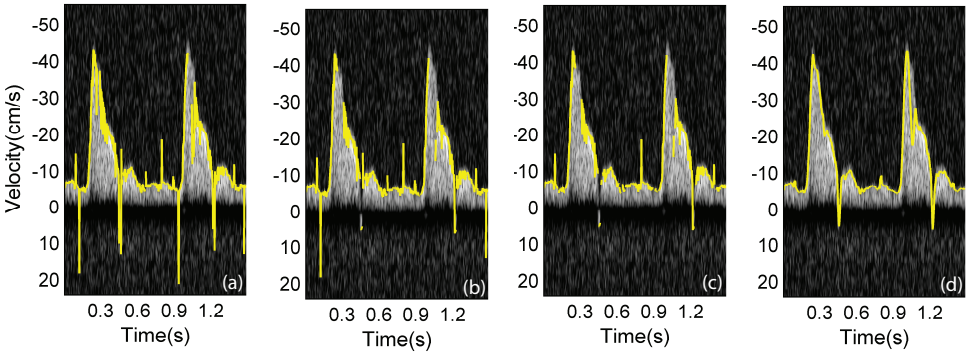

Figure 4.3: Maximum velocity points detected for a carotid artery spectrogram (displayed here with dynamic range set to 40 dB), (a) before introducing $1/3^{rd}$ condition, (b) after introducing $1/3^{rd}$ condition on (a), (c) after introducing power thresholding on (b), (d) after interpolation and smoothing on (c).

4.2.2 Maximum Velocity Envelope Estimation

In order to obtain a correct estimate of the spectral envelope, the maximum velocity identified at each time point should be accurate. After the f_{max} points are detected, the spectral envelope is estimated using the following steps.

Making f_{max} detections rigorous

In case of SNSI, the location of knee center frequency point is fixed at $f_S + D/8$ with the knee region extending from f_S to $f_S + D/4$. Since the proposed method uses altered GM for locating the knee center, there are no restrictions on the location of knee center frequency point based on distance from f_S. In such a case, if there is some signal loss resulting in a distorted IPS curve, an erroneous knee center may be identified by GM as implemented in this work, leading to inaccurate f_{max} detection as shown in Fig. 4.3(a). With f_S to $f_S + D/4$ in mind as the typical extension of the knee region as according to SNSI, the range was slackened with f_S fixed until $f_S + D/3$ worked out as the optimal distance to restrict the location of knee center with. The location of knee center beyond this range seemed improbable and the condition helped to avoid many erroneous detections. Fig. 4.3(b) shows the spectral envelope after exclusion of spectral bins from the maximum velocity estimation for which the location of knee

center does not satisfy the above criteria. Hereafter, this criteria of exclusion will be referred to as the '$1/3^{rd}$ condition' and the maximum frequency points contained in the envelope after application of this exclusion criteria as the 1^{st} estimate of the envelope.

Power Threshold Requirement and Automated Estimation

Erroneous detections of f_{max} can be reduced further by validation of the signal quality at each point in time. This is assessed by comparing the mean spectral power with a given threshold, and excluding estimates at times with poor signal quality. As the noise level may vary for different signal acquisitions, the threshold should be adaptive to the noise in that spectrogram.

To obtain this threshold value, the power values in the frequency bins of the spectrogram present above the maximum frequency points in the 1^{st} estimate of the envelope for the first 1s or 2s of the spectrogram are taken depending on the duration of the recording. These bins are expected to lie in the noise region. Threshold is then chosen as the 90^{th} percentile of noise power spectral density distribution. The percentile was experimentally determined after application of different percentile values to spectrograms with different SNR levels.

This threshold value can then be applied to the part from which it is obtained as well as the rest of the spectrogram to exclude those time points from envelope estimation at which the mean power spectral value is less than the threshold. Fig. 4.3(c) shows the estimated f_{max} points after power thresholding. If no f_{max} points are detected for a continuous period of 0.1 s or more, the f_{max} values for these periods are set to zero. Finally, the good set of detected f_{max} points are interpolated to obtain the spectral envelope. It is then smoothed further using a moving average filter of length five equivalent to temporal averaging of 7.5 ms. Fig. 4.3(d) shows the estimated envelope after interpolation and smoothing.

4.2.3 Algorithm for Pulsatility Index Estimation

Once the spectral envelope is obtained, automated Doppler Index measurements are possible. An algorithm was developed for estimating PI for the umbilical and uterine artery flow. PI measurements are relevant to quantify the impedance to blood flow in placenta. It is assumed that the direction of flow is constant, that the sign of maximum velocity values does not vary throughout the cardiac cycle. This is a valid assumption for umbilical and uterine flow in which the flow direction is constant. The severe case of absence or reversal of diastolic flow is an extreme condition and itself reflective of abnormal placental development [7].

The direction of flow is assessed by checking for the sign of maximum velocity values in the envelope. The magnitude of maximum velocity values in the envelope is used for further calculations in the algorithm for PI estimation. The maximum value and the minimum value from the envelope over entire chosen time range are obtained and the average of the two values set as the threshold for locating peak systolic velocities (PSV). The peaks should lie above this value. Also, the minimum

time period between the peaks to be detected is set as 0.5 s in case of uterine flow and 0.25 s in case of umbilical flow, keeping in mind the duration of one flow cycle in each of the arteries, with sufficient margin not to miss any PSV point.

The envelope is then inverted about itself and the minima now located by finding maxima in the inverted envelope in the same way as for detecting systolic peaks. The minimum time period between these maxima is however set as 0.03s as more than one minima can occur during diastolic flow. Once the time points at which the minima occur are identified, the velocity values at these points can be estimated using the original envelope. The diastolic end velocities (EDV) are then chosen by keeping only the minima which have occurred just before the occurrence of systolic peaks of corresponding successive cycles.

The time averaged velocity (TAV) for a cycle can then be estimated by taking the cumulative sum of the envelope values from the EDV of the previous cycle to the EDV of that cycle and dividing by the time duration between their occurrence. Finally, PI for each cycle is calculated as

$$PI = PSV - EDV/TAV. \tag{4.3}$$

4.3 Evaluation Methods

4.3.1 Signal Model for Simulations

To compare the f_{max} points detected by the algorithm with true maximum frequency as well as test the robustness of the envelope to a wide range of SNRs, a signal model that simulates parabolic flow in blood vessels is introduced.

In parabolic flow distribution, the variation of velocity in a vessel, v as a function of distance r measured from the axis will be as follows

$$v(r) = v_{max}(1 - (r/R)^2), \tag{4.4}$$

where v_{max} is the velocity of the blood cells moving along the axis and R is the radius of the vessel. To obtain r as a function of v, the above equation can be written as

$$r(v) = R\sqrt{1 - v/v_{max}}. \tag{4.5}$$

Considering uniform distribution of blood cells in the vessel, the probability p_r that a blood cell is present at a distance r from the axis is

$$p_r(r) = 2\pi r dr. \tag{4.6}$$

The probability p_v that a blood cell possesses velocity v can then be obtained using Jacobian transformation,

$$p_v(v) = p_r(r)\left|\frac{\partial r}{\partial v}\right|. \tag{4.7}$$

Differentiating equation (4.5) and substituting in equation (4.7), we obtain

$$p_v(v) = R^2/v_{max}. \tag{4.8}$$

As the probability density function of velocity is constant for a particular vessel, it can be inferred that, the number of blood cells that are moving with a certain velocity is the same for each velocity when the flow profile is parabolic.

In the model, a focused beam with beamwidth greater than the vessel diameter is assumed to insonate the vessel and the sample volume to enclose the vessel width. As transit time and geometrical broadening at the focus are equivalent [14], broadening occurring as a result of the former phenomenon is introduced.

The signal from each scatterer will be non zero only for a short interval of time, called transit time (T_T), when it is passing through the ultrasound beam. The signal received would be a sinusoidal signal of Doppler shift frequency (f_d), modulated by the beam profile, a sinc squared function ($sinc^2(t/T_T)$ where t represents time) resulting from pulsed wave focused transmission and use of rectangular apodization at both the transmit and receive apertures of the transducer. This will give a triangular function in frequency domain with center frequency f_d and bandwidth equal to $2/T_T$ [29, 30]. Transit time, $T_T = f_{num}\lambda/vsin(\theta)$ where θ is the beam to flow angle, f_{num}= focal depth/aperture and λ is the wavelength of the transmitted ultrasound beam. Thus,

$$Bandwidth(v) = 2v\sin(\theta)/f_{num}\lambda. \tag{4.9}$$

In parabolic flow, as the probability density function for the velocities (Doppler frequency shifts) observed is a constant, the area under the triangular function obtained at each velocity would be a constant. With the bandwidth and area, these triangular functions can be completely determined. The sum of these triangular functions at each Doppler frequency shift gives the simulated blood flow power spectrum [31]. Lower frequencies are excluded from the model as infinitely large spectral power values will be obtained from the computation for these frequencies. Tissue clutter with a normalized frequency bandwidth of 0.05 was introduced at low frequencies with power value 40 dB higher than the blood flow signal power. Simulations were done for two different peak velocities, each at two different Doppler angles. The parameters that were used for the simulations are listed in Table 4.1.

Table 4.1: Simulation parameters

Parameter	
Blood flow maximum velocity, v_{max} [cm/s]	60, 100
Radius of the vessel,R [mm]	1
Center frequency,f_0 [MHz]	5
PRF [kHz]	10.62
F-number, f_{num}	4
Beam to flow angle, θ [degrees]	27, 58
Speed of sound, c [m/s]	1540

Thermal noise is completely white in modern ultrasound scanners with digital signal processing. This is because the correlation length of the signal is much shorter

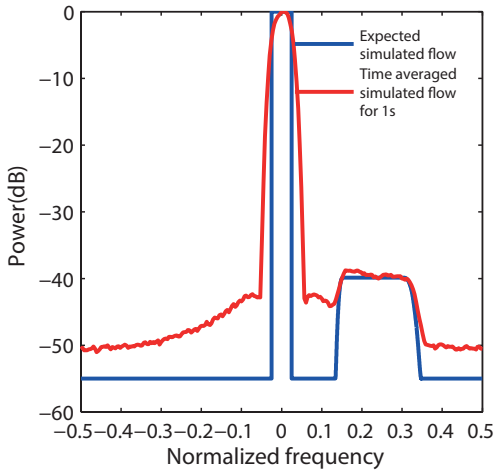

Figure 4.4: Power spectrum for parabolic flow velocity profile with spectral SNR 15 dB — expected (blue), time averaged over 1s time interval / 660 spectra (red).

than the pulse repetition time (Doppler signal received is in megahertz range but is sampled in kilohertz range (pulse repetition frequency)). To obtain spectrograms of desired SNR, that were required to be used in experiments to test the envelope robustness to SNR (Section 4.4.2), a constant noise floor was added to the power spectra. The Doppler signal from a large number of blood cells would add up to a Gaussian random process. The square root of power spectrum was then multiplied with the Fourier transform of a Gaussian complex random signal to achieve the required power spectrum. Inverse Fourier transform of this signal, yields the required Doppler signal. The linearity of the Fourier transform ensures that the simulated Doppler signal will be a complex Gaussian signal. Fig. 4.4 shows the expected and time averaged power spectrum averaged over 1s / using 660 spectra for SNR of 15 dB. Finite window size used in the spectral analyzer introduces further broadening.

4.3.2 Data Acquisition and Processing

Beam-formed IQ data were acquired from umbilical, uterine, carotid and subclavian arteries using Vivid E9 (GE Vingmed Ultrasound, Horten, Norway) in PW-Doppler mode. Umbilical and uterine recordings were obtained from two pregnant volunteers at gestational age of 29 and 39 weeks. Common carotid, external carotid, internal carotid and subclavian recordings were acquired from a healthy volunteer.

For all phantom flow acquisitions, Doppler string phantom Mark 4 (JJ&A Instruments, Duvall, WA, USA) was used with plain tap water as the fluid in the tank. Beam-formed IQ data was acquired using GE Vivid E9. Four acquisitions were made for steady velocity at two values — 60 cm/s and 100 cm/s, each at a Doppler angle of 27° and 58°. Two acquisitions were made for pulsatile string velocity mimicking

physiological flow in Ductus Arteriosus with peak systolic velocity of 100 cm/s at Doppler angles of 27° and 58°. The Doppler angles chosen here were in accordance with the clinical guidelines which recommend a Doppler angle of 60° or less.

The IQ data acquired was clutter filtered and the spectrogram obtained by using 256 point FFT on a 64 point Hamming windowed signal with 75% overlap. The phantom recordings were clutter filtered to keep the conditions the same as for the *in vivo* case. The spectrograms were averaged in time using an averaging filter of window size 8 for the string phantom acquisitions, resulting in a temporal averaging of 12 ms. Spectrograms for *in vivo* acquisitions were averaged using a window size of 4 or 8 depending upon the resulting averaging in time, which it was ensured remains less than 24 ms.

To test for robustness of envelope estimation to SNR variability in case of *in vivo* and phantom data, the desired noise power was obtained by multiplying mean spectral power in the spectrogram with the required relative noise level. Noise was then generated by multiplying the square root of power with a normally distributed complex random signal and added to the acquired Doppler signal.

To enable a direct comparison between phantom and simulation results, the Doppler angles chosen while simulating data were the same as for the phantom acquisitions — 27° and 58° (Table 4.1). In case of flow simulations, clutter filter was applied and spectrogram obtained in the same way, using 256 point FFT on a 64 point Hamming windowed signal with 75% overlap. Spectrogram averaging in time was then done using an averaging filter of window size 8, resulting in a temporal averaging of 12 ms.

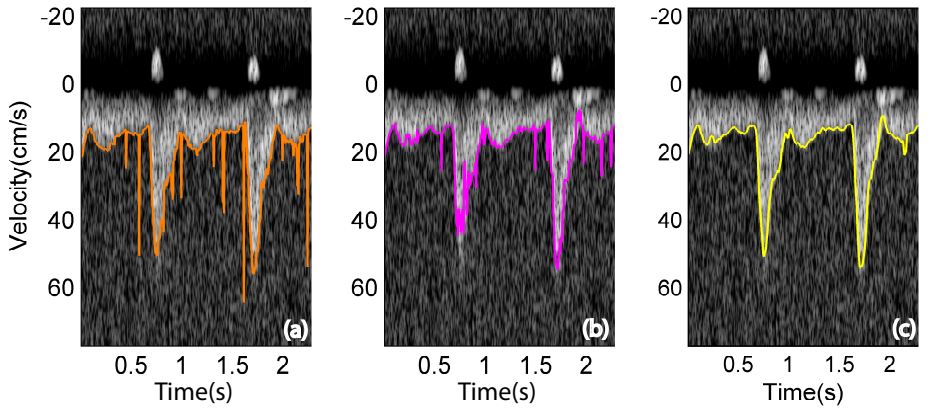

Figure 4.5: A comparison of the spectral envelope estimated using proposed algorithm (c) with that obtained by GM (a) and SNSI (b), on a uterine artery spectrogram (displayed here with dynamic range set to 40 dB).

4.4 Results

The proposed algorithm was tested on 7 carotid, 4 uterine, 4 umbilical and 2 subclavian artery *in vivo* recordings as well as 4 steady and 2 pulsatile flow phantom recordings. Also, flow simulations were performed and the algorithm tested on them. In this section, results obtained from tests done to evaluate the accuracy of envelope estimation and its robustness to SNR are presented.

4.4.1 Comparison with Existing Methods

Geometric Method and Signal Noise Slope Intersection — using *in vivo* data

Fig. 4.5 shows the spectral envelope points obtained by GM and SNSI against those obtained by the proposed method for a uterine artery spectrogram with SNR approximated to 6.3 dB using the equation below.

$$SNR = 10\log_{10}\frac{< P_S > - < P_N >}{< P_N >}, \tag{4.10}$$

where $< P_S >$ is the mean power contained in the entire spectrogram and $< P_N >$, mean power contained in a region containing only noise. A region containing only noise was identified while estimating the spectral envelope using proposed method. This step has been discussed in section 4.2.2.

Reduction in false f_{max} detections and variance in the the envelope is visible when the proposed method is used.

Signal Noise Slope Intersection — using string phantom data

Fig. 4.6(a) and Fig. 4.6(b) illustrate the envelope obtained for steady phantom flow using SNSI and the proposed method respectively. Fig. 4.6(c) and 4.6(d) show the envelope results using the two methods for pulsatile phantom flow. Noise has been added to the acquired flow spectra. The SNR estimated using equation (4.10) was 1.9 dB for the illustrated steady flow and 3.7 dB for the illustrated pulsatile flow spectrograms.

Method by Vilkomerson et al. — using simulations

The method proposed by Vilkomerson et al. [22] for obtaining accurate peak velocity has been derived for a model with parabolic flow profile and uniform insonation. The resulting power spectrum features a plateau similar to that obtained by the model used in this work (discussed in Section 4.3.1).

In this section, we make an analysis of our results for parabolic flow simulation against the results obtained using the method proposed by Vilkomerson et al., suggested particularly for plateaued power spectra. However, the simulations done here assume a focused-beam insonation instead of uniform insonation of the vessel as assumed by the Vilkomerson method.

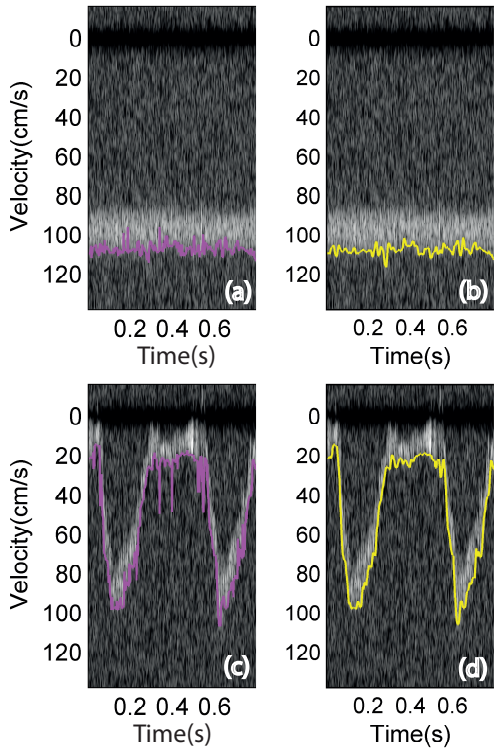

Figure 4.6: Spectral envelope on steady phantom flow using SNSI (a) and proposed method (b), spectral envelope on pulsatile phantom flow using SNSI (c) and proposed method (d). (All spectrograms have been displayed in this figure with dynamic range set to 40.)

According to Vilkomerson et al., the maximum frequency point occurs at spectral power ST_M, which is equal to 0.5 times the spectral power at the beginning of the plateau, ST_P. ST_P is estimated using an iterative method. An initial power threshold Th_0 is chosen to be above the noise level. The spectrum is scanned from high to low frequencies until initial frequency point f_0 is located where bin power exceeds Th_0. Thereafter, the frequency points f_i and the thresholds Th_i are recursively determined as

$$f_i = (1 - \alpha) f_{i-1}, \tag{4.11}$$

$$Th_i = \frac{1}{f_{i-1} - f_i} \int_{f_i}^{f_{i-1}} S(x)\,\mathrm{d}x, \tag{4.12}$$

where Th_i is the average spectral density between the frequency points f_{i-1} and f_i, α is a parameter which affects the dimension of the averaging region, and i is the step index. The procedure quickly converges to the plateau level, and stops when $f_i = f_{i-1}$.

When implementing this algorithm to our simulations, we take α= 0.05 and Th_0 is decided based on SNR of the simulated flow. The maximum value of Th_is is chosen as ST_P if Th_i values are monotonically increasing. However, if noise may cause fluctuations in the calculated Th_is, the Th_i value just after the slope in power spectrum is chosen as ST_P. Also, we do not make an interpolation in the power spectrum values to obtain the maximum frequency point beyond the frequency resolution in the spectrogram.

The proposed method and the method by Vilkomerson et al. were implemented on steady flow simulated with peak velocity 60 cm/s and Doppler angle 27° for the cases of spectral SNR 30 dB and 12 dB. The percentage bias and standard deviation of maximum frequencies normalized with respect to pulse repetition frequency (PRF) were estimated for 660 time points / 1s time interval. For the case of spectral SNR equal to 30 dB, bias in f_{max} point estimation was found to be 1.21% and -0.90%, and standard deviation over envelope was found to be 0.54% and 1.65%, by the proposed and the Vilkomerson methods respectively. For the case of spectral SNR equal to 12 dB, bias in f_{max} point estimation was found to be 1.14% and -1.10%, and standard deviation over envelope was found to be 1.14% and 2.02%, by the proposed and Vilkomerson methods respectively. The envelope over spectrogram and the corresponding bias and standard deviation on time averaged power spectrum are depicted in Fig. 4.7 and Fig. 4.8.

4.4.2 Testing for Robustness to Varying SNR

To test the robustness of envelope estimation to varying noise level in the spectrogram, experiments were done by adding noise to simulated and *in vivo* data.

Simulated Flow with Varying SNR: Spectral noise was added to the simulated flow spectra yielding signals with spectral SNR (level of signal power amplitude to noise power amplitude) ranging from 30 dB to 10 dB. Actual SNR for each case was calculated as the ratio of total power contained in the signal and noise over the entire frequency range. Table 4.2 shows the percentage values of bias and standard deviation of maximum frequencies, normalized with respect to PRF, calculated for 660 time points / 1s time interval for each SNR case. The error in f_{max} estimation at time point i (E_i), bias and standard deviation (σ) are estimated as

$$E_i = \frac{(f_{max})_i - ((f_{max})_{true})_i}{PRF}, \tag{4.13}$$

$$Bias = \frac{1}{N}\sum_{i=1}^{i=N} E_i, \tag{4.14}$$

$$\sigma = \sqrt{\frac{1}{N-1}\sum_{i=1}^{i=N}\left|E_i - \frac{1}{N}\sum_{i=1}^{i=N} E_i\right|^2}, \tag{4.15}$$

where $(f_{max})_i$ is the maximum frequency at any time point i, $((f_{max})_{true})_i$ is the true maximum frequency at that time point (equal to a constant value $(f_{max})_{true}$ at all

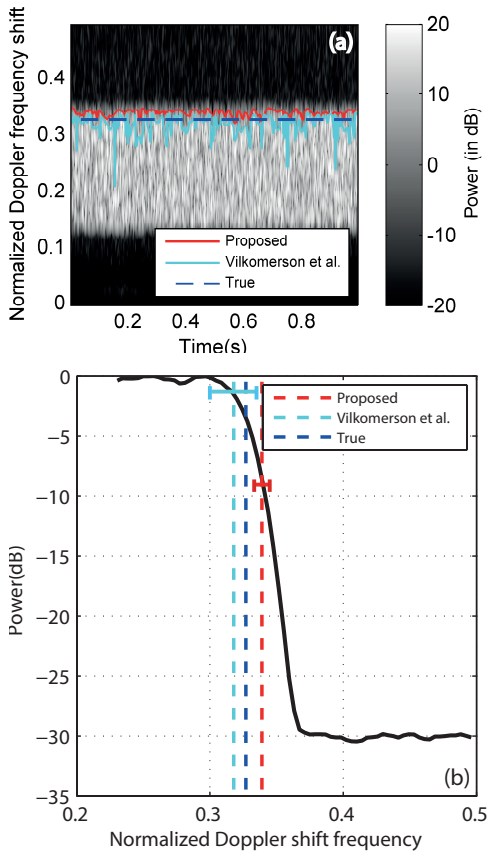

Figure 4.7: (a) Comparison of spectral envelope over simulated flow (SNR=30 dB) spectrogram (displayed here with 40 dB dynamic range) using the proposed method with method by Vilkomerson et al., (b) illustration of bias in f_{max} point estimation and standard deviation in the envelope by the proposed and Vilkomerson methods on time averaged power spectrum.

time points for steady simulated flow) and N is the number of time points considered.

Noise addition to *in vivo* data: Blood flow spectrogram with 1422 time points from a uterine artery recording lasting 3.98 s was obtained. The SNR of the recording was calculated approximately as 14 dB using equation (4.10).

Increasing level of noise was added to the spectrogram, using a desired level relative to the mean power contained in the spectrogram. As the recording would have some inherent noise, the resulting SNR value (in dB) was then estimated using equation (4.10). The percentage bias and standard deviation of estimated normalized maximum velocities was calculated for each case as shown in Table 4.3, the true normalized maximum velocity at each time point being considered as obtained in the case without

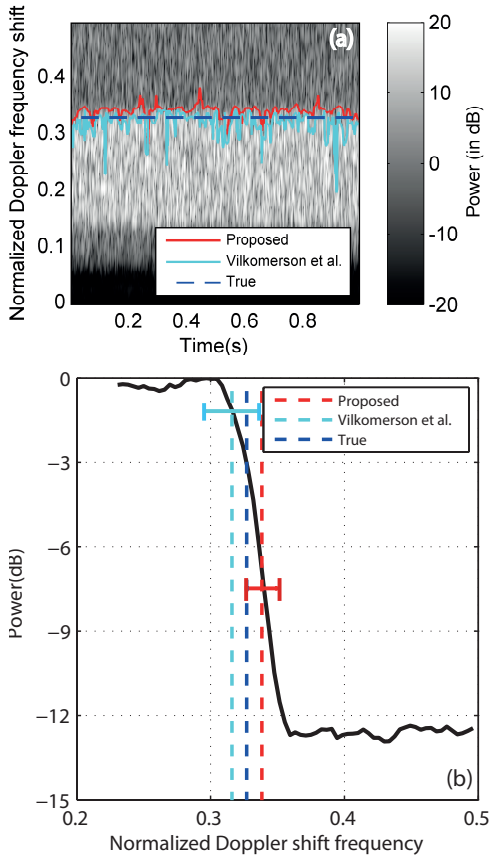

Figure 4.8: (a) Comparison of spectral envelope over simulated flow (SNR=12 dB) spectrogram (displayed here with 40 dB dynamic range) using the proposed method with method by Vilkomerson et al., (b) illustration of bias in f_{max} point estimation and standard deviation in the envelope by the proposed and Vilkomerson methods on time averaged power spectrum.

any additional noise in the spectrogram. The normalization of velocities was done with respect to twice the Nyquist velocity. The error, bias and standard deviation are estimated according to (4.13), (4.14), (4.15) respectively.

Visual analysis for a poor SNR signal: The spectral envelope obtained using proposed method on a subclavian artery spectrogram whose SNR was approximated using equation (4.10) to 5.4 dB was compared with its corresponding autotrace on the commercial scanner with trace sensitivity set to maximum. Fig. 4.9 illustrates the example.

Table 4.2: Envelope estimation for varying SNR in simulated flow

Spectral SNR [dB]	**SNR [dB]**	**Bias of normalized maximum frequencies (%)**	**Standard Deviation of normalized maximum frequencies (%)**
30	22.6	1.21	0.54
20	12.6	0.98	0.96
15	7.6	0.89	0.97
12	4.6	1.14	1.14
10	2.6	1.59	2.00

Table 4.3: Envelope estimation for varying SNR in in vivo data

Approximate resulting SNR [dB]	**Bias of normalized maximum velocities(%)**	**Standard deviation of normalized maximum velocities(%)**
13.3	-0.008	0.15
10.3	-0.007	0.33
6.6	0.028	0.60
1.9	0.226	1.62
-0.7	0.909	2.84

4.4.3 Varying Doppler angle and peak velocity

Maximum velocity envelope estimation for several cases of peak velocity and beam to flow angle was done for phantom and simulated flow. Table 4.4 shows the different cases and the corresponding bias and standard deviation in estimation of maximum velocities normalized with respect to twice the Nyquist velocity. The measures of error have been obtained for each case of steady thread phantom flow using a spectrogram of time duration 6 s discretized over 3979 time points and for simulated flow using a spectrogram of 1s discretized over 660 time points. Note that in case of pulsatile flow, peak velocity is the peak systolic velocity and the bias and standard deviation shown

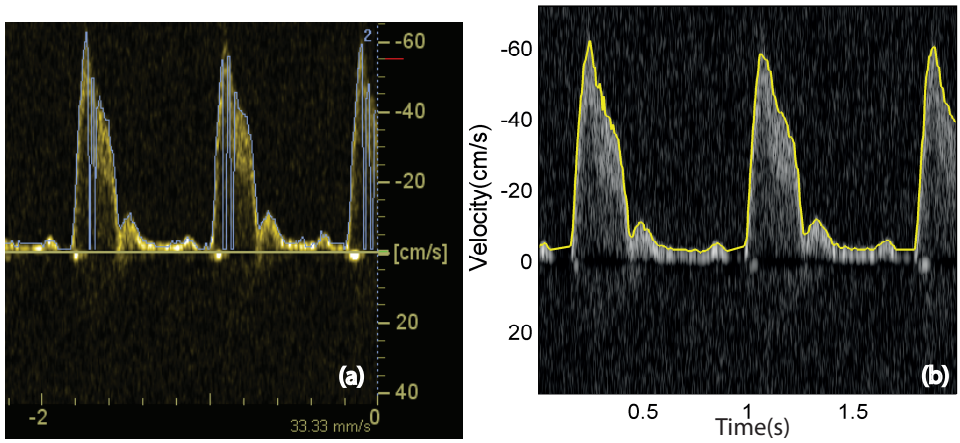

Figure 4.9: Comparison of maximum velocity (a) autotrace on a commercial scanner with trace sensitivity set to maximum and (b) envelope obtained using algorithm on subclavian artery spectrogram (spectrogram (b) is displayed with dynamic range set to 38 dB).

for each of the two cases of pulsatile phantom flow is for 16 peak systolic points.

4.4.4 Estimation of Clinical Indices based on Spectral Envelope

Using the algorithm discussed in section 4.2.3, PI can be calculated based on the spectral envelope after identification of peak systolic and end diastolic velocities. The envelope on a uterine artery spectrogram and the identified peak systolic and end diastolic velocities for three cardiac cycles are shown in Fig. 4.10.

The accuracy of PI estimation depends highly on the estimated envelope and thus the robustness of the envelope to varying SNR is important. The variation in PI estimation based on the proposed method with SNR is shown in Table 4.5.

Fig. 4.11 is a scatter plot showing variation of PI estimated using spectral envelope obtained by the proposed method with that obtained using the commercial scanner. The plot compares a total of 37 PI measurements (obtained from 18 uterine and 19 umbilical artery cardiac cycles — from 5 PW Doppler recordings acquired from two pregnant volunteers). The line shown is the line of identity. Considering the PIs obtained from the commercial scanner as reference, the mean absolute error and standard deviation as calculated for all data points is 0.046 and 0.062 respectively. The mean PI value (averaged over three consecutive cycles) for uterine artery in case of Patient 1 (at 29 weeks of gestation), was found to be 1.20 from the scanner and 1.20 using the proposed algorithm. For Patient 2 (at 39 weeks of gestation), mean uterine PI from scanner was 2.06 and PI from algorithm was 2.04. PI reference ranges from clinical perspective of assessing placenta associated diseases have been discussed

Table 4.4: Envelope estimation for varying peak velocity and Doppler angle

Flow type	**Peak velocity (cm/s)**	**Doppler angle (°)**	**Bias of normalized maximum velocities (%)**	**Standard Deviation of normalized maximum velocities (%)**
Phantom flow				
Steady	60	27	3.47	0.88
Steady	60	58	12.35	1.36
Steady	100	27	5.20	1.37
Steady	100	58	19.09	1.85
Pulsatile	100	27	3.26	2.89
Pulsatile	100	58	18.16	2.35
Simulated flow				
Steady	60	27	0.98	0.96
Steady	60	58	1.89	0.84
Steady	100	27	1.71	0.81
Steady	100	58	2.26	1.78

in [32]. The 95^{th} centile value (upper limit for patients considered normal) at 29 weeks of gestation is 1.13 and at 39 weeks of gestation is 0.91. The estimated and reference PI values are found to fall in the same reference range (greater than 95^{th} centile) for both the patients.

Table 4.5: PI variation with varying SNR, Reference PI =1.20

Approximate resulting SNR [dB]	**Estimated PI**
14.0	1.20
12.1	1.21
10.3	1.22
6.6	1.24
3.0	1.23

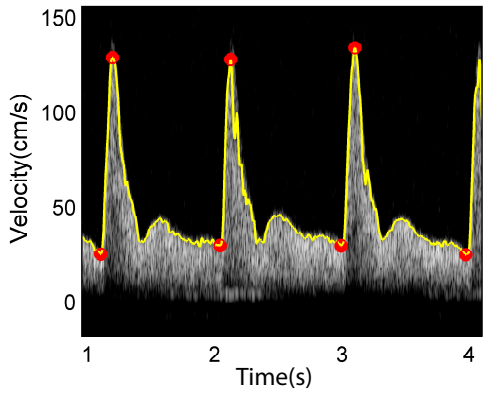

Figure 4.10: Spectral envelope on a uterine artery spectrogram (displayed here with dynamic range set to 40 dB) with identified peak systolic and end diastolic velocity points for three cardiac cycles.

4.5 Discussion

4.5.1 Method Establishment

The existing methods — GM and SNSI have been tested on simulated and steady phantom flow in earlier works [17,19,20]. When implemented on *in vivo* spectrograms susceptible to signal loss and greater variance in the power spectrum estimate, these methods tend to result in erroneous maximum velocity estimations (Fig. 4.5). The proposed method for f_{max} estimation is designed with its main basis as SNSI, a method which follows a heuristic approach designed for clinically relevant acquisition settings. However, in the proposed method, SNSI has been modified in several ways to overcome its limitations.

We extend the use of SNSI to short time averaged pulsatile flow, which is

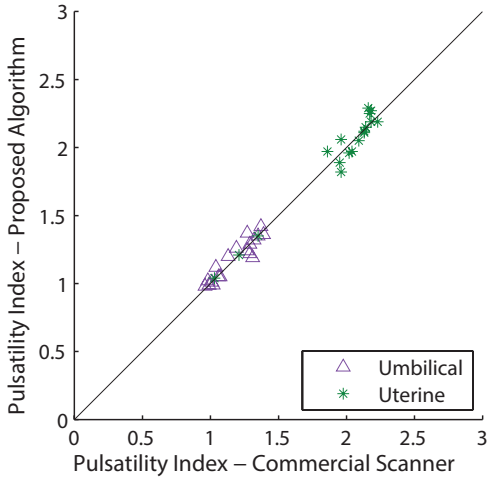

Figure 4.11: Scatter plot showing correlation between PI estimated using proposed method and that obtained from commercial scanner.

the requirement on the clinical side, although in earlier works, the technique was implemented on steady flow with power spectra averaged over long ensemble lengths. Pre-defined location of the knee center and consequently noise start point, as fraction of the distance between maximum analyzed frequency and end of signal region, lead to failure of the method for several cases in our data (Fig. 4.5(b)). These locations would probably have held true in case of constant flow phantom data on which the method was tested by its authors [19,20]. Fig. 4.6. also supports this fact. Observation of IPS for these cases revealed that the knee center identified this way did not correspond to the actual knee center. The use of altered GM for location of knee center turned out to be promising as it helps to locate the center of the transition region between signal and noise more accurately.

To obtain accurate results, SNSI requires the use of ensemble averaged PS while GM requires an optimal f_H which is not too close to f_{max}. In other words, the use of both methods requires a good IPS representative of its characteristic shape. This is a requirement that holds for the proposed f_{max} point detection technique. For pulsatile flow with moderate or low SNR, this can never really be achieved at each time point. The limitation of not being a 'good IPS' is thus used to our advantage by eliminating the time points at which these occur for f_{max} detection. The envelope is obtained by interpolating and smoothing the good set of f_{max} points.

4.5.2 Reliability of Maximum Velocity Estimation

There are numerous possible sources of error in estimating the maximum velocity, and these combine to form a maximum velocity error. The primary factors that contribute to these have been summarised in Christopher et al. [33]. Errors arise from the assumed

value of the variables used in the Doppler equation (4.1) while estimating maximum velocity from maximum frequency. Moreover, if the maximum frequency used is that as observed by the naked eye or based on threshold crossing methods (summarised in Section 4.1), the effect of intrinsic spectral broadening gets ignored. The degree of spectral broadening and the associated error varies based on the data acquisition settings like sample volume length, sample volume shape and aperture size.

The choice of SNSI as a basis for f_{max} detections for the spectral envelope estimation technique described in this work was based on the fact that results obtained using SNSI have been shown to have little intratransducer and intra/intermachine variability. The results were also found to be sufficiently robust to changes in focal depth and beam-steering. Though it was shown that overestimation errors occurred, increasing with an increase in the Doppler angle, these errors were significantly less at clinically relevant Doppler angles in comparison to errors without the use of SNSI correction [20, 34, 35].

Using the proposed method, the bias of normalized maximum velocities in the case of simulations for different peak velocities and Doppler angles was found to be less than 2.5% (Table 4.4). In the case of phantom experiments, for a smaller Doppler angle (27°) bias of up to 5% was seen while for a larger Doppler angle (58°), bias of 12-19% was observed. The main cause for greater bias in the case of phantom flow as compared to simulated flow seemed to be vibrations of the phantom string happening in a direction transverse to the desired mimicked fluid flow due to the motor driving the string motion. This also helps to understand the significant increase in bias at the higher angle in which case contribution to the signal received by the transducer from these transverse vibrations would be higher than at a smaller Doppler angle. In addition, slight misalignment of the angle correction cursor at greater angles may also have contributed to the large velocity estimation errors. For both phantom and simulation results, greater bias at a higher Doppler angle and maximum velocity indicates that with an increase in spectral broadening, the accuracy of maximum velocity estimation is reduced. This is probably because of greater spectral broadening resulting in a larger knee region in the IPS. The detected f_{max} in such a situation has higher probability to be located farther away from true f_{max}. Standard deviation in f_{max} estimation is considerably low — less than 2% for steady string phantom and simulated flow and less than 3% for pulsatile string phantom, indicating high precision in f_{max} estimation. Slightly higher standard deviation in case of string phantom velocity when compared to simulated flow, despite similar conditions, can be attributed to vibrations in the case of the string phantom and frequent spikes in the spectrogram due to bubbles.

Parabolic blood flow simulations also enabled comparison of the errors in maximum velocity estimation using the developed technique with the model based method developed by Vilkomerson et al.. f_{max} detection technique by Vilkomerson et al. is specifically meant for plateaued power spectra derived for a model based on continuous laminar flow with parabolic velocity distribution, fully insonated by a probe. The method is not designed to be used as such for *in vivo* flow. It is seen that while the proposed method overestimates the maximum velocity, the Vilkomerson method tends to underestimate it. Also, for the cases of spectral SNR 30 dB and 12 dB,

while the magnitude of bias observed in f_{max} estimation using the proposed method is very slightly higher than the Vilkomerson method, the standard deviation of the f_{max} points in the envelope is much lower. Overall, the values of percentage bias estimated for the two methods, for both SNR cases, are small relative to other sources of error in maximum velocity estimation. The true maximum velocity is found to lie at -3 dB and thus the plateaued power spectrum model assumed seems consistent with the findings of the model described by Vilkomerson et al. However, the location of the point detected as f_{max} in the Vilkomerson method in Fig. 4.7(b) and 4.8(b), seems to be around -2 dB and not around the expected -3 dB as the figures represent average of f_{max} points for each power spectral line in the spectrogram on the time averaged power spectrum of the spectrogram and not the f_{max} estimate for the averaged power spectrum.

4.5.3 Robustness to SNR

The bias being low and steady (0.9-1.6%) over an SNR range of 22.6 dB to 2.6 dB, in the case of steady flow simulated for a velocity of 60 cm/s and Doppler angle of 27°, indicates that the maximum velocities estimated in the envelope have very low sensitivity to SNR (Table 4.2).

Also, fairly low standard deviation is found in the observed maximum velocities. Less than 2% standard deviation in normalized maximum velocities is observed down to 2.6 dB SNR in simulated flow and 1.9 dB approximate SNR in *in vivo* flow. Envelope estimated for *in vivo* data seems to show better performance as compared to envelope for simulated data at the same SNR level, probably because the bandwidth for *in vivo* data is lower resulting in a higher spectral SNR.

4.5.4 Blood flow measurements based on envelope

Low variability in the observed envelope with variable SNR is promising from the point of view of automated Doppler indices estimation. Results in Table 4.5, showing consistency of PI estimation for varying SNR strongly support this fact. It is difficult to know the true maximum velocity of blood flow *in vivo*. However, considering that the broadening suffered by the maximum velocity at a time point in the Doppler spectrogram is proportional to the velocity value at that time point and the other parameters remain constant over the analysed part of spectrogram as can be deduced from equation (4.9), it can be said that the Doppler indices like PI, being a ratio of maximum velocities are independent of spectral broadening. Here, we are neglecting the effect of spectral broadening due to finite window size used while taking Fourier transform of the acquired Doppler signal as it produces very little effect compared to transit time broadening. Also, it can be fairly safely assumed, that the maximum velocities observed from a commercial scanner, suffer a broadening proportional to the true maximum velocities at corresponding points, yielding a PI independent of spectral broadening.

Fig. 4.11 indicates a very good agreement between PI estimated using spectral envelope obtained by the proposed method with that obtained using the commercial

scanner. The mean absolute error of estimated PI values when compared to the reference PI values is small, equal to 0.046. Also, the estimated and reference values are found to fall in the same clinical reference range of uterine artery PI for the case of two volunteer patients, even though Patient 1 is a case close to the deciding borderline.

4.6 Conclusion

In this work we presented a method for spectral envelope estimation which is fully automatic and independent of gain settings. The f_{max} detection technique for this method is developed by modifying an existing experimental approach (SNSI). In addition, the use of a threshold estimated based on noise level in the spectrogram ensures exclusion of erroneous f_{max} detections that may occur for certain power spectral estimates.

Experiments to test the performance of the envelope estimator were done for several cases of Doppler angles, peak velocities and SNR levels. Low errors in maximum velocity estimation are observed for simulated flow. Standard deviation in the envelope formed of the maximum velocity estimates is significantly low for simulated, phantom as well as *in vivo* flow. These results point towards robust envelope estimation with low sensitivity to SNR and variance in the power spectrum.

Consistency in PI estimation for different SNR levels and good agreement of PI values with their reference values from the commercial scanner suggest that the envelope can be used in automated measurement of clinical indices. While making diagnosis possible by users less exposed to ultrasound technology, the spectral envelope as well as automated measurements will be useful in reducing inter/intra observer, inter/intra machine variability.

Acknowledgment

The authors would like to thank Bente Simensen, for the acquisition of patient uterine and umbilical PW Doppler recordings.

This work was supported by the MedIm Bridging Grant provided by Norwegian Research School in Medical Imaging (MedIm) and the project UMOJA - Ultrasound for midwives in rural areas, Helse Midt-Norge RHF.

References

[1] E. Grant, C. Benson, G. Moneta, A. Alexandrov, J. Baker, and E. Bluth, "Carotid artery stenosis: gray-scale and Doppler US diagnosis society of radiologists in ultrasound consensus conference," *Radiology*, vol. 229, no. 2, pp. 340–346, 2003.

[2] M. Heijenbrok-Kal, E. Buskens, P. Nederkoorn, Y. V. D. Graaf, and M. Hunink, "Optimal peak systolic velocity threshold at duplex US for determining the need for carotid endarterectomy: a decision analytic approach," *Radiology*, vol. 238, no. 2, pp. 480–488, 2006.

[3] R. Albayrak, B. Degirmenci, M. Acar, A. Haktanir, M. Colbay, and M. Yaman, "Doppler sonography evaluation of flow velocity and volume of the extracranial internal carotid and vertebral arteries in healthy adults," *J Clin Ultrasound*, vol. 35, pp. 27–33, 2007.

[4] K. V. Canneyt, A. Swillens, L. Lovstakken, L. Antiga, P. Verdonck, and P. Segers, "The accuracy of ultrasound volume flow measurements in the complex flow setting of a forearm vascular access," *J. Vasc. Access*, vol. 14, no. 3, pp. 281–290, 2012.

[5] J. Lee, J. Kim, S. Yoon, Y. Lim, Y. Jeon, and C. Bahk, J.and Kim, "Evaluation of corrected flow time in oesophageal Doppler as a predictor of fluid responsiveness," *Br. J. Anaesth.*, vol. 99, no. 3, pp. 343–348, 2007.

[6] H. Gardiner, J. Brodszki, A. Eriksson, and K. Marsal, "Volume blood flow estimation in the normal and growth-restricted fetus," *Ultrasound Med. Biol*, vol. 28, no. 9, pp. 1107–1113, 2002.

[7] K. Nicolaides, G. Rizzo, K. Hecher, and R. Ximenes, "Doppler in Obstetrics," *The Fetal Medicine Foundation*, 2002.

[8] J. Cnossen, R. Morris, B. ter Riet G., Mol, J. van der Post, A. Coomarasamy, A. Zwinderman, S. Robson, P. Bindels, J. Kleijnen, and K. Khan, "Use of uterine artery Doppler ultrasonography to predict pre-eclampsia and intrauterine growth restriction: A systematic review and bivariable meta-analysis," *CMAJ*, vol. 178, pp. 701–711, 2008.

[9] D. Evans, W. McDicken, R. Skidmore, and J. Woodcock, "Doppler ultrasound, physics, instrumentation, and clinical application," 1989.

[10] V. Newhouse, P. Bendick, and L. Varner, "Analysis of transit-time effects on Doppler flow measurements," *IEEE Transactions on Biomedical Engineering*, vol. 23, pp. 381–387, 1976.

[11] V. Newhouse, L. Varner, and P. Bendick, "Geometrical spectrum broadening in ultrasonic Doppler systems," *IEEE Transactions on Biomedical Engineering*, vol. 24, pp. 478–480, 1977.

[12] P. Bascom, R. Cobbold, and B. Roelofs, "Influence of spectral broadening on continuous wave Doppler ultrasound spectra: a geometric approach," *Ultrasound Med Biol*, vol. 12, pp. 387–395, 1986.

[13] V. Newhouse, E. Furgason, G. Johnson, and D. Wolf, "The dependence of ultrasound Doppler bandwidth on beam geometry," *IEEE Transactions on Sonics and Ultrasonics*, vol. 27, pp. 50–59, 1980.

[14] G. Guidi, C. Licciardello, and S. Falteri, "Intrinsic spectral broadening (ISB) in ultrasound Doppler as a combination of transit time and local geometrical broadening," *Ultrasound Med Biol*, vol. 26, pp. 853–862, 2000.

[15] L. Mo, L. Yun, and R. Cobbold, "Comparison of four digital maximum frequency estimators for Doppler ultrasound," *Ultrasound Med. Biol.*, vol. 14, no. 5, pp. 355–363, 1988.

[16] T. D. Alessio, "'objective' algorithm for maximum frequency estimation in Doppler spectral analysers," *Medical & Biological Engineering & Computing*, vol. 23, pp. 63–68, 1985.

[17] K. Marasek and A. Nowicki, "Comparison of the performance of three maximum Doppler frequency estimators coupled with different spectral estimation methods," *Ultrasound Med. Biol.*, vol. 20, no. 7, pp. 629–638, 1994.

[18] R. Moraes, N. Adin, and D. Evans, "The performance of three maximum frequency envelope detection algorithms for doppler signals," *Journal of Vascular Investigation*, vol. 1, pp. 126–134, 1995.

[19] A. H. Steinman, J. Tavakkoli, J. G. Myers, R. S. Cobbold, and K. W. Johnston, "A new approach for determining maximum frequency in clinical Doppler ultrasound spectral estimates," *22nd Annual EMBS International Conference, Chicago*, 2000.

[20] A. Steinman, J. Tavakkoli, J. Myers, R. Cobbold, and K. Johnston, "Sources of error in maximum velocity estimation using linear phased-array Doppler systems with steady flow," *Ultrasound Med. Biol.*, vol. 27, no. 5, pp. 655–664, 2001.

[21] K. Fernando, V. J. Mathews, and E. Clark, "A mathematical basis for the application of the modified geometric method to maximum frequency estimation," *IEEE Transactions on Biomedical Engineering*, vol. 51, pp. 2085–2088, 2004.

[22] D. Vilkomerson, S. Ricci, and P. Tortoli, "Finding the peak velocity in a flow from its Doppler spectrum," *IEEE Transactions on Ultrasonics, Ferroelectrics, and Frequency Control*, vol. 60, no. 10, pp. 2079–2088, 2013.

[23] S. Ricci, R. Matera, and P. Tortoli, "An improved Doppler model for obtaining accurate maximum blood velocities," *Ultrasonics*, vol. 54, pp. 2006–2014, 2014.

[24] S. Ricci, D. Vilkomerson, R. Matera, and P. Tortoli, "Accurate blood peak velocity estimation using spectral models and vector Doppler," *IEEE Transactions on Ultrasonics, Ferroelectrics, and Frequency Control*, vol. 62, pp. 686–696, 2015.

[25] J. Tschirren, R. M. Lauer, and M. Sonka, "Automated analysis of Doppler ultrasound velocity flow diagrams," *IEEE Transactions on Medical Imaging*, vol. 20, pp. 1422–1425, 2001.

[26] O. Shechner, M. Sheinovitz, M. Feinberg, and H. Greenspan, "Image analysis of Doppler echocardiography for patients with atrial fibrillation," *IEEE International Symposium on Biomedical Imaging: Nano to Macro, 2004*, vol. 1, pp. 488–491, 2004.

[27] D. Doherty, I. James, and J. Newnham, "Estimation of the Doppler ultrasound maximal umbilical waveform envelope: I. Estimation method," *Ultrasound Med Biol*, vol. 28, pp. 1251–1259, 2002.

[28] A. Kathpalia, Y. Karabiyik, B. Simensen, E. Tegnander, S. Eik-Nes, H. Torp, I. Ekroll, and G. Kiss, "A robust Doppler spectral envelope detection technique for automated blood flow measurements," *2015 IEEE International Ultrasonics Symposium*, pp. 1–4, 2015.

[29] V. Newhouse, D. Censor, T. Vontz, J. Cisneros, and B. Goldberg, "Ultrasound Doppler probing of flow transverse with respect to beam axis," *IEEE Transactions on Biomedical Engineering*, vol. 34, pp. 779–788, 1987.

[30] D. Censor, V. Newhouse, T. Vontz, and H. Ortega, "Theory of ultrasound Doppler spectra velocimetry for arbitrary beam and flow configurations," *IEEE Transactions on Biomedical Engineering*, vol. 35, pp. 740–751, 1988.

[31] G. Guidi, V. Newhouse, and P. Tortoli, "Doppler spectrum shape analysis based on the summation of flow-line spectra," *IEEE Transactions on Ultrasonics, Ferroelectrics and Frequency Control*, vol. 42, pp. 907–915, 1995.

[32] O. Gomez, F. Figueras, S. Fernandez, B. M., J. Martnez, B. Puerto, and E. Gratacos, "Reference ranges for uterine artery mean pulsatility index at 11-41 weeks of gestation," *Ultrasound Obstet Gynecol*, vol. 62, pp. 128–132, 2008.

[33] D. Christopher, P. Burns, J. Hunt, and F. Foster, "The effect of refraction and assumed speeds of sound in tissue and blood on Doppler ultrasound blood velocity measurements," *Ultrasound Med Biol*, vol. 21, pp. 187–201, 1995.

[34] P. Hoskins, "Accuracy of maximum velocity estimates made using Doppler ultrasound systems," *Br J Radiol*, vol. 69, pp. 172–177, 1996.

[35] P. Hoskins, "A comparison of single- and dual-beam methods for maximum velocity estimation," *Ultrasound Med Biol*, vol. 25, pp. 583–592, 1999.

Chapter 5

Quantitative Doppler Analysis using Conventional Color Flow Imaging Acquisitions

Yücel Karabiyik[1], Ingvild Kinn Ekroll[1,2], Sturla Eik-Nes[3], and Lasse Løvstakken[1]
[1] Dept. of Circulation and Medical Imaging, NTNU, Norway
[2] St. Olavs Hospital, Trondheim University Hospital, Norway
[3] National Center for Fetal Medicine, St. Olavs University Hospital, Norway

Interleaved acquisitions used in conventional triplex mode results in a trade-off between the frame rate and the quality of velocity estimates. On the other hand, work-flow becomes inefficient when the user has to switch between different modes, and measurement variability is increased. This work investigates the use of power spectral Capon estimator in quantitative Doppler analysis using data acquired with conventional color flow imaging (CFI) schemes. To preserve the number of samples used for velocity estimation, only spatial averaging was utilized, and clutter rejection was performed after spectral estimation. The resulting velocity spectra were evaluated in terms of spectral broadening using an adaptive maximum velocity estimator. The spectral envelopes were also used for Doppler index calculations using *in vivo* and string phantom acquisitions. *In vivo* results demonstrated that the Capon estimator can provide spectral estimates with sufficient quality for quantitative analysis using packet based CFI acquisitions. The calculated Doppler indices were similar to the values calculated using spectrograms estimated on a commercial ultrasound scanner.

5.1 Introduction

Blood velocity measurements using ultrasound are normally dependent on anatomical B-mode images for navigation, color flow imaging (CFI) for detecting abnormal blood flows, and spectral-Doppler, i.e., pulsed wave (PW)-/continuous wave (CW)-Doppler, for quantitative measurements. While these sources of image data are available near simultaneously using interleaved acquisition schemes on clinical scanners, so-called duplex/triplex modes, the trade-off in image quality and/or spectral quality can be quite severe. Therefore, the recommendation is that spectral-Doppler is done individually for most blood velocity measurements. This implies that the placement of the Doppler sample volume is positioned based on image data that is not necessarily

current, that spectral velocity information is only available at one location at a time, and the current workflow often involves switching back and forth between modalities.

Conventional CFI scanning schemes employ focused transmits scanned over a region of interest (ROI) using a given pulse repetition frequency (PRF) to acquire slow-time Doppler ensembles. Mean velocities in this region are estimated for each pixel and displayed using color coding. For several reasons, it would be beneficial to extract the quantitative information directly from 2-D CFI. First, this would have the potential to simplify the work flow, and second new information could be obtained simultaneously by analyzing spectral traces from several positions. However, quantitative analysis based on conventional CFI is currently hampered by several factors. First, the frame rate is often too low to follow rapid changes in blood flow. Secondly, the mean velocity estimator may be biased due to sub-optimal clutter filtering and have a high variance. Third, it is usually not the mean, but the maximum velocity trace that is used clinically, and conventional CFI ensembles are too small to perform standard spectral analysis. While spectral information currently can be extracted from CFI data sets, the limited number of pulses available with conventional acquisition schemes leads to a very poor frequency resolution. Fast imaging based on broad emissions and synthetic transmit aperture techniques have been used to bypass these limitations [1–3], are suitable for high-end systems with substantial memory and processing capabilities [4], and may also suffer from reduced penetration in clinical use due to decreased acoustic intensities.

To be able to estimate velocity waveforms with sufficient quality for quantitative Doppler analysis, the spectral estimator should yield power spectral densities (PSDs) with sufficient side lobe suppression and minimum spectral broadening; moreover, the temporal resolution of the Doppler waveform should be high enough to follow accelerations during the cardiac cycle. Conventionally, Welch's method [5] is used for estimating the velocity waveforms in commercial scanners. This method requires long observation windows (OWs), e.g., 64-128 time samples, for estimation of PSDs to achieve low side lobe levels and high frequency resolution. One way to acquire PW-Doppler data is to interleave B-mode, CFI and PW-Doppler acquisitions. A uniform sampling scheme sets an upper limit on the maximum PRF, therefore on the maximum measurable velocity. Alternatively, interrupting PW-Doppler data acquisition with B-mode and CFI acquisitions leaves gaps in the spectrogram. Several methods have been proposed to reconstruct these gaps in order to regenerate continuous spectrograms [6,7] or methods that can generate spectrograms using randomly or periodically sampled sparse data sets [8–11]. The performance of these methods depends heavily on the amount of the available data, and therefore these methods are mainly suitable for duplex imaging where only B-mode and PW-Doppler acquisitions are made. Additionally, they allow for only one or a limited number of spatial locations where velocity spectra can be analyzed simultaneously with sufficient quality.

Data adaptive spectral estimators have been used in medical ultrasound and demonstrated to produce high quality PSDs using shorter OWs than used for the traditional Welch's method. Filter bank methods [11–14], such as Capon and APES, have been shown to produce Doppler spectra with lower side lobe levels and increased frequency resolution using observation window sizes comparable to data

lengths used in CFI for mean velocity estimation, e.g., 8-16 [15]. Recently, a method that combines the Capon spectral estimator and plane wave imaging was used for retrospective qualitative Doppler analysis using short window sizes and interleaved B-mode acquisitions and showed promising results [1].

This work aims to improve the quantitative abilities of duplex CFI. Data acquired for color Doppler image generation are used for estimation of velocity waveforms. 2-D spatial averaging is utilized for covariance matrix estimation and the PSDs are estimated with the power spectral Capon estimator. Further, a recent adaptive maximum velocity envelope estimator [16] is employed for maximum velocity and Doppler index calculation to evaluate the performance of the proposed method. The adaptive spectral estimation methods have been shown to improve frequency resolution and contrast in spectral Doppler [11, 14, 17]. In this work, performance of the power spectral Capon method is evaluated in terms of spectral broadening with ensemble lengths used in conventional CFI.

The paper is organized as follows. In Section 5.2, the PSD estimators, the maximum velocity envelope estimator and the data acquisition setup are presented. In Section 5.3 *in vivo* and string phantom results are presented and discussed in Section 5.4. Concluding remarks are given in section 5.5.

5.2 Methods

The acquisition, beamforming and post-processing methods in this work are all chosen to address the aforementioned CFI limitations, while retaining the possibility for implementation also on a conventional low- to mid-end ultrasound system. For an in-depth analysis, both plane wave imaging and conventional CFI scanning schemes were used for acquisition of data sets. A 2-D averaging region is used for each estimation.

Let $x_{r,b}(n)$ represent a sample in CFI or plane wave data set at depth r in radial, beam b in lateral direction and emission n after demodulation. It consists of echoes from stationary or slowly moving tissue which is regarded as clutter, signal from blood and zero mean white Gaussian noise. An ensemble acquired at this location that has N temporal samples, can be expressed as $\mathbf{x}_{r,b} = [x_{r,b}(1)\ x_{r,b}(2)\ \cdots\ x_{r,b}(N)]^T$. N is usually referred to as ensemble length or packet size (PS) in CFI.

5.2.1 PSD Estimators

The ensemble can be subdivided into smaller segments for temporal averaging to decrease the variance. Let l denote the index for the sub-segments $\tilde{\mathbf{x}}_{r,b}$

$$\tilde{\mathbf{x}}_{r,b}(l) = [x_{r,b}(l)\ x_{r,b}(l+1)\ \cdots\ x_{r,b}(l+M-1)]^T, \tag{5.1}$$

where M is the length of the sub-segment.

Including the spatial averaging in radial and lateral directions, the Welch PSD estimator is expressed as

$$\hat{\mathbf{P}}_{Welch}(f_k) = \frac{1}{RBL}\sum_{r=1}^{R}\sum_{b=1}^{B}\sum_{l=1}^{L}\left|\sum_{m=0}^{M-1} w(m)x_{r,b}(l+m)e^{-i2\pi f_k m}\right|^2, \quad (5.2)$$

where $w(m)$ is a tapering window, f_k is the normalized frequency with respect to PRF, L is the number of sub-segments and $M = N-L+1$. In this work, a Hamming window is chosen as the tapering window and $L = 1$, i.e. no subdivision of the ensemble.

The Capon estimator is a filter bank method that generates a unique filter for each frequency estimate. The filter minimizes the power output while keeping the power estimate of the frequency of interest undistorted. As CFI data sets are used for estimation, the estimator is evaluated using only 2-D spatial averaging without any temporal averaging. The estimator can be given as [12]

$$\hat{P}_{Capon}(f_k) = \frac{1}{\mathbf{a}_{f_k}^{\mathrm{H}}\hat{\mathbf{R}}_{Capon}^{-1}\mathbf{a}_{f_k}}, \quad (5.3)$$

where $\mathbf{a}_{f_k} = [1\ e^{i2\pi f_k}\ \cdots\ e^{i2\pi f_k(N-1)}]^T$ is the Fourier vector and the covariance matrix $\hat{\mathbf{R}}_{Capon}$ is

$$\hat{\mathbf{R}}_{Capon} = \frac{1}{RB}\sum_{r=1}^{R}\sum_{b=1}^{B}\mathbf{x}_{r,b}\mathbf{x}_{r,b}^{\mathrm{H}}. \quad (5.4)$$

Fig. 5.1 shows two spectrograms generated using data acquired from the common carotid artery (CCA) when $N = 16$. A 2-D averaging kernel with dimensions of $0.5mm \times 1.2mm$ used for spatial averaging. The Capon method (Fig. 5.1(b)) can isolate the clutter while the Welch method (Fig. 5.1(a)) has high side lobe levels and the clutter affects the low velocity estimations.

5.2.2 Maximum Velocity Envelope Estimation

A recent method [16] proposed for maximum velocity and spectral envelope estimation is used for maximum velocity estimation. The method is a combination of two existing maximum velocity estimation methods, an altered version of the Geometric Method (GM) [18] and the Signal Noise Slope Intersection (SNSI) [19], and employs further steps for exclusion of low quality estimates to achieve low variance maximum velocity envelopes.

The method requires spectrograms without clutter, which are also non-aliased or baseline shifted. In this work, baseline shifts were done manually by inspecting the spectrograms. For each bin in the spectrogram, the spectral values are integrated from zero frequency to the maximum analyzed frequency, generating an integrated power spectrum (IPS). A characteristic IPS has three distinct regions: signal, noise and knee (the transition region between signal and noise) regions. After the regions are detected, the algorithm fits lines to the curves in the signal and noise regions and

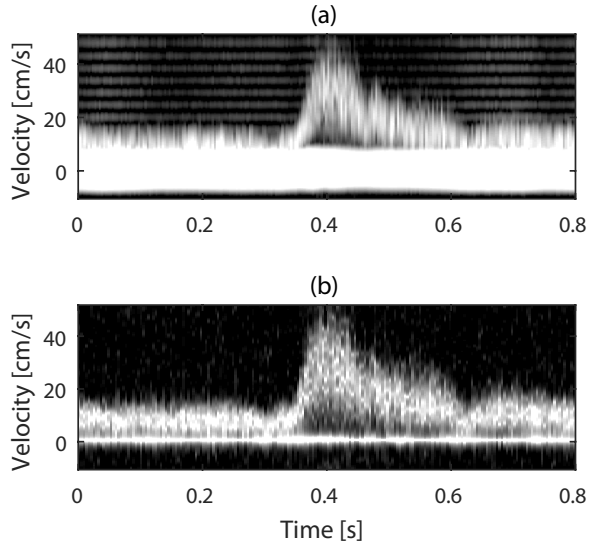

Figure 5.1: Spectrograms estimated with the Welch estimator (a) and the Capon estimator (b) when the ensemble length is short ($N = 16$). The spectrograms are displayed with 40 dB dynamic range.

finds the slope of the fitted lines. Next, the maximum frequency point $f_{d_{max}}$ is found by finding the point in the knee region which has the slope closest to the slope m, defined as

$$m(x) = m_s x + m_n(1 - x), \tag{5.5}$$

where m_s and m_n are the slopes of the lines fitted to the curves of signal and noise regions respectively, while x is chosen as 0.1. This value was found empirically by qualitative assessments for beam-to-flow angles up to 60° [19, 20].

The low quality estimates are excluded based on power thresholding and the location of the knee center where a maximum limit is introduced on its location. The excluded estimations are later interpolated. In the original algorithm, linear interpolation is used for this purpose while in this work, the time resolution of the spectrograms is a limitation. Therefore, spline interpolation is employed instead to improve the reconstruction of the true spectral trace. Finally the maximum velocity, v_{max}, is found by

$$v_{max} = f_{d_{max}} PRF c / 2 f_0 \cos\theta, \tag{5.6}$$

where f_0 is the center frequency and θ is the beam-to-flow angle.

The method has previously been evaluated on spectrograms generated using Welch's method. In this work, the method was applied to Capon spectograms generated from low packet sizes and with a relatively low time resolution.

The maximum velocity envelopes were further used for PI calculation. PI is for instance known to be an effective indicator for the prediction of pre-eclampsia [21] in pregnancy and calculated as

$$PI = (PSV - EDV)/TAV, \tag{5.7}$$

where the time averaged velocity (TAV) is calculated between the detected peak systolic velocity (PSV) and end diastolic velocity (EDV) for each cycle.

5.2.3 Data Acquisition and Processing

String phantom acquisitions

The quantitative assessments were done on string phantom data sets recorded using a Doppler string phantom, Mark 4 (JJ&A Instruments, Duvall, WA, USA). This system provided both constant velocity movement as well as physiological waveforms, such as umbilical artery flow. A rubber 1.6 mm diameter o-ring cord was used as the string. Stationary and umbilical artery waveforms were chosen for performance evaluation. The angular positioner of an Acoustic Intensity Measurement System AIMS III (Onda, Sunnyvale, California, USA) was employed to accurately set the beam-to-flow angle in the investigation. The probe was placed above the string and aligned to minimize out of plane motion by manually inspecting the acquired B-mode images. Later, the probe moved in azimuth and radial plane while keeping the elevation position fixed in order to record data with different beam-to-flow angles and velocities. Table 5.1 summarizes the setup and acquisition parameters of the string phantom recordings.

String phantom data were recorded using a Verasonics ultrasound system (Verasonics Inc., Redmond, WA, USA) with a L11-4V linear probe. A plane wave acquisition scheme was here used in order to be able to generate spectrograms using arbitrary packet sizes and compare the Welch and Capon power spectral estimators based on the data from the same recording. A continuous scanning scheme was used with 10 and 6 kHz PRFs for stationary flow and umbilical artery flow waveforms respectively.

In order to investigate spectral broadening with different scenarios, the string was moved with a constant velocity, mimicking flow conditions of velocities 20, 60 and 100 cm/s. For each velocity, the recordings were done with 30°, 45°, 60° and 75° beam-to-flow angles. For each angle and velocity 1 second of data was recorded. Continuous plane wave acquisitions were divided into packets with sizes 8, 12 and 16 for the Capon PSD estimations. The data with 16 packet size were further used with the Welch estimator to demonstrate what could be achieved with a conventional estimator ($L = 1$ and no time overlap). The packet data were filtered with a 6th order FIR filter to be used with the Welch estimator to avoid the clutter effect shown in Fig. 5.1. This resulted in effective OW length 11 after filter initialization. Reference Welch PSD estimations were done with 64 OW length and 75% overlap resulting in 1872 maximum velocity estimations for each beam-to-flow angle and velocity. The number of estimations done for packet based estimations were PRF/PS. The dimensions of the

2-D spatial averaging region, $0.7mm \times 1mm$ in lateral and radial directions respectively, was the same for all methods.

The umbilical artery waveform recordings were processed in the same manner. The estimated spectrograms were used for PI estimation and the effect of broadening on PI calculations was investigated.

As the transmit pulse parameters are different for actual CFI and PW-Doppler recordings, the recorded data were also filtered with narrow and wide bandwidth filters during IQ demodulation to mimic using long and short pulse lengths for PW and CFI recordings respectively. See Table 5.1 for the signal bandwidths ratio where the bandwidth is defined as the full width at -30 dB in the power spectrum.

Table 5.1: String phantom acquisition setup

Parameter	stationary	umbilical
Center frequency [MHz]	6	6
Pulse periods	2.5	2.5
PRF [kHz]	10	6
F-number	1.4	1.4
CFI/PW-Doppler bandwidth ratio	2.23	2.23

In vivo acquisitions

In vivo acquisitions from healthy volunteers were performed to evaluate the method using conventional CFI recordings. Recordings from umbilical artery at gestational age 32 weeks, common carotid artery recording from 30 year old male and aortic flow from a 28 year old male volunteer were acquired.

In vivo recordings were done using Vivid E95 (GE Vingmed Ultrasound, Horten, Norway) clinical scanner and CFI scanning schemes with different packet sizes and frame rates. ROIs were chosen that would make it possible to acquire a 2-D region with dimensions sufficient for interpretation of the anatomy, while providing sufficient frame rate for the investigation of the performance for high and low frame rates using different frame downsampling factors. In this setting, frame rate of the color Doppler image corresponds to the time resolution of the velocity waveform. Table 5.2 summarizes the imaging setup and post-processing parameters. The 2-D averaging regions used for the Capon spectral estimations were $3mm \times 0.6mm$, $5.5mm \times 3.1mm$ and $2.25mm \times 1.12mm$ in lateral and radial directions for the CCA, aortic flow and the umbilical artery recordings respectively. After the CFI data acquisition, a PW-Doppler reference spectrogram was recorded while keeping the probe approximately in the same position. The spectrograms estimated with the Capon estimator were compared to spectrograms estimated on the scanner in terms of broadening. The reference scanner spectrograms were generated in PW-Doppler only mode in order to achieve high quality. In addition, the calculated PI values were compared for the umbilical artery case.

Table 5.2: Acquisition setup and processing parameters

Parameter	umbilical	carotid	cardiac
CFI			
Center frequency [MHz]	3.125	5	2.2
Pulse periods (cycles)	2.5	4	3
PRF [kHz]	5	5	5
Packet size	14	10	12
Frame rate	104	94	97
Cut-off velocity [cm/s]	8	15	30
Probe type	C1-6-D	11L-D	M4Sc-D
PW			
Center frequency [MHz]	2.5	5.9	2
Pulse periods (cycles)	12	6.5	12
PRF [kHz]	2.8	5.3	5.8
F-number	5	5	5.5
Frame rate	479	531	485

Clutter filtering

Ideally, the clutter filter should have a short transition region and high stop band attenuation which are difficult to achieve with the short ensemble lengths used in CFI. Adaptive spectral estimation methods are shown to have low side lobe levels and can confine the clutter signal in a narrow region around zero frequency [17]. Recently this was utilized for clutter removal in CFI [22]. Clutter filtering for Capon spectrograms in this work was performed after spectral estimation as proposed in [22], by setting spectral estimates between defined cut-off frequencies to zero. The cut-off frequencies were chosen manually by visually inspecting the spectrograms (Table 5.2). Due to insufficient spectral resolution and higher side lobe levels, this approach is not applicable for the Welch method with small packet sizes. Finite impulse response (FIR) filters were used for the data used for the Welch spectral estimation methods.

5.3 Results

The performance of the Capon estimator was evaluated in terms of spectral broadening with different beam-to-flow angles and packet sizes using data recorded from the string phantom, umbilical artery, CCA and aorta. The results were compared to the conventional Welch method with long OW length or the reference spectrogram estimated on the commercial scanner. Later, the effect of broadening on the

quantitative PI calculation was investigated using *in vivo* and string phantom recordings.

5.3.1 String phantom results

Constant velocity waveform

Table 5.3 shows maximum velocity estimates (in cm) for different beam-to-flow angles and velocities. The bias is calculated using the data from the same recordings; however, the data were filtered differently to mimic different settings for CFI and PW-Doppler recordings. Bias in maximum velocity estimation increases with increasing beam-to-flow angle and velocity for all methods. Increased angle and velocity limit the time that the scatterers are observed in the sample volume, which in turn increases the broadening. Comparing the Capon method with packet size 16 to Welch's with the same packet size, it can be seen that the Capon method can decrease the spectral broadening significantly, especially for low velocities. Increasing the packet size from 8 to 12 decreases the standard deviation and bias of the maximum velocity estimates for the Capon method. Increasing the packet size further improves the estimates only marginally. Welch's method with packet 64 size performs better for all beam-to-flow angles and velocities except for 75° and 20 cm/s case where Capon method with packet size 16 performed slightly better. Absolute bias increases more for the Capon estimator than the Welch estimator (with 64 OW length) as velocity increases.

Table 5.3: String phantom stationary flow pattern results

	20 cm/s						60 cm/s						100 cm/s					
30°		Welch		Capon				Welch		Capon				Welch		Capon		
	PS	**64**	**16**	**8**	**12**	**16**	**PS**	**64**	**16**	**8**	**12**	**16**	**PS**	**64**	**16**	**8**	**12**	**16**
	M	23.4	37.1	26.6	25.7	25.2	**M**	65.4	77.2	73.6	73.1	73.2	**M**	107.9	119.1	122.9	122.8	122.5
	S	0.6	0.8	1.8	1.3	0.9	**S**	1.1	0.9	2.3	1.8	1.9	**S**	2.4	1.5	4	3.7	4.1
45°		Welch		Capon				Welch		Capon				Welch		Capon		
	PS	**64**	**16**	**8**	**12**	**16**	**PS**	**64**	**16**	**8**	**12**	**16**	**PS**	**64**	**16**	**8**	**12**	**16**
	M	24.3	40.9	25.9	25.9	25.9	**M**	67.7	82.1	75.4	76.1	76.7	**M**	111.4	123.9	125.5	125.9	125.4
	S	0.6	0.6	1.2	1	0.9	**S**	1.2	1.15	2	1.8	1.7	**S**	2	1.8	4	3.4	3.6
60°		Welch		Capon				Welch		Capon				Welch		Capon		
	PS	**64**	**16**	**8**	**12**	**16**	**PS**	**64**	**16**	**8**	**12**	**16**	**PS**	**64**	**16**	**8**	**12**	**16**
	M	26.2	49.8	28.3	27.9	27.9	**M**	71.8	91.7	81	81.3	82	**M**	114.4	142.6	126.6	127.2	126.8
	S	0.9	0.9	1.4	1	1.1	**S**	1.8	1.4	2.6	2.1	2	**S**	2.9	2.4	3.8	3.9	3.9
75°		Welch		Capon				Welch		Capon				Welch		Capon		
	PS	**64**	**16**	**8**	**12**	**16**	**PS**	**64**	**16**	**8**	**12**	**16**	**PS**	**64**	**16**	**8**	**12**	**16**
	M	34.9	82.6	37.7	34.6	33.9	**M**	79.2	120.8	95.9	94	94.4	**M**	129.4	163.8	155.4	154.6	157.2
	S	4.9	15	3.2	2.3	2.1	**S**	3.1	3.3	5.7	3.8	3.9	**S**	7.8	5.3	7.8	6.1	5.8

PS: Packet size, M: Mean, S: Standard deviation

Fig. 5.2 shows spectrograms generated using data recorded with 60 ° beam-to-flow angle and 60 cm/s velocity with OW lengths 16 and 64 for Welch's method and 8 and 16 for the Capon method. Welch's method with 64 provides the envelope estimation with lowest bias and has better dynamic range than the other estimations. Welch's method with 16 packet size yields spectrogram with considerably higher broadening. Even though the envelope estimations done on Capon spectrograms yield similar values, 16 packet size provides better contrast than the 8 case. This is also shown in Fig 5.2(e) where the spectra estimated at the same time instance are plotted together. Note that the Capon-based results in Table III and Fig. 2 are based on wideband filtering, whereas the reference (Welch 64) used a narrow bandwidth.

Fig. 5.3 shows the maximum velocity estimation results for the Capon with wide and narrow bandwidth filtered data. The OW lengths are 64 and 16 for the Welch and the Capon methods respectively. The maximum velocities based on the Capon spectra are more similar to the reference method when a narrowband filter is applied. For low velocities, e.g., 20 cm/s, the methods yield similar results. However, the increase in bias with increasing velocity is higher for the Capon based estimates than the Welch based estimates.

Umbilical artery waveform

Umbilical artery waveform recordings were done to evaluate the effect of broadening on Doppler index estimations. Similar to the stationary waveform recordings, umbilical artery waveform recordings were done with beam-to-flow angles 30°, 45°, 60° and 75°. Table 5.4 shows the estimated PI values for different beam-to-flow angles and packet sizes. Since the bias increases for increasing beam-to-flow angles, especially for high velocities, PI values increases with increased beam-to-flow angle except for Welch's method with packet size 16. This is due to the increased mean velocity which is the denominator in the PI formula. Standard deviation also increases with increasing beam-to-flow angle although the increase is not significant.

Fig. 5.4 shows the resulting spectrograms from the umbilical waveform recorded with 60° beam-to-flow angle. The center of the red circles show the detected peak systolic and end diastolic velocities. Similar to Fig. 5.2, the reference method (Welch 64) provides the best contrast and spectral resolution. Welch 64 and Capon with packet sizes 16 and 8 give similar PSV and EDV values while Welch with packet size 16 yielded considerably higher maximum velocity results throughout each cycle. As expected from the stationary flow experiment, the Capon method had higher bias for peak systolic velocities compared to Welch 64 OW length.

5.3.2 In vivo results

Fig. 5.5 shows a comparison between a conventional PW-Doppler recording and a CFI recording from the CCA. Fig. 5.5(a) shows B-mode image of the artery. The yellow parallel lines in the image show the sample volume used for the generation of the spectrogram shown in Fig. 5.5(c) while the green line shows the chosen flow direction. The beam-to-flow angle used for velocity correction was 77 °. Fig. 5.5(b) shows color

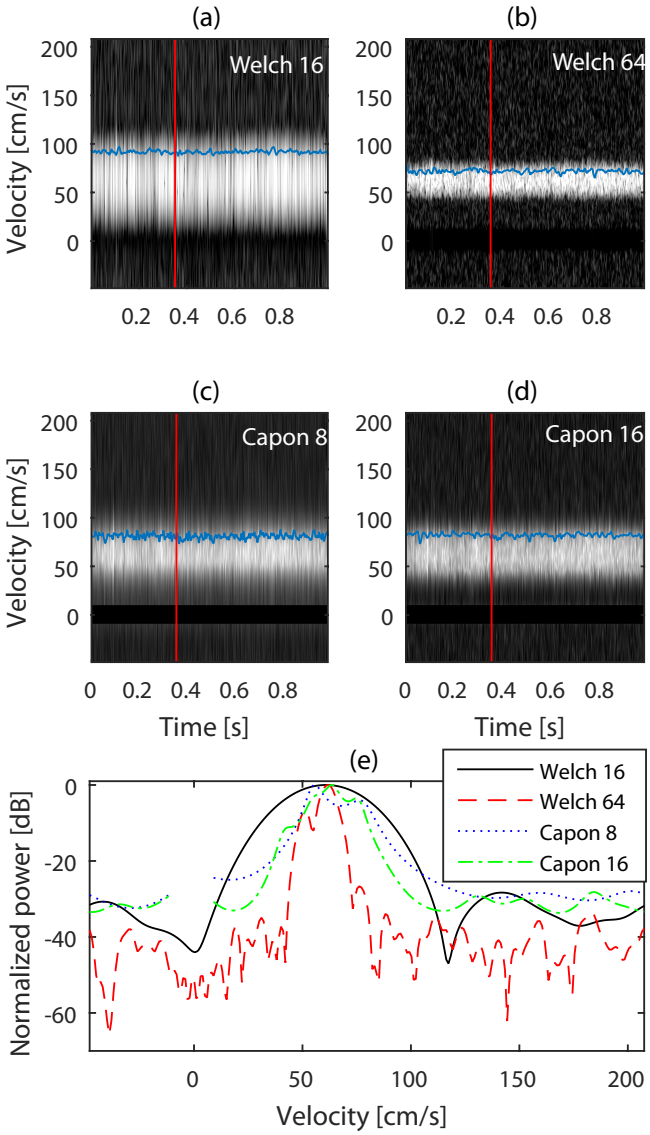

Figure 5.2: The spectrograms estimated with (a) Welch with packet size 16, (b) Welch with packet size 64, (c) Capon with packet size 8 and (d) Capon with packet size 16 and the corresponding estimated envelope plotted on top. The string velocity is 60 cm/s and the beam-to-flow angle is 60°. The dynamic range used for the display is 50 dB. The spectra shown in (e) correspond to the spectra estimated at the time point indicated with the vertical red lines for all estimations.

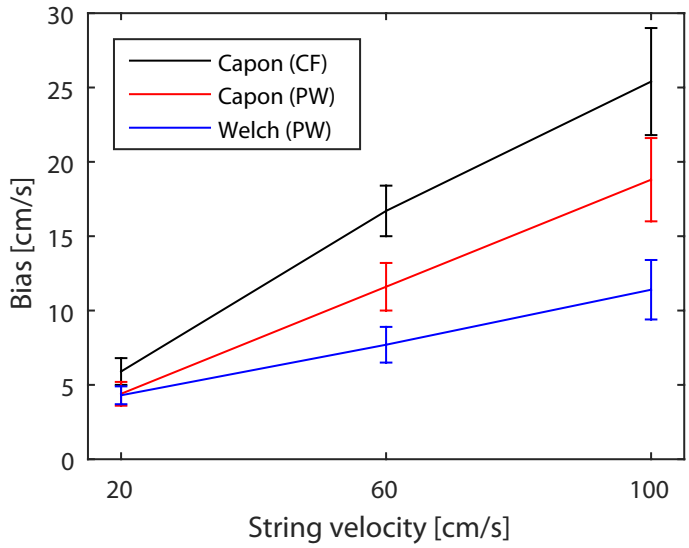

Figure 5.3: The estimated maximum velocities for different velocities when the beam-to-flow angle is 45° and the OW lengths are 16 for the Capon and 64 for the Welch estimator. The red and blue curves are estimated using the narrowband filtered data where the black on is estimated on the widerband filtered data. CF: Color flow

Table 5.4: String phantom umbilical artery flow pattern PI estimation results

		Welch		Capon		
	PS	**64**	**16**	**8**	**12**	**16**
30°	**M**	0.85	0.66	0.92	0.90	0.90
	S	0.03	0.02	0.03	0.03	0.03
45°	**M**	0.85	0.63	0.92	0.90	0.89
	S	0.03	0.02	0.02	0.03	0.03
60°	**M**	0.88	0.56	0.94	0.91	0.90
	S	0.03	0.02	0.03	0.03	0.04
75°	**M**	0.89	0.45	0.99	0.95	0.94
	S	0.04	0.02	0.05	0.05	0.05

PS: Packet size, M: Mean, S: Standard deviation

flow image generated offline from the recorded CFI data using the autocorrelation method [23] and the green box in the image show the sample volume used for generation of the spectrogram shown in Fig. 5.5 (c). Capon spectra were generated using OW length 10 samples. The time resolution of the spectrograms are 10.6 ms and 1.9 ms which corresponds to 97 and 531 bins/second for the CFI generated and the PW-Doppler generated spectrograms respectively. The mean PSV was found to be 105

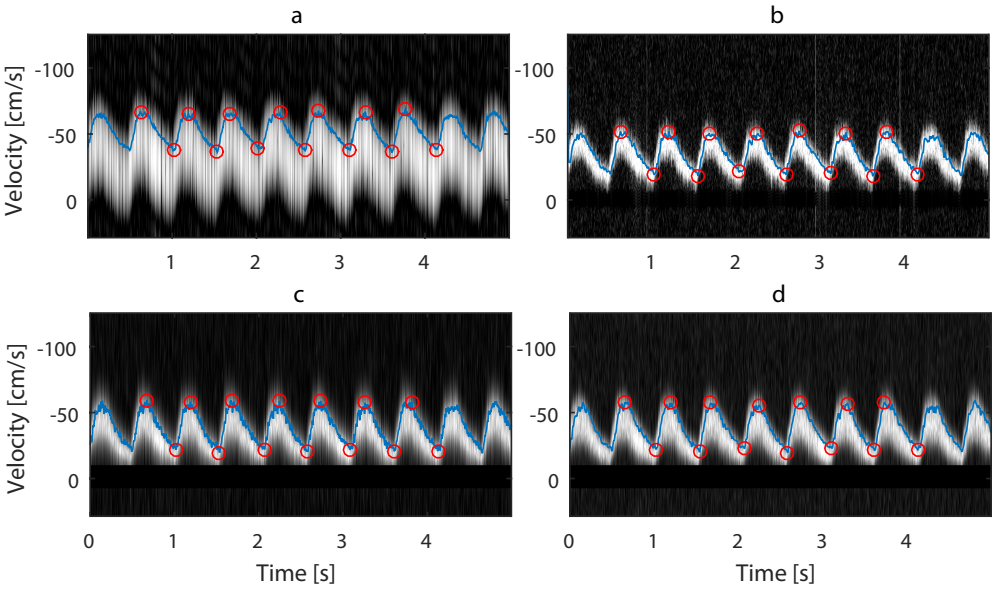

Figure 5.4: String phantom umbilical artery waveform results displayed along with the estimated envelopes and PSV and EDV estimations. Spectrograms estimated with a) FFT with packet size 16, b) FFT with packet size 64, (c) Capon with packet size 8 and (d) Capon with packet size 16 and the corresponding estimated envelope plotted on top. Beam-to-flow angle 60° and the dynamic range used for the display is 50 dB.

cm/s for the CFI generated spectrogram while it was 112.4 cm/s for the PW-Doppler. The standard deviations were 3.6 cm/s and 5.7 cm/s for the CFI estimates and PW-Doppler estimates respectively.

Fig. 5.6 shows the results of umbilical artery recordings. Fig. 5.6(a) and Fig. 5.6(c) show the color flow image and the spectrogram generated on the scanner respectively. Fig. 5.6(b) shows the color flow image generated using the CFI data set and the Fig. 5.6(d) shows the Capon spectrogram. The packet size was 14. The mean PSV were found to be 46.4 cm/s and 44.5 cm/s while the EDV were 15.2 cm/s and 12.5 cm/s for the Capon spectra and the reference spectra respectively. The estimated mean PI was 1.11 for the Capon estimator and 1.22 for the reference spectrogram while the mean PI at gestational age 32 weeks is 0.98 [24].

Fig. 5.7 shows the aortic flow comparison. Similar to Fig. 5.6, the top left figure shows the color flow image recorded on the scanner and the offline generated image next to it. Fig. 5.7(c) shows the spectrogram generated on the scanner while Fig. 5.7(d) shows the Capon estimation using the CFI data set. The sample volume depth is around 11 cm. The recordings have high velocity clutter due to the movement of the aortic valve. The spectral envelope estimator assumes that the clutter is filtered sufficiently which would be removal of velocities up to 30 cm/s. In order not to obscure low velocities, the spectrograms were estimated using low cut-off filters while the power

of velocities between 0-30 cm/s were set to zero in the calculation of each IPS.

The mean peak systolic velocities were found to be 111.7 cm/s and 114.8 cm/s and the standard deviations of the PSVs were 2.1 cm/s and 9.8 cm/s using the reference spectrogram and the offline generated spectrogram respectively. The PSV found in the second heart cycle shown in Fig. 5.7(c) is not included in the calculation as the envelope estimator clearly fails in this case.

In order to investigate the effect of frame rate on the PSV, EDV and PI estimation, the umbilical artery recording spectrogram was downsampled by factors 2 and 4 yielding spectrograms with frame rates 52 Hz and 26 Hz, shown in Fig. 5.8(b) and 5.8(c) respectively. Fig. 5.8(a) shows the original sampling rate spectrogram. The envelopes found using the downsampled spectrograms were upsampled to the original frame rate 104 after exclusion of the low quality estimates and interpolated. Table 5.5 shows the mean PSV, EDV and the calculated PI results for each frame rate. The results show that downsampling of the spectrogram caused a decrease in the estimated PSV end EDVs while no significant effect was observed on the PI calculation.

Table 5.5: Time resolution effect on qualitative parameter estimation

	FR [FPS]	**104**	**52**	**26**
PSV	**M [cm/s]**	46.4	45	42.6
	S [cm/s]	3	3	2.4
EDV	**M [cm/s]**	15.2	14.7	13.3
	S [cm/s]	0.8	0.8	0.8
PI	**M**	1.1	1.1	1.1
	S	0.06	0.04	0.08

FR: Frame rate, M: Mean, S: Standard deviation

5.4 Discussion

An adaptive spectral estimation method, the power spectral Capon has been investigated in terms of quantitative use for ensemble lengths used in conventional CFI, e.g., 8-16. Quantitative Doppler analysis was made with CFI data acquired using commercial scanners and compared to conventional PW-Doppler spectrograms. The method has been investigated in these setting for its performance in mean velocity estimation [22] and has also previously been evaluated in terms of frequency resolution with short and long OW lengths [14,15,17]. It was seen from the *in vivo* results that the conventional PW-Doppler spectrograms and the Capon spectrograms yielded similar maximum velocity estimations for high and low velocities. PI estimations done on *in vivo* umbilical artery recordings were comparable and both fell into the normal PI value range ($mean \pm 2 \times standard\ deviation$) for 32 weeks gestational age [24].

Additionally, string phantom experiments were done to quantify spectral broadening for different beam-to-flow angles and velocities. The Capon estimator with OW

length 16 yields similar results to Welch's method with 64 samples for low velocities when same data sets are used for comparison. For high velocities, the Welch's method with long OW outperformed Capon estimator. This effect was not seen to the same extent in the *in vivo* recordings. This may be because the sample volume was not placed exactly at the same location, the time resolution was not high enough to detect the real maxima in the spectrograms, or the effect of using a shorter pulse was less than expected.

It has been previously shown that the Capon method has improved frequency resolution, especially for low velocities. It has also been shown that the Capon method with OW length 16 has approximately the same spectral resolution as 64 samples [15], which was also observed in this work, e.g., Fig. 5.3 for 20 cm/s. However, the advantage of the Capon, which is a narrow band spectral estimator, is lost when the correlation length of the signal is reduced. This effect is more apparent in high velocity and large beam-to-flow angle situations. Table 5.3 shows the effect of beam to flow angle. In practice, less than 60 ° beam-to-flow angle is used for measurements as a rule of thumb and can be said that this holds true for the Capon estimator as well. In addition, it was shown that the Welch's estimator cannot be used with this concept due to limitations of the estimator. Spectral broadening of the Welch's method with OW length 16 was significantly higher for all beam-to-flow angles and velocities. Therefore, the Doppler index estimations clinically were not valuable (Table 5.5).

It was seen that the improvement in dynamic range is marginal when the Capon estimator is used. The Welch method with OW 64 length produced spectrograms with better contrast for all cases. The effect of having lower sidelobe levels for the Welch's method was, however, not significant for maximum velocity estimation in this work.

Providing simultaneous B-mode, CFI and spectral information can be achieved by using broad-wave imaging and software beamforming, such as plane or diverging wave imaging, or synthetic transmit aperture imaging. However, in order to achieve a sufficient (high) PRF for the Doppler imaging, the gain from coherent compounding or synthetic transmit aperture is limited, leading to poorer quality B-mode images. Further, these techniques are based on the assumption of stationary imaging objects, and it has been shown that the motion of blood can lead to underestimation in Doppler imaging [25]. In addition, the acquisition and processing of such techniques brings extra processing power and hardware requirement which makes it possible to implement only on high-end ultrasound scanners.

A major disadvantage of the proposed method is that the time resolution of the spectrogram is dependent on the CFI frame rate. In this work the ROI was restricted to achieve high frame rates. The frame rate needed to display the accelerations in the spectrogram is dependent on the application. Waveforms with high accelerations will need higher time resolutions. It was seen that around 50 FPS was adequate to capture the details of the waveforms that were investigated and provided sufficient time resolution for the given scenario. However, this is not necessarily the case for abnormal cases with higher accelerations, e.g., in presence of intrauterine growth restriction in obstetrics [26]. Decreasing the frame rate down to 26 resulted in decreasing PSV estimates and the spectrogram had a low visual quality. However, EDVs could be retrieved through spline interpolation, i.e., estimated mean EDV approached the

reference mean EDV. The low resolution can be alleviated by combining spectral bins or maximum velocity estimates from several heart cycles into one representative cycle. This can be done, for instance, by aligning data based on the detected PSVs and EDVs. However this requires a steady heart rate and sample volume location.

It was observed that the standard deviation of the estimated maximum velocities were higher for the Capon estimator. However, the difference was marginal and smooth maximum velocity envelopes could be achieved for all methods. A limitation of the maximum envelope estimator is that the clutter has to be removed completely. Residuals from the clutter can alter the standard shape of the IPS and cause false detection.

In PW Doppler, long pulses are used to increase SNR and decrease spectral broadening, and the beam-to-flow angle is adjusted to minimize broadening effects. In CFI, however, short pulses are used in order to increase spatial resolution. The transmissions can be steered to adjust beam-to-flow angle although this does not guarantee to have and optimal beam-to-flow angle for all parts of the image. Therefore, the quantitative analysis done in all spatial points in the ROI may not have the same reliability.

The proposed method for estimation of the PSDs combined with the method proposed in [22] for mean velocity estimation can provide a complete system for triplex mode. The mean velocities can be calculated on the estimated PSDs and quantitative analysis can be done anywhere on the color flow image without switching between different modalities. Additionally, Doppler indices can be calculated using the maximum envelope estimator. This, for example, can be used to provide color coded index maps in addition to the color flow image. This allows the physician to get Doppler indices and velocity waveforms simultaneously from all spatial points in the color flow image. However, this requires a robust automatic baseline shift algorithm and the user has to ensure that the optimal beam-to-flow angle is achieved or automatic quality assessment criteria have to be introduced.

5.5 Conclusions

Quantitative spectral analysis of blood velocities was extracted and evaluated for conventional CFI with limited ensemble sizes (8-16), using the data adaptive Capon spectral estimator. Results showed that clutter and associated sidelobes were sufficiently suppressed, providing comparable accuracy to PW-Doppler for relevant flow phantom and *in vivo* data. While encouraging, results are dependent on the CFI frame rate and the beam-to-flow angle, and further *in vivo* evaluation is warranted.

5.6 Acknowledgements

This work was supported by the UMOJA - Ultrasound for midwives in rural areas (Helse Midt-Norge HMF) project. Authors would like to thank E. Tegnander, L. M. Saxhaug and M. S. Wigen for the *in vivo* acquisitions and A. R. Molares for his help with the string phantom setup.

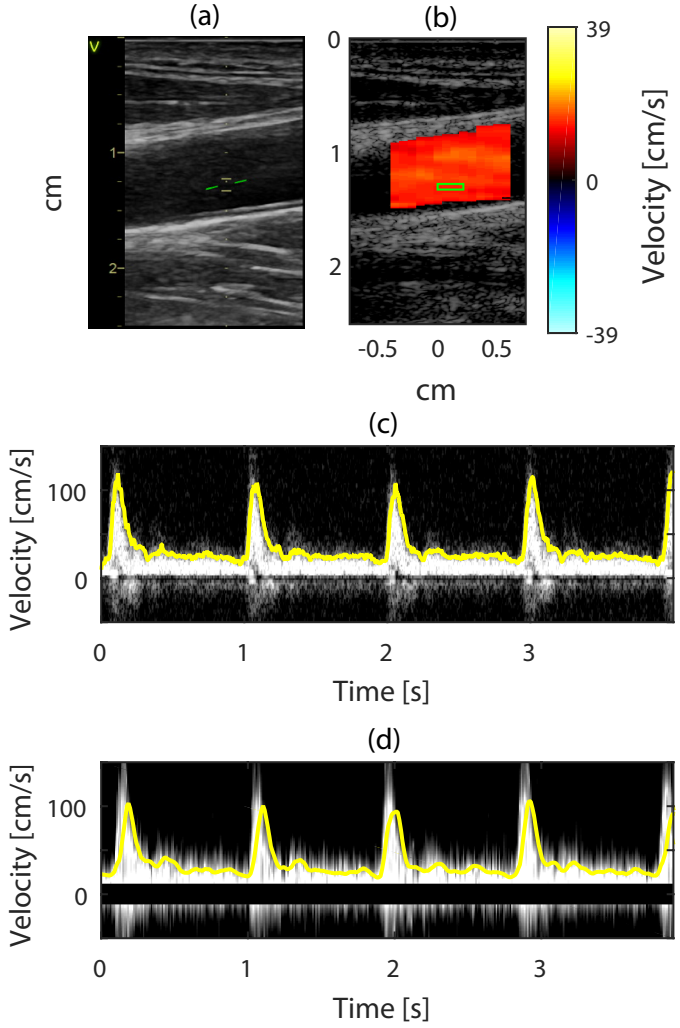

Figure 5.5: Comparison of conventional PW recording with the spectrogram generated with the Capon estimator using the recorded CFI data from the CCA. The B-mode image (a) and the estimated spectrogram (c) are as displayed on the scanner while the CFI (a) and the Capon spectrogram (d) are generated offline using the recorded B-mode and CFI data. The beam-to-flow angle is 77° and the OW length used for Capon is 10. The spectrograms are displayed with 40 dB dynamic range.

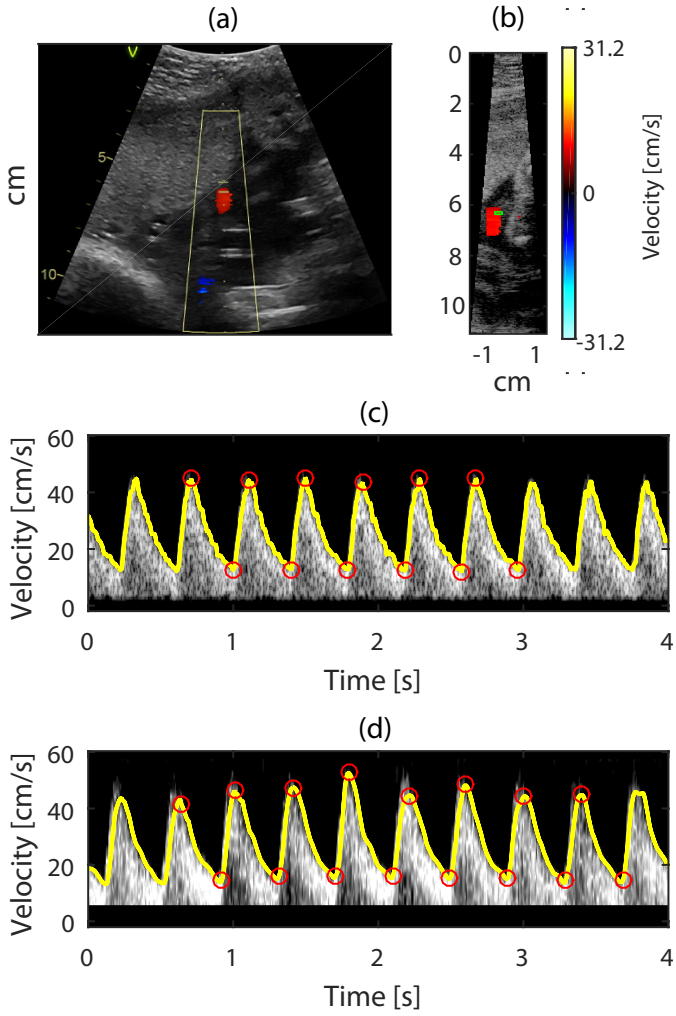

Figure 5.6: Comparison of conventional PW recording with the spectrogram generated with the Capon estimator using the recorded CFI data from the umbilical artery. The B-mode image (a) and the estimated spectrogram (c) are as displayed on the scanner while the CFI (a) and the Capon spectrogram (d) are generated offline using the recorded B-mode and CFI data. The OW length used for Capon is 14. The spectrograms are displayed with 40 dB dynamic range.

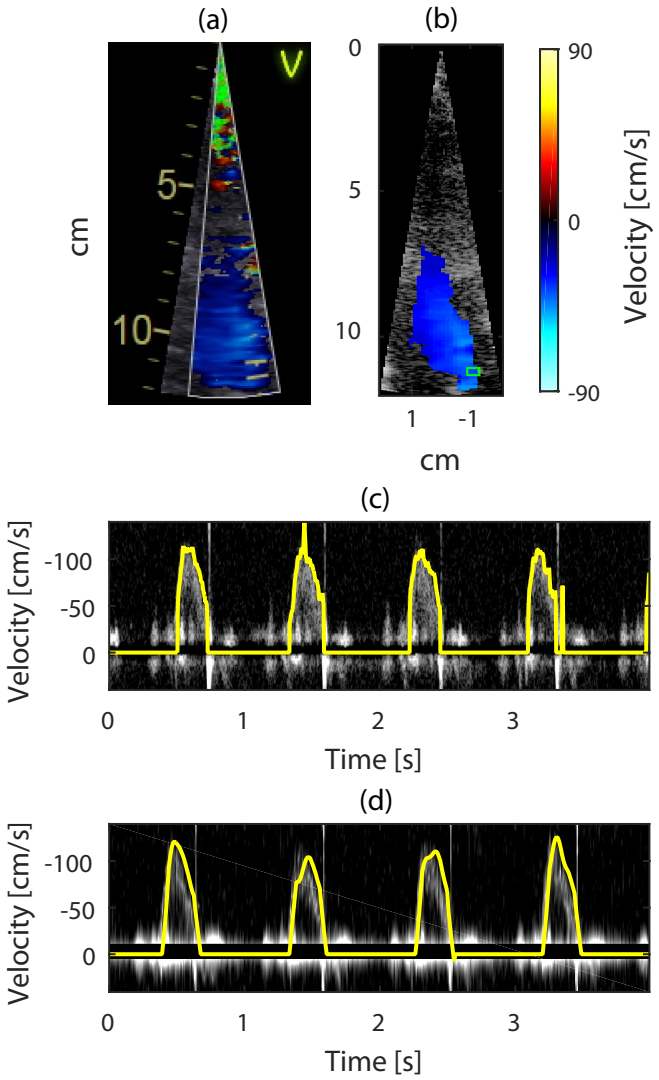

Figure 5.7: Comparison of conventional PW recording with the spectrogram generated with the Capon estimator using the recorded CFI data from the aorta. The B-mode image (a) and the estimated spectrogram (c) are as displayed on the scanner while the CFI (a) and the Capon spectrogram (d) are generated offline using the recorded B-mode and CFI data. The OW length used for Capon is 12. The spectrograms are displayed with 40 dB dynamic range.

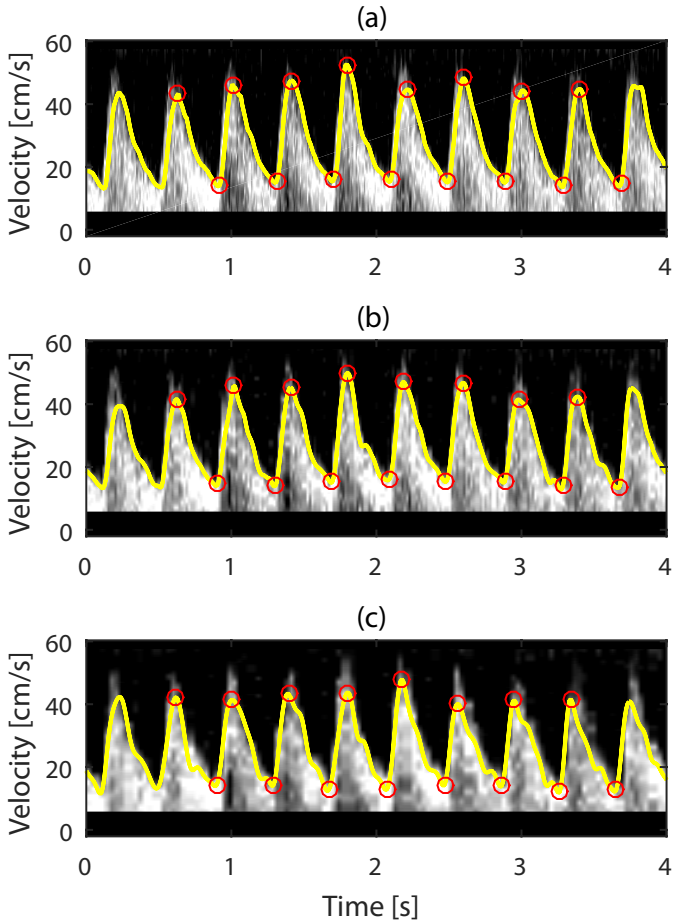

Figure 5.8: The effect of frame rate on the estimated qualitative parameters and the visual spectrum quality. The original frame rate spectrogram (a) and the downsampled by factor 2 (b) and 4 (c) spectrograms are displayed with 40 dB dynamic range.

References

[1] I. K. Ekroll, T. Dahl, H. Torp, and L. Løvstakken, "Combined vector velocity and spectral Doppler imaging for improved imaging of complex blood flow in the carotid arteries," *Ultrasound in medicine & biology*, vol. 40, no. 7, pp. 1629–1640, 2014.

[2] J. Bercoff, G. Montaldo, T. Loupas, D. Savery, F. Meziere, M. Fink, and M. Tanter, "Ultrafast compound Doppler imaging: providing full blood flow characterization," *IEEE Transactions on Ultrasonics, Ferroelectrics, and Frequency Control*, vol. 58, pp. 134–147, January 2011.

[3] J. A. Jensen, S. I. Nikolov, K. L. Gammelmark, and M. H. Pedersen, "Synthetic aperture ultrasound imaging," *Ultrasonics*, vol. 44, pp. e5–e15, 2006.

[4] M. Tanter and M. Fink, "Ultrafast imaging in biomedical ultrasound," *IEEE transactions on ultrasonics, ferroelectrics, and frequency control*, vol. 61, no. 1, pp. 102–119, 2014.

[5] P. D. Welch, "The use of fast Fourier transform for the estimation of power spectra: A method based on time averaging over short, modified periodograms," *IEEE Transactions on audio and electroacoustics*, vol. 15, no. 2, pp. 70–73, 1967.

[6] K. Kristoffersen and B. A. Angelsen, "A time-shared ultrasound Doppler measurement and 2-D imaging system," *IEEE transactions on biomedical engineering*, vol. 35, no. 5, pp. 285–295, 1988.

[7] H. Klebæk, J. A. Jensen, and L. K. Hansen, "Neural network for sonogram gap filling," in *Ultrasonics Symposium, 1995. Proceedings., 1995 IEEE*, vol. 2, pp. 1553–1556, IEEE, 1995.

[8] J. A. Jensen, "Spectral velocity estimation in ultrasound using sparse data sets," *Acoustical Society of America. Journal*, vol. 120, no. 1, pp. 211–220, 2006.

[9] P. Liu and D. Liu, "Periodically gapped data spectral velocity estimation in medical ultrasound using spatial and temporal dimensions," in *2009 IEEE International Conference on Acoustics, Speech and Signal Processing*, pp. 437–440, IEEE, 2009.

[10] J. Richy, D. Friboulet, A. Bernard, O. Bernard, and H. Liebgott, "Blood velocity estimation using compressive sensing," *IEEE transactions on medical imaging*, vol. 32, no. 11, pp. 1979–1988, 2013.

[11] E. Gudmundson, A. Jakobsson, J. A. Jensen, and P. Stoica, "Blood velocity estimation using ultrasound and spectral iterative adaptive approaches," *Signal Processing*, vol. 91, no. 5, pp. 1275–1283, 2011.

[12] P. Stoica and R. L. Moses, *Spectral analysis of signals*. Pearson/Prentice Hall Upper Saddle River, NJ, 2005.

[13] J. Capon, "High-resolution frequency-wavenumber spectrum analysis," *Proceedings of the IEEE*, vol. 57, no. 8, pp. 1408–1418, 1969.

[14] F. Gran, A. Jakobsson, and J. A. Jensen, "Adaptive spectral Doppler estimation," *IEEE transactions on ultrasonics, ferroelectrics, and frequency control*, vol. 56, no. 4, pp. 700–714, 2009.

[15] K. L. Hansen, F. Gran, M. M. Pedersen, I. K. Holfort, J. A. Jensen, and M. B. Nielsen, "In-vivo validation of fast spectral velocity estimation techniques," *Ultrasonics*, vol. 50, no. 1, pp. 52–59, 2010.

[16] A. Kathpalia, Y. Karabiyik, S. Eik-Nes, E. Tegnander, I. Ekroll, G. Kiss, and H. Torp, "Adaptive spectral envelope estimation for Doppler ultrasound," *IEEE Transactions on Ultrasonics, Ferroelectrics, and Frequency Control*, vol. PP, no. 99, pp. 1–1, 2016.

[17] I. K. Ekroll, H. Torp, and L. Lovstakken, "Spectral Doppler estimation utilizing 2-D spatial information and adaptive signal processing," *IEEE transactions on ultrasonics, ferroelectrics, and frequency control*, vol. 59, no. 6, pp. 1182–1192, 2012.

[18] K. Marasek and A. Nowicki, "Comparison of the performance of three maximum Doppler frequency estimators coupled with different spectral estimation methods," *Ultrasound in medicine & biology*, vol. 20, no. 7, pp. 629–638, 1994.

[19] A. Steinman, J. Tavakkoli, J. Myers, R. Cobbold, and K. Johnston, "A new approach for determining maximum frequency in clinical Doppler ultrasound spectral estimates," in *Engineering in Medicine and Biology Society, 2000. Proceedings of the 22nd Annual International Conference of the IEEE*, vol. 4, pp. 2640–2643, IEEE, 2000.

[20] A. H. Steinman, J. Tavakkoli, J. G. Myers, R. S. Cobbold, and K. W. Johnston, "Sources of error in maximum velocity estimation using linear phased-array Doppler systems with steady flow," *Ultrasound in medicine & biology*, vol. 27, no. 5, pp. 655–664, 2001.

[21] N. Onwudiwe, C. Yu, L. Poon, I. Spiliopoulos, and K. Nicolaides, "Prediction of pre-eclampsia by a combination of maternal history, uterine artery Doppler and mean arterial pressure," *Ultrasound in obstetrics & gynecology*, vol. 32, no. 7, pp. 877–883, 2008.

[22] Y. Karabiyik, I. K. Ekroll, S. H. Eik-Nes, J. Avdal, and L. Løvstakken, "Adaptive spectral estimation methods in color flow imaging," *IEEE transactions on ultrasonics, ferroelectrics, and frequency control*, vol. 63, no. 11, pp. 1839–1851, 2016.

[23] C. Kasai, K. Namekawa, A. Koyano, R. Omoto, *et al.*, "Real-time two-dimensional blood flow imaging using an autocorrelation technique," *IEEE Trans. Sonics Ultrason*, vol. 32, no. 3, pp. 458–464, 1985.

[24] S. Gudmundsson and K. Maršál, "Umbilical artery and uteroplacental blood flow velocity waveforms in normal pregnancya cross-sectional study," *Acta obstetricia et gynecologica Scandinavica*, vol. 67, no. 4, pp. 347–354, 1988.

[25] I. K. Ekroll, M. M. Voormolen, O. K.-V. Standal, J. M. Rau, and L. Lovstakken, "Coherent compounding in Doppler imaging," *IEEE transactions on ultrasonics, ferroelectrics, and frequency control*, vol. 62, no. 9, pp. 1634–1643, 2015.

[26] E. Berkley, S. P. Chauhan, A. Abuhamad, S. for Maternal-Fetal Medicine Publications Committee, *et al.*, "Doppler assessment of the fetus with intrauterine growth restriction," *American journal of obstetrics and gynecology*, vol. 206, no. 4, pp. 300–308, 2012.

Chapter 6

Data Adaptive 2-D Tracking Doppler

Yücel Karabiyik[1], Jørgen Avdal[1], Ingvild Kinn Ekroll[1,2], Hans Torp[1], and Lasse Løvstakken[1]
[1] Dept. of Circulation and Medical Imaging, NTNU, Norway
[2] St. Olavs Hospital, Trondheim University Hospital, Norway

Spectral broadening in pulsed wave Doppler caused by the transit time effect deteriorates the frequency resolution and may cause overestimation when tracing the maximum velocities in high velocity blood flow regions. Data adaptive spectral estimators have been shown to provide improved frequency resolution, especially for small window sizes, but offer little or no improvement when the transit time effect dominates. A method, presented as 2-D tracking Doppler where the scatterers are tracked in space was shown to reduce transit time effect. However, the method requires long tracking lengths to provide sufficient improvement. In this work, a method is presented that combines the Capon data adaptive spectral estimation method and the 2-D tracking Doppler to increase the frequency resolution for both high and low velocities. The broadening could be decreased by 66% compared to 2-D tracking Doppler using 16 time samples.

6.1 Introduction

Pulsed wave Doppler is an effective method used in various fields in medicine such as cardiology and obstetrics to estimate the spectrum of blood velocities. Conventionally, ultrasonic pulses are fired along a direction and echoes are sampled at a fixed location of interest to estimate and display the spectrum of velocities present in the region. Depending on the ultrasound pulse transmit parameters and the beam-to-flow angle, the scatterers are observed for a limited amount of time. Decreased observation time results in broadening of the velocity spectrum, especially in the presence of high velocities. This effect is called transit time effect and causes deterioration of velocity resolution and overestimation of velocities.

A method presented as velocity matched spectrum [1] has been shown to reduce transit time spectral broadening by tracking the scatterers in space to increase observation time. However, this method provides improvement for a limited range of beam-to-flow angles as the tracking is done only in the beam direction. Extension of this method to 2-D, called 2-D tracking Doppler [2], resolves this problem by tracking

the scatterers in a wider region in 2-D made possible by parallel receive beamforming. A limitation of these methods is that they require relatively long observation windows (OWs) to achieve good frequency resolution. As the scatterers are tracked in space, long OWs may violate the assumption of stationary flow in space and time. This is a potential problem in case of complex flow fields with rapid acceleration.

Adaptive spectral estimation methods [3], [4] have been adapted to ultrasound Doppler blood flow imaging and have been shown to produce velocity spectra with increased frequency resolution and contrast using significantly fewer time samples than used for Welch's method [5] which is conventionally used for velocity spectrum estimation. However, these methods use signals sampled at a fixed location for spectral estimation and as a result suffer from spectral broadening for high velocities due to transit time effect.

In this work, a method is proposed to achieve high spectral resolution for high and low velocities using a limited number of time samples. The tracking Capon is combination of 2-D tracking Doppler and an adaptive spectral estimation method, power spectral Capon [3] where time samples are extracted tracking the blood scatterers and subsequently used in the Capon estimator to get the velocity spectrum.

6.2 Methods

Extraction of time samples in the direction of the flow is done in a similar manner to the method 2-D tracking Doppler. Signal after demodulation and low pass filtering is represented by $u(x, z, k)$ where x and z are lateral and radial coordinates respectively and k represents time index. Data are interpolated along a line with an angle given by the user using 2-D spline interpolation.

For the defined beam-to-flow angle θ, an interpolated sample can be written as

$$u_\theta(r, k) = u(r \sin\theta + x_0, r \cos\theta + z_0, k), \tag{6.1}$$

where r is the distance from the line center $[x_0, z_0]$ to the interpolated point. Interpolation is done for all velocities of interest. Data sampled for velocity v can be represented as vector $\mathbf{u}_{\theta,v}$ with elements

$$u_{\theta,v}(kvT, k_0 + k),\ k = -(K-1)/2,\ \cdots,(K-1)/2, \tag{6.2}$$

where T is pulse repetition time, K is the number of samples used for spectral estimation and k_0 is the center point in time. A 2-D averaging region is used for estimation of the covariance matrix for spectral power estimation. A set of spatial points moving with defined velocity and angle generates parallel lines. Denoting the direction of flow towards the probe as positive, a sample from line n after phase correction can be written as

$$u_{\theta,v,n}(r, k) = u(r \sin\theta + x_{0,n}, r \cos\theta + z_{0,n}, k) e^{-i\omega_d k \Delta t}, \tag{6.3}$$

where ω_d is the angular demodulation frequency and

$$\Delta t = \frac{2vT\cos\theta}{c}. \tag{6.4}$$

Consequently, the data vector consisting of samples interpolated along line n for velocity v can be represented as

$$u_{\theta,v,n}(kvT, k_0 + k), \quad k = -(K-1)/2, \ \cdots, (K-1)/2. \tag{6.5}$$

The covariance matrix estimated using the extracted signals can be written as

$$\hat{\mathbf{R}}_v = \frac{1}{N}\sum_{n=1}^{N} \mathbf{u}_{\theta,v,n}\mathbf{u}_{\theta,v,n}^{\mathrm{H}}. \tag{6.6}$$

The estimated power for velocity v is later found by using spectral Capon estimator

$$\hat{\mathbf{P}}(v) = \frac{1}{\mathbf{a}_f^{\mathrm{H}}\hat{\mathbf{R}}_v^{-1}\mathbf{a}_f}. \tag{6.7}$$

where $\mathbf{a}_f = [1 \ e^{i2\pi f} \ \cdots \ e^{i2\pi f(K-1)}]^T$ is the Fourier vector and f is the normalized frequency. Interpolated time samples should match in phase when the sampling velocity matches the velocity of the scatterer. Therefore, only the zero frequency ($f = 0$) is investigated for each velocity. Finally, the proposed estimator can be given as

$$\hat{\mathbf{P}}(v) = \frac{1}{\sum_{i=1}^{K}\sum_{j=1}^{K} R_{ij}}, \tag{6.8}$$

where R_{ij} represents the element of $\hat{\mathbf{R}}_v^{-1}$ in row i and column j. Fig. 6.1 shows the concept of sampling done for power spectrum density (PSD) estimation. The averaging region is a grid of points moving in space and time with a defined angle. The resulting tracking lines have a spatial extent proportional to the velocity of interest and the length of the OW. Therefore, the number of averaging lines is equal to the number of spatial points used for averaging.

6.3 Experiments

Evaluation of the method was done using data acquired from a flow phantom experiment and *in vivo* recording from common carotid artery of a healthy volunteer. SonixMDP ultrasound system (Ultrasonix, Richmond, BC, Canada) with a 5 MHz linear probe was used for recordings. Plane wave transmission steered straight down at 4 kHz pulse repetition frequency (PRF) was used for both phantom and *in vivo* experiments.

The flow phantom (Model 524 Peripheral Vascular Doppler Flow Phantom, ATS laboratories, Bridgeport, CT, USA) consisted of a tissue mimicking material

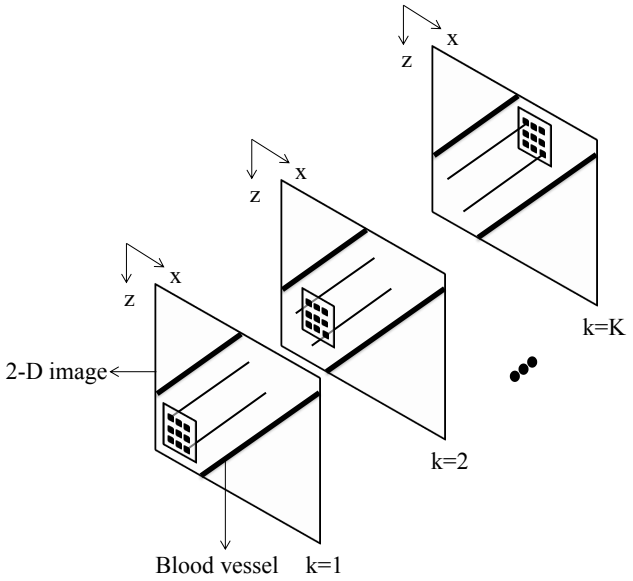

Figure 6.1: The concept of extracting samples for each velocity of interest. A 2-D averaging region moves in space with a defined angle and velocity forming parallel lines.

surrounding a straight tube was used for the recording. The PhysioPulse 100 flow system (Shelley Medical Image Technologies, London, ON, Canada), pumping blood mimicking fluid, was connected to the flow phantom to form a flow loop. The system was set to give 1 Hz sinusoidal flow.

The recordings were done with 70 ° and 62 ° beam-to-flow angles for *in vivo* and flow phantom recordings respectively.

Table 6.1 summarizes the acquisition parameters. Acquired data were clutter filtered using an FIR filter that has cutoff at 210 Hz. Welch and Capon PSD estimations were done on 512 frequency points and 512 spectral power estimations were done for the tracking methods for velocities between ± 2 m/s and ± 1.15 m/s for *in vivo* and flow phantom results respectively.

Table 6.1: Acquisition setup

Parameter	flow phantom & carotid artery
Center frequency [MHz]	5
Pulse periods	2.5
PRF [kHz]	4
F-number	1.4

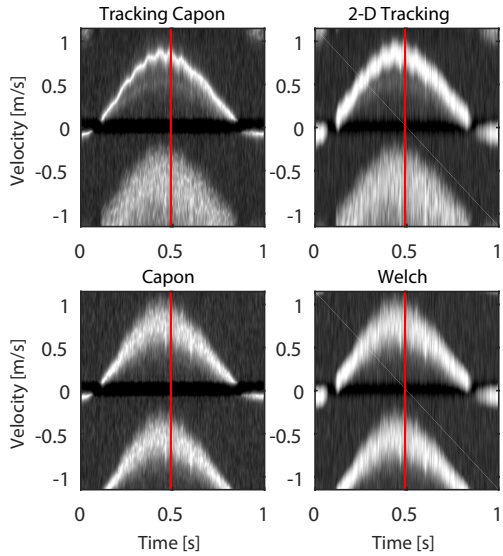

Figure 6.2: Spectrograms that are generated with tracking Capon, 2-D tracking, Capon and Welch's method using flow phantom recording. The beam-to-flow angle is 62 °. The dynamic range used for display is 40 dB.

6.4 Results

Fig. 6.2 shows spectrograms generated using the flow phantom recording where the proposed method is compared to the 2-D tracking Doppler, power spectral Capon and Welch's method. A 2-D averaging region corresponding to 1.5 mm x 1.5 mm and 10 ms temporal averaging is used for PSD estimations. OW length for all methods were chosen to be 16. This results in a maximal tracking length of 0.8 cm, corresponding to the highest investigated velocity of 2 m/s. The proposed method yields spectrograms with reduced spectral broadening for low and high velocities compared to other methods.

Fig. 6.3 shows spectra corresponding to the vertical lines in the spectrograms in Fig. 6.2 where the mean velocity is approximately 0.85 m/s. The spectral width at -3 dB were found to be approximately 5 cm/s, 15 cm/s, 26 cm/s and 32 cm/s for this mean velocity for the proposed method, 2-D tracking, Capon and Welch's approach respectively.

Spectrograms generated using the *in vivo* carotid recording are shown in Fig. 6.4. Except for the averaging region, the imaging and processing parameters were equal to those used for the flow phantom recordings. The 2-D averaging region has dimensions of 1.4 mm x 0.6 mm in lateral and radial directions respectively. There is a clear improvement in spectral broadening for the proposed method, especially for high velocities, e.g., peak systolic velocity. Upper panel in Fig. 6.5 shows the spectra correspond to the red vertical lines in Fig. 6.4 while the lower panel corresponds to

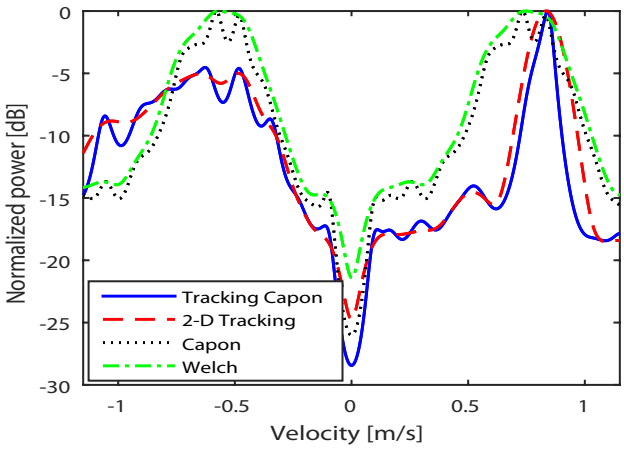

Figure 6.3: Doppler power spectra corresponding to the time instances marked with red lines in Fig. 6.2.

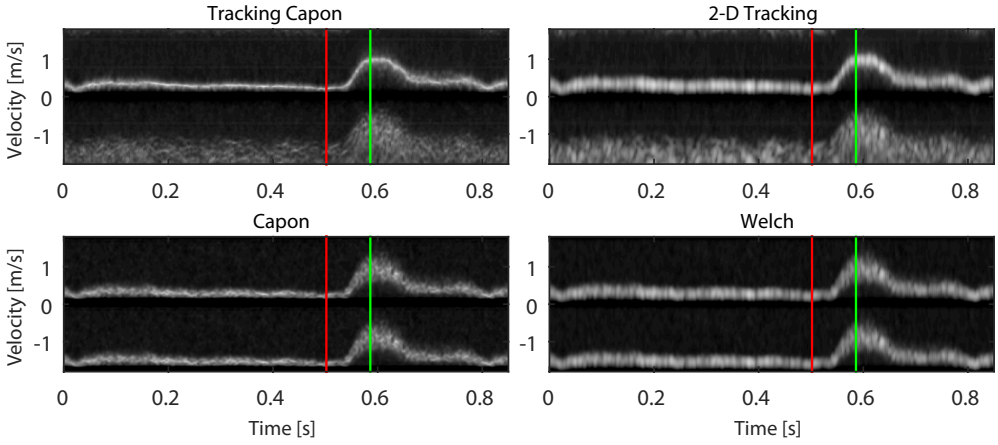

Figure 6.4: Spectrograms that are generated with tracking Capon, 2-D tracking, Capon and Welch's method using *in vivo* recording. The beam-to-flow angle is 70 °. The dynamic range used for display is 40 dB.

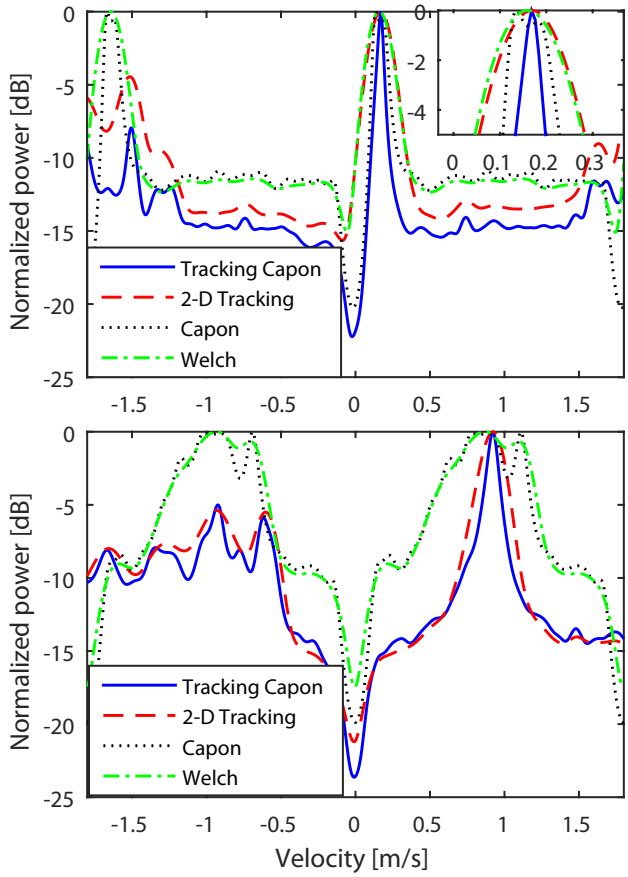

Figure 6.5: The upper and lower panels show velocity spectra corresponding to the time instances marked in Fig. 6.4 with red and green lines respectively.

the green lines. The mean velocity for the time instants are approximately 0.2 m/s and 1 m/s for red and green lines respectively. The proposed method provides the best spectral resolution for low and high velocities. In addition, the aliased part of the tracking Capon and 2-D tracking spectra has lower power compared to other methods.

6.5 Discussion

The results show that for a limited number of Doppler samples, the proposed data adaptive method can reduce spectral broadening further than what can be achieved with regular 2-D tracking Doppler. Both methods are based on tracking the movement of the scatterers to increase the transit time. Power spectral Capon, however, generates a data dependent filter which minimizes the output power while preserving the power

of frequency of interest. This adaptive property is utilized in the proposed method, instead of summing the interpolated samples as done in regular 2-D tracking Doppler, the samples are filtered with a data dependent filter with center frequency around zero. This results in a suppression of interfering velocity components and decreases spectral broadening. Improved resolution can make delineating the true maximum velocity easier which is crucial for applications as Doppler index calculation in obstetrics.

The use of data adaptive methods such as power spectral Capon can by itself decrease spectral broadening for low velocities and short OW sizes as shown in Fig. 6.5. However, for high velocities, increased spectral broadening is inevitable when the spectral broadening due to transit time effect dominates as shown in Fig. 6.3.

The proposed method reduces the number of samples needed to generate high frequency resolution PSDs. Tracking lengths required for 2-D tracking Doppler can be too long to satisfy the stationary flow assumption in space and time. This introduces additional broadening and the improvement achieved by the method may be lost. It was observed that the proposed method can decrease the tracking length to half while preserving the frequency resolution achieved by 2-D tracking Doppler.

As the signal extraction is based on the same approach, 2-D tracking and the proposed method has similar advantages and challenges. Out of plane motion of the scatterers or incorrect flow angle estimation results in broadening of the main lobe. However, if the extracted samples are in phase, the methods can yield PSDs with high SNR and frequency resolution as shown in Fig. 6.3.

It was observed that the aliased part of the spectrum can have lower power for the proposed method. This helps to distinguish between the true and aliased velocity components.

A disadvantage of tracking Capon is that it requires relatively larger averaging region to generate robust estimates. This may increase spectral broadening in case the velocity profile is not constant in the averaging region.

6.6 Conclusion

A method that improves the frequency resolution for high velocities using short OW sizes is presented. Increased transit time is made possible by tracking scatterers in 2-D space, combined with the high resolution spectral estimation properties of the Capon estimator, the proposed method could yield PSDs that have considerably higher frequency resolution, especially for high velocities. A 66% of reduction in spectral broadening was achieved compared to 2-D tracking Doppler for 0.85 m/s mean velocity and with 62 $^\circ$ beam-to-flow angle. Being able to produce high resolution PSDs with short OW size can potentially extend the use of 2-D tracking concept to complex flow fields with rapid accelerations.

Acknowledgment

This work was funded by the project "Umoja - Ultrasound for Midwives in Rural Areas" (Helse Midt-Norge RHF).

References

[1] H. Torp and K. Kristoffersen, "Velocity matched spectrum analysis: A new method for suppressing velocity ambiguity in pulsed-wave Doppler," *Ultrasound in medicine & biology*, vol. 21, no. 7, pp. 937–944, 1995.

[2] T. D. Fredriksen, I. K. Ekroll, L. Lovstakken, and H. Torp, "2-D tracking Doppler: a new method to limit spectral broadening in pulsed wave doppler," *IEEE transactions on ultrasonics, ferroelectrics, and frequency control*, vol. 60, no. 9, pp. 1896–1905, 2013.

[3] F. Gran, A. Jakobsson, and J. A. Jensen, "Adaptive spectral Doppler estimation," *IEEE transactions on ultrasonics, ferroelectrics, and frequency control*, vol. 56, no. 4, pp. 700–714, 2009.

[4] E. Gudmundson, A. Jakobsson, J. A. Jensen, and P. Stoica, "Blood velocity estimation using ultrasound and spectral iterative adaptive approaches," *Signal Processing*, vol. 91, no. 5, pp. 1275–1283, 2011.

[5] P. D. Welch, "The use of fast Fourier transform for the estimation of power spectra: A method based on time averaging over short, modified periodograms," *IEEE Transactions on audio and electroacoustics*, vol. 15, no. 2, pp. 70–73, 1967.